ABSTRACT

PILLAI, PRIYA RAMACHANDRAN. Nitrous Oxide Emissions from Biofuel Crops and Atmospheric Aerosols: Associations with Air Quality and Regional Climate (Under the direction of Dr. Viney P. Aneja and Dr. John T. Walker)

Emissions of greenhouse gases (GHG) and primary release and secondary formation of aerosols alter the earth's radiative balance and therefore have important climatic implications. Savings in carbon dioxide (CO_2) emissions accomplished by replacing fossil fuels with biofuels may increase the nitrous oxide (N_2O) emissions. Among various atmospheric trace gases, N_2O, irrespective of its low atmospheric concentration, is the fourth most important gas in causing the global greenhouse effect. Major processes, those affect the concentration of atmospheric N_2O, are soil microbial activities leading to nitrification and denitrification. Therefore, anthropogenic activities such as industrial emissions, and agricultural practices including application of nitrogenous fertilizers, land use changes, biomass combustion all contribute to the atmospheric N_2O concentration. The emission rates of N_2O related to biofuel production depend on the nitrogen (N) fertilizer uptake efficiency of biofuel crops. However, crops with less N demand, such as switchgrass may have more favorable climate impacts when compared to crops with high N demands, such as corn. Despite its wide environmental tolerance, the regional adaptability of the potential biofuel crop switch grass varies considerably. Therefore, it is important to regionally quantify the GHG emissions and crop yield in response to N-fertilization. A major objective of this study is to quantify soil emissions of N_2O from switchgrass and corn fields as a function of N-fertilization. The roles of soil moisture and soil temperature on N_2O fluxes were analyzed. These N_2O observations may be used to parameterize the biogeochemical models to better understand the impact of different N_2O emission scenarios. This study allows for

improvements in climate models that focus on understanding the environmental impacts of the climate change mitigation strategy of replacing fossil fuels with biofuels.

As a second major objective, the top of the atmosphere (TOA) shortwave aerosol direct radiative forcing (SWARF) by regionally nucleated particles over a forest site in the Southeastern United States was estimated. Particle size distributions (aerodynamic diameter, D_p 10.2 nm to 250 nm), total number concentrations of nucleation mode (D_p < 25 nm) and fine mode (25 < D_p < 250 nm) particles, and growth rates were analyzed to identify regional nucleation events during November 2005 to September 2007. Shortwave flux from Clouds and Earth's Radiant Energy System (CERES) and aerosol optical depth at 550 nm (AOD, τ_{550}) from Moderate Resolution Imaging Spectroradiometer (MODIS) instruments onboard the Earth Observing System (EOS) Terra satellite were used to estimate SWARF. AOD was highest (0.38 ± 0.20) in summer (period of highest particle growth rate) and lowest (0.06 ± 0.05) in winter (period of lowest particle growth rate). The nucleation day SWARF forcing was -24 ± 11 Wm^{-2} in summer and -15 ± 19 Wm^{-2} in spring. The radiative forcing efficiency was lower (-54 Wm^{-2}, τ_{550}^{-1}) in summer (period of highest τ_{550} and organic $PM_{2.5}$ concentrations) as compared to spring (-93 Wm^{-2}, τ_{550}^{-1}). The results show that, during spring and summer 2006 and 2007, the radiative forcing efficiency of regionally nucleated aerosols was -73 Wm^{-2}, τ_{550}^{-1}. Formations of particles during regional nucleation events introduced significant radiative forcing that need to examine for other regions of the globe where intense regional nucleation events occur frequently.

Nitrous Oxide Emissions from Biofuel Crops and Atmospheric Aerosols: Associations with Air Quality and Regional Climate

by
Priya Ramachandran Pillai

A dissertation submitted to the Graduate Faculty of
North Carolina State University
in partial fulfillment of the
requirements for the degree of
Doctor of Philosophy

Marine, Earth, and Atmospheric Sciences

Raleigh, North Carolina

2016

APPROVED BY:

_____	_____
Dr. Viney P. Aneja Committee Co-Chair	Dr. John T. Walker Committee Co-Chair
_____	_____
Dr. S. Pal Arya	Dr. Anantha Aiyyer

DEDICATION

I dedicate this work to my family and in the loving memory of my father

S. Ramachandran Pillai

BIOGRAPHY

Curriculum Vitae

Priya Pillai
Department of Marine, Earth, and Atmospheric Sciences
North Carolina State University
Raleigh, NC 27606

Education

North Carolina State University	Ph.D. Candidate Atmospheric Sciences
University of Alabama in Huntsville	M.S. Atmospheric Sciences
Cochin University of Sci & Technology, India	M.Sc. Meteorology
Mahatma Gandhi University, India	B.Sc. Physics (Chemistry & Mathematics)

Professional Positions

Research Engineer/Science	NOAA through I.M. Systems Group	2015 – present
Graduate Research Assistant	North Carolina State University	2009 – 2015
Graduate Researcher	U.S. EPA, Durham, NC	2013 – 2015
Graduate Research Assistant	University of Alabama in Huntsville	2007 – 2009
Junior Research Fellow	Indian Institute of Technology, New Delhi	2004 – 2006
Junior Research Fellow	National Aerospace Lab, Bangalore	2003 – 2004

Teaching Experience

Instructor	Introduction to Weather & Climate Laboratory	2010 – 2014
Graduate Teaching Assistant	Fundamentals of Air Quality& Climate Change	2012 – 2015
	Fundamentals of Air pollution	2012 – 2013
	The Global Atmosphere	2011
	Introduction to Weather & Climate	2011
	Air Quality Modeling & Forecasting	2010

Publications

Pillai P., Khlystov, A., Walker, J. T., Aneja, V. P., (2013), "Observation and Analysis of Particle Nucleation at a Forest Site in the Southeast U.S.", *Atmosphere*, 4, 72-93.

Aneja V. P., **Pillai P.,** Isherwood, A., Morgan, P., and Aneja, S. P., (2015), "Particulate Matter Pollution in the Coal-Producing Regions of the Appalachian Mountains: Integrated Ground Based Measurements and Satellite Retrievals", (*Journal of Air and Waste Management*)

Yu, F., Luo, G., Pryor, S. C., **Pillai, P. R.**, Lee, S. H., Ortega, J., Schwab, J. J., Hallar, A. G., Leaitch, W. R., Aneja, V. P., Smith, J. N., Walker, J. T., Hogrefe, O., and Demerjian, K. L., (2015), "Spring and summer contrast in new particle formation over nine forest areas in North America", *Atmos. Chem. Phys. Discuss.*, 15, 21271–21298.

Pillai P., V. P. Aneja, J. Walker, (2015), "Satellite Based Estimation of Shortwave Aerosol Radiative Forcing by Regional Nucleation Events at a forest site in the Southeast US", (submitted)

Walker, J. , **Pillai P.,** V. P. Aneja, and coauthors, "Soil Nitrous Oxide Emissions from Corn and Switch grass Crops" (to be submitted)

Pillai P., A. Khlystov, J.T. Walker, V. P. Aneja, "Formation and growth of atmospheric particles at a forest site in the southeast US", AIP Conf. Proc. 1527, 401 (2013), DOI:10.1063/1.4803288.

Pillai P., A. Khlystov, J.T. Walker, and V. P. Aneja, "Relationships between particle nucleation and radiative forcing at a forest site in the Southeast US", 16th International Symposium for the Advancement of Boundary-Layer Remote Sensing, Boulder, CO, June 2012.

Awards and Assistantships

Doctoral Poster Competition (2nd Place) &ACE Travel Scholarship	Air & Waste Management Association (A&WMA)	June 2015
National Science Foundation Travel Grant	Boulder, CO	July 2013
National Science Foundation Travel Grant	Fort Collins, CO	June 2013
GCC Student Scholarship	Climate Conference, WA	October 2012
ISARS Travel Grant	16th ISARS, CO	June, 2012
CSIR/UGC Fellowship	Council of Scientific & Industrial Research, India	2002 & 2003

ACKNOWLEDGMENTS

I would like to thank the North Carolina State University (NCSU), Raleigh, North Carolina for this wonderful opportunity and the financial support and all those individuals who supported me to make this dissertation possible. Also, I would like to thank the U.S. Environmental Protection Agency (U.S. EPA) for the partial financial support.

Special thanks go to my advisors Dr. Viney Aneja and Dr. John T. Walker. Dr. Aneja was not only my advisor but also a mentor. He gave me the freedom to explore my passion. I would like to thank him for his patience and constant encouragement for my doctoral research. Dr. Walker was my support to keep going and the guidance to follow through. It has been an honor as well as a responsibility to learn from him.I would like to express my sincere gratitude to Dr. Arya and Dr. Aiyyer. I could not have finished this work without their help and guidance. Thanks to Dr. Lisa Dean for her suggestions in finishing this dissertation. Special thanks go to the NCSU, Raleigh professors Dr. Gary Lackmann who made it possible for me to teach at the university, Dr. Robinson, Department Head and Dr. Sukanta Basu, Professor.

Thanks to Aleksandra, for her help in data collection and the laboratory analysis. I also thank Air Quality Lab members William Battye, Casey Brey, and Dennis Mikel for their encouragements and the fruitful discussions we had. There are several people outside of academia who made this journey possible. I would also like to acknowledge the staff of BASF at Holly Springs for site access and management in support of the N_2O study.

Most importantly I would like to thank my family: husband Praju, mom Valsa, grand mom Devaki, siblings Deepa and Rajesh, and niece Deya for their selfless love and constant support. I also would like to thank all my friends for their encouragement towards achieving my goal.

TABLE OF CONTENTS

LIST OF TABLES

LIST OF FIGURES

Chapter 1

1. INTRODUCTION

Greenhouse gases (GHGs) modify the earth's climate directly through their interactions with outgoing terrestrial (longwave) radiation. GHGs have a positive feedback on the earth's radiative balance. Radiative forcing is the quantification of the capacity of forcing agents such as GHGs, clouds, and aerosols in affecting the earth's radiative balance (IPCC, 2007). Nitrous Oxide (N_2O), irrespective of its low atmospheric concentration, is the third largest contributor to radiative forcing (0.17 ± 0.03 W m^{-2}) by well mixed GHGs. It has an average life time of 121 years and accounts for ~ 6.25% of the global greenhouse effect (Forster et al., 2007). The 100 years averaged global warming potential of N_2O is about 300 (Myhre et al., 2013). This means that the greenhouse effect or in other words, the radiative forcing produced by unit mass of N_2O is ~300 times intense than that produced by the same mass of carbon dioxide (CO_2). N_2O plays another important role in the concentration of stratospheric Ozone (O_3). N_2O through its reaction with oxygen atom ($O(^1D)$), produced primarily by the photo-dissociation of O_3, acts as a stratospheric source of mono-nitrogen oxides (NO_x) (Seinfeld and Pandis, 2006). With the declining levels of chlorofluorocarbons (Montzka et al., 2011), N_2O therefore turns to be the leading cause of stratospheric ozone depletion (Ravishankara et al., 2009).

The present day global concentration of atmospheric N_2O is about 327 parts per billion by volume (ppb) (IPCC, 2013). Based on National Oceanic and Atmospheric Administration (NOAA) flask program's monthly mean global N_2O data from 1995 to 2013 (Figure 1.1), the N_2O concentration has increased by about 5% at approximately 0.86 ppb yr^{-1}.

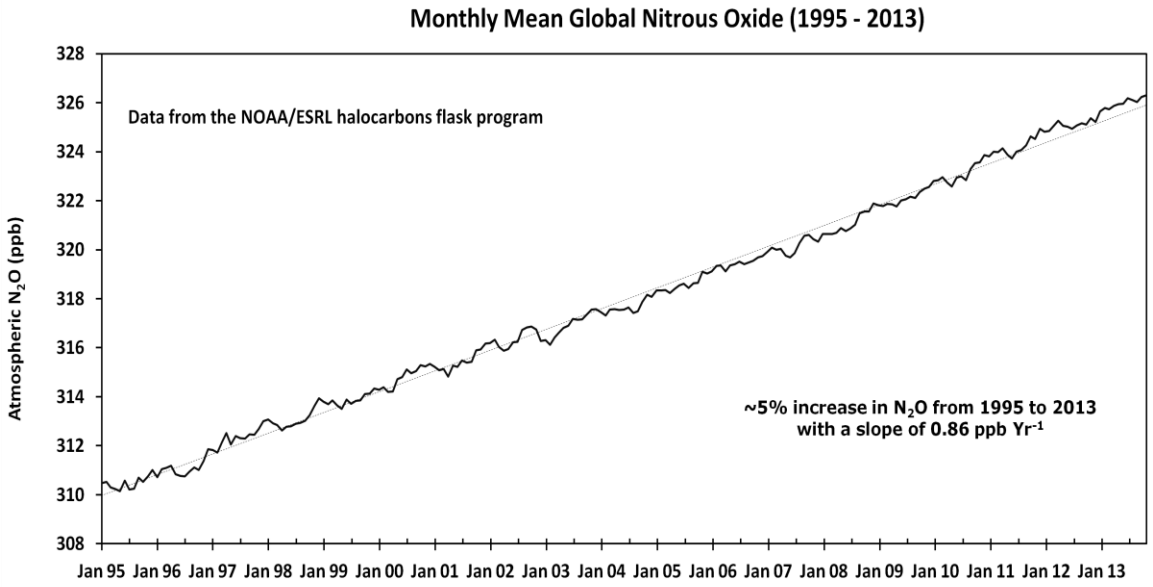

Figure 1.1. Monthly averages of global mean N_2O from January 1995 to July 2013 (Data Source: NOAA/ESRL halocarbons flask program).

Soil N_2O emissions will continue to rise in order to meet the growing demands for food and fuel as well as the rising dependence of agriculture on N-fertilizers (Schnepf and Yacobucci, 2010; U.S. EPA 2010; IPCC 2013). The U.S. Renewable Fuels Standards (U.S. RFS) has set a goal of the use of 36 billion gallons of renewable transportation fuels by 2022 in the United States (Schnepf and Yacobucci, 2010) and is expected to be

associated with economic and environmental benefits (U.S. EPA 2011). As a result of the growing biofuel demands, expansions in crop land, expansions in fertilized land use, and the accompanying intense agricultural activities including irrigation, tillage operations, and associated increase in soil microbial activities may lead to enhanced soil N_2O emissions. About 78% of the global nitrous oxide emissions come from agriculture of which ~67% comes from agricultural soils mainly through microbial transformation of nitrogen (N) compounds in the soil (Mosier et al, 1998). Therefore, anthropogenic activities such as industrial emissions, agricultural practices including application of nitrogenous fertilizers, land use changes, and biomass combustion all contribute to the atmospheric N_2O concentration (Hillel, 1998).

The need for an alternate climate friendly fuel to mitigate fossil fuel driven climate change as well as the rising energy demands are the two major factors responsible for the rapid growth in biofuel production. Crutzen et al., (2008) concluded that soil N_2O emissions from N-fertilizer application in biofuel production can be 3 to 5 times greater than current estimates and can partially offset the greenhouse gas mitigation expected to accomplish by replacing fossil fuels, the primary anthropogenic source of CO_2, with biofuels. For these reasons, an efficient shift from fossil fuel to biofuel may only be associated with both economic and environmental benefits.

To reach the 36 billion gallons biofuel production goal set by US RFS, 2010, the biofuel industry will need an increased supply of current feedstock such as corn and large scale production of promising crops such as switchgrass. This goal mandates the production of 16 billion gallons of cellulosic and agricultural waste-based biofuel and to qualify in this

undertaking, the cellulosic biofuels must be efficient enough to decrease its lifecycle GHG emissions by no less than 60% (Schnepf and Yacobucci, 2010). Therefore, it is of extreme interest to the researches around the world to identify alternate energy crops, to quantify their contribution to N_2O emissions in relation to reduction in CO_2 emissions achieved by replacing fossil fuels with biofuel, and further to quantify their role in the GHG mitigation. Switchgrass is a tall-grass prairie native to North America and can grow in a wide spectrum of ecotypes in various geographic locations (Palmer et al, 2014; Parrish et al, 2003; Parish et al, 2016). Initial considerations on switchgrass focused primarily on its potential as a crop on marginal land. A study by Robertson et al in 2008 demonstrated the environmental benefits of lignocellulosic feedstock. Over the years, switchgrass has grown from a common tall-grass prairie to one of the widely mentioned potential energy crop (Hamilton et al, 2015; Wolf and Fiske, 2009). It was proposed as a model crop for energy feedstock by the US Department of Energy (U.S. DoE) due to multiple factors including relatively higher biomass yield over wide range of geographical and climatic conditions, lower fertilization and water demands than corn. Additional benefits of these warm season grasses are their relatively lower requirement for routine management practices (as a perennial crop), role as a wildlife habitat because of the complex fibrous root system, and its positive contribution in the soil carbon credits. Switchgrass has the potential to reduce soil-N losses through nitrate (NO_3^-) leaching and N_2O emissions (Smith et al, 2013). Additional benefits of switchgrass as a biofuel crop include the reduction in wind flow at the soil surface and evaporation and enhancement in infiltration (Dale et al, 2011). Moreover, these crops can be grown on marginal lands or can be

rotated with other crops. The deep fibrous rooting system of switchgrass can serve as an invertebrate habitat in addition of being an excellent carbon sink. The soil organic carbon sequestration by switchgrass is two to four times greater than was parameterized in crop models (Follet et al, 2012). Increase in soil organic carbon further improves soil structure (Lal, 2009).

Emission rates of N_2O depend on the N- fertilizer uptake efficiency of crops. Therefore, crops with less N demand and high N-uptake efficiency, such as switchgrass, may have more favorable climate impacts as compared to crops with high N demands and relatively low N-uptake efficiency, such as corn. Like corn, in order to realize optimal crop yields, nitrogen fertilizer must be applied, resulting in N_2O emissions.

In North Carolina, switchgrass has the potential to become a favorable (smaller N to dry matter ratio) lignocellulosic bio-energy feedstock (Palmer et al, 2014). For the aforementioned reasons (Dale et al, 2011; Follet et al, 2012; Hamilton et al, 2015; Palmer et al, 2014; Smith et al, 2013; Wolf et al., 2008), switchgrass based cellulosic biofuels may be a promising greener alternative to food-crop or fossil fuel based liquid transportation fuels. However, a recent study (Ruan et al, 2016) pointed out the importance of minimizing the use of N-fertilizers, in order to achieve climate benefits, in the second generation biofuel crops such as switchgrass. Their study showed a reduction by about 2.74 Mg CO_2e ha^{-1} yr^{-1} in the GHG mitigation capacity in bio-ethanol production from switchgrass fertilized at 196 kg N ha^{-1} compared to that fertilized at 56 kg N ha^{-1}. Moreover, the energy replacement ratio (energy delivered per unit of fossil energy consumption as part of energy production) between cellulosic ethanol and fossil fuel is

~10 and that between corn ethanol and fossil fuel is ~1.4 (U.S. DoE, 2006). At present, there is only limited knowledge on the N_2O emissions from switchgrass fields, which precludes comparison to other crops and development of a full life-cycle analysis of the cost of switchgrass production. Moreover, the complex influences of N-fertilizer on the N_2O emission rates during switchgrass cultivation are not yet fully characterized. In this study, the N_2O fluxes from switchgrass and corn are examined and compared.

The objectives of this study are to (i) quantify the soil N_2O emissions, as a function of three different N-fertilizer application rates, from a potential biofuel crop of high N-uptake capacity, switchgrass; (ii) at the same N-fertilizer application rates, compare with N_2O emission from the current major biofuel crop, corn; and (iii) analyze the complex interactive influences of nitrogen fertilization, soil moisture, and soil temperature on soil N_2O fluxes. The current study therefore attempts to establish an improved understanding on the adaptation of switchgrass as a potential biofuel crop in the southeastern US.

We further examined the associations of newly formed particles with the air quality and the regional climate of the southeast U.S. Atmospheric aerosols contribute to acid rain, and impair visibility. Aerosols, similar to GHGs, also alter the earth's radiation budget. Depending on the type of aerosols or their chemical compositions, these radiative interactions can either be direct by scattering incoming solar radiation and absorbing outgoing long wave radiation or be indirect by acting as cloud condensation nuclei to modify cloud micro-physical properties (Ramanathan et al., 2007). However, large uncertainties in the understanding aerosols and their formation mechanisms and the estimation of their effects on regional or global climate persist (IPCC, 2007; IPCC 2013).

Aerosols can either be directly emitted (primary) from natural and anthropogenic sources, or formed from gas phase precursors (secondary). Aerosol production mechanisms, number concentrations, and chemical composition are highly dependent on geographical location, air mass origin, source type, meteorology, and atmospheric chemistry. As a second major objective, the top of the atmosphere (TOA) shortwave aerosol direct radiative forcing (SWARF) by regionally nucleated aerosols over the suburban Duke forest site in the Southeastern United States were estimated. Particle size distributions (aerodynamic diameter, D_p 10.2 nm to 250 nm), total number concentrations of nucleation mode (D_p < 25 nm) and fine mode (25 < D_p < 250 nm) particles, and growth rates were analyzed to identify regional nucleation events during November 2005 to September 2007. Shortwave flux from Clouds and Earth's Radiant Energy System (CERES) and aerosol optical depth at 550 nm (AOD, τ_{550}) from Moderate Resolution Imaging Spectroradiometer (MODIS) instruments onboard the Earth Observing System (EOS) Terra satellite were used to estimate SWARF.

These two major objectives or studies are presented as two separate sections in this thesis. Each of these sections includes scientific background, experimental, results, discussions, and conclusions. These sections are followed by a chapter detailing the overall conclusions and the future directions.

REFERENCES

Crutzen, P.J., Mosier, A.R., Smith, K.A. and Winiwarter, W., 2008. N_2O release from agro-biofuel production negates global warming reduction by replacing fossil fuels. *Atmospheric chemistry and physics*, *8*(2), pp.389-395.

Dale, V.H., Kline, K.L., Wright, L.L., Perlack, R.D., Downing, M. and Graham, R.L., 2011. Interactions among bioenergy feedstock choices, landscape dynamics, and land use. *Ecological Applications*, *21*(4), pp.1039-1054.

Follett, R.F., Vogel, K.P., Varvel, G.E., Mitchell, R.B. and Kimble, J., 2012. Soil carbon sequestration by switchgrass and no-till maize grown for bioenergy. *BioEnergy Research*, *5*(4), pp.866-875.

Forster, A., Schouten, S., Baas, M. and Damsté, J.S.S., 2007. Mid-Cretaceous (Albian–Santonian) sea surface temperature record of the tropical Atlantic Ocean. *Geology*, *35*(10), pp.919-922.

Hamilton S.K., Hussain M.Z., Bhardwaj A.K., Basso B. and Robertson G.P., 2015. Comparative water use by maize, perennial crops, restored prairie, and poplar trees in the US Midwest. *Environmental Research Letters*, 10(6), p.064015.

Hillel, D., 1998. *Environmental soil physics: Fundamentals, applications, and environmental considerations*. Academic press.

IPCC, 2007: Climate Change 2007: The Physical Science Basis. Contribution of Working Group I to the Fourth Assessment Report of the Intergovernmental Panel on Climate Change. Solomon, S., Qin, D., Manning, M., Chen, Z., Marquis, M., Averyt, K.B., Tignor, M. and Miller, H.L. (*Eds.*). Cambridge University Press, Cambridge, United Kingdom and New York, NY, USA, 996 pp.

IPCC, 2013. Climate Change 2013: The Physical Science Basis. Contribution of Working Group I to the Fifth Assessment Report of the Intergovernmental Panel on Climate Change. *Stocker, T.F., Qin, D., Plattner, G.K., Tignor, M., Allen, S.K., Boschung, J., Nauels, A., Xia, Y., Bex, V. and Midgley, P.M. (eds.)*. Cambridge University Press, Cambridge, United Kingdom and New York, NY, USA, 1535 pp.

Lal, R., 2009. Challenges and opportunities in soil organic matter research.*European Journal of Soil Science*, *60*(2), pp.158-169.

Montzka, S.A., Dlugokencky, E.J. and Butler, J.H., 2011. Non-CO2 greenhouse gases and climate change. *Nature*, *476*(7358), pp.43-50.

Mosier, A., Kroeze, C., Nevison, C., Oenema, O., Seitzinger, S. and Van Cleemput, O., 1998. Closing the global N_2O budget: nitrous oxide emissions through the agricultural nitrogen cycle. *Nutrient cycling in Agroecosystems*, *52*(2-3), pp.225-248.

Myhre, G., Shindell, D., Bréon, F.M., Collins, W., Fuglestvedt, J., Huang, J., Koch, D., Lamarque, J.F., Lee, D., Mendoza, B., Nakajima, T., Robock, A., Stephens, G., Takemura, T. and Zhang, H., 2013. Climate Change 2013: The Physical Science Basis. Contribution of Working Group I to the Fifth Assessment Report of the Intergovernmental Panel on Climate Change. *Stocker, T.F., Qin, D.,* Plattner, *G.K., Tignor, M., Allen, S.K., Boschung, J., Nauels, A., Xia, Y., Bex, V., and Midgley, P.M. (eds.), Cambridge University Press Cambridge,* United Kingdom and New York, NY, USA.

Palmer, I.E., Gehl, R.J., Ranney, T.G., Touchell, D. and George, N., 2014. Biomass yield, nitrogen response, and nutrient uptake of perennial bioenergy grasses in North Carolina. *Biomass and Bioenergy*, 63, pp.218-228.

Parish, E.S., Dale, V.H., English, B.C., Jackson, S.W. and Tyler, D.D., 2016. Assessing multimetric aspects of sustainability: Application to a bioenergy crop production system in East Tennessee. *Ecosphere*, *7*(2).

Parrish, D.J., Wolf, D.D., Fike, J.H. and Daniels, W.L., 2003. Switchgrass as a Biofuels Crop for the Upper Southeast: Variety Trials and Cultural Improvements–Final Report for 1997 to 2001. *ORNL/SUB-03-19XSY163/01*.

Ramanathan, V., Ramana, M.V., Roberts, G., Kim, D., Corrigan, C., Chung, C. and Winker, D., 2007. Warming trends in Asia amplified by brown cloud solar absorption. *Nature*, *448*(7153), pp.575-578.

Ravishankara, A.R., Daniel, J.S. and Portmann, R.W., 2009. Nitrous oxide (N_2O): The dominant ozone-depleting substance emitted in the 21st century. *Science, 326*(5949), pp.123-125.

Robertson, G.P., Dale, V.H., Doerig, O.C., Hamburg, S.P., Melillo, J.M., Wander, M.M., Parton, W.J., Adler, P.R., Barney, J.N. and Cruse, R.M., 2008. Sustainable Biofuels Redux. *Science*. *322*, pp.49-50.

Ruan, L., Bhardwaj, A.K., Hamilton, S.K. and Robertson, G.P., 2016. Nitrogen fertilization challenges the climate benefit of cellulosic biofuels. *Environmental Research Letters*, 11(6), p.064007.

Seinfeld, J., and Pandis, S. N., 2006, *Atmospheric Chemistry and Physics: From Air Pollution to Climate Change*, John Wiley & Sons Inc., Hoboken, New Jersey.

Smith, C.M., David, M.B., Mitchell, C.A., Masters, M.D., Anderson-Teixeira, K.J., Bernacchi, C.J. and DeLucia, E.H., 2013. Reduced nitrogen losses after conversion of row crop agriculture to perennial biofuel crops. *Journal of environmental quality*, 42(1), pp.219-228.

Schnepf, R., and Yacobucci, B.D., July, 2010. Renewable fuel standard (RFS): overview and issues. In *CRS Report for Congress* (No. R40155).

U.S. DoE, 2006. Breaking the biological barriers to cellulosic ethanol: A joint research agenda. *U.S. Department of Energy*, Washington.

U.S. EPA, 2010. Regulation of fuels and fuel additives: changes to renewable fuel standard program; final rule, *Federal register*, vol. 75, No. 58, March 26, 40 CFR Part 80

U.S. EPA, 2011. Biofuels and the environment: first triennial report to congress. EPA/600/R-10/183F. *National Center for Environmental Assessment, Office of Research and Development, U.S. Environmental Protection Agency*, Washington DC

Wolf, D. and Fiske, D., 2009. Planting and Managing Switchgrass for Forage, Wildlife, and Conservation. *Virginia Cooperative Extension*. Publication 418-013.

Nitrous Oxide Emissions from Biofuel Crops: Associations with Air Quality and Regional Climate

Chapter 2

2. SCIENTIFIC BACKGROUND ON N_2O EMISSIONS

Most of the nitrogen present in the ecosystem is in the rocks in the lithosphere followed by the atmosphere where nitrogen is present as molecular nitrogen (N_2). N_2 cannot be directly broken apart and taken up by plants or microorganisms.

2.1. The Biological Nitrogen Cycle in the Soil

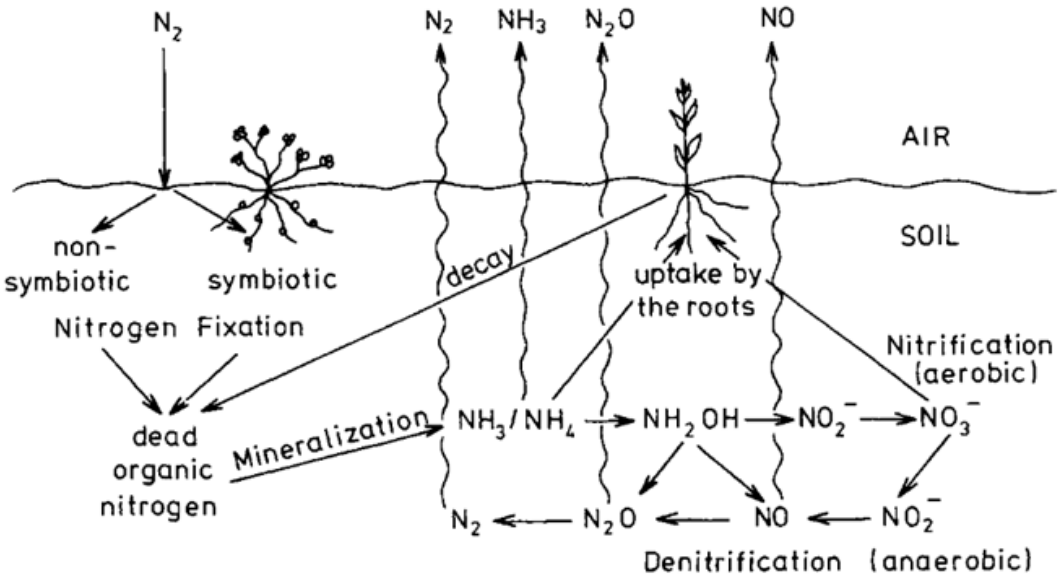

Figure 2.1. The biological nitrogen cycle in the soil atmosphere interface (Source: Chemistry of the Natural Atmosphere by Peter Warneck, 2000)

2.1.1. Nitrogen Fixation and Mineralization

N_2 enters the soil through nitrogen fixation, where the fixed N can be taken up by plants and microorganisms to be incorporated in their living cells. During bacterial nitrogen fixation, N_2 is reduced by heterotrophic bacteria such as azotobactor and clostridia or by Rhizobia living in the root nodules of leguminous plants. Once these nitrogen incorporated plants or microorganisms decay, the organic matter is decomposed and undergoes mineralization to ammonium (NH_4^+) and ammonia (NH_3) (Rosswall, 1981).

2.1.2. Nitrification

In well aerated soils, nitrification (oxidation of NH_4^+ via the intermediate hydroxylamine, NH_2OH) takes place through microbial activity. Nitrosomonas bacteria oxidize NH_4^+ to nitrite (NO_2^-) and Nitrobactor bacteria further oxidize NO_2^- to NO_3^-.

$$NH_4^+ \rightarrow NH_2OH \rightarrow NO_2^- \rightarrow NO_3^- \qquad (2.1)$$

Under oxygen limiting conditions, the NO_2^- can serve as an electron acceptor for the NH_4^+ oxidizers and N_2O can be released. The end product of nitrification is NO_3^-, which can be taken up by plants and microorganisms. Once these plants/organisms die, the fixed nitrogen again enters back in the soil through bacterial degradation (Warneck, 2000).

2.1.3. Denitrification

A portion of this fixed N undergoes denitrification which closes the N-cycle. Under anaerobic conditions, denitrifying bacteria utilize oxides of nitrogen as a source of oxygen and therefore reduce NO_3^- to N_2 in which case NO_2^-, NO, and N_2O are the intermediate products. Figure 2.1 shows the biological nitrogen cycle in soils and its connection with the atmosphere (Warneck, 2000).

$$NO_3^- \rightarrow NO_2^- \rightarrow NO \rightarrow N_2O \rightarrow N_2 \qquad (2.2)$$

In oxygen deficient (high soil water content) conditions denitrification of NO_3^- is the primary N_2O production pathway.

2.2. Factors Affecting Soil N-Cycle

Major contributors of atmospheric N_2O are soils and these emissions are governed by soil microbial processes and the amount of suitable mineral nitrogen substrates such as NH_4^+ or NO_3^-. In soils, N_2O is produced at the intermediate stage during both nitrification (oxidation of NH_4^+ to NO_3^-) and denitrification (reduction of $NO_3^-$to NH_4^+) (Hillel, 1998). Soil microbial processes are influenced by temperature and precipitation. Therefore, the N_2O emissions from soil show strong diurnal and seasonal variations. Depending on the soil aeration conditions, N_2O or nitric oxide (NO) can be the dominant end product during denitrification. Under anaerobic soil conditions, denitrifying bacteria make use of the

oxygen in nitrogen compounds and therefore NO is further reduced before escaping the soil, and the more reduced oxide, N_2O will be the end product. Soil microbial activity depends on both soil temperature and soil volumetric water content. In oxygen deficient (high soil water content) conditions, denitrification (Russow et al., 2000) of NO_3^- to N_2 and N_2O is regarded as the primary N_2O production pathway. Denitrification happens primarily in wet soils where denitrifying bacteria reduce NO_3^- to N_2 and N_2O to gain oxygen. Anaerobic soil conditions with wet soils having Water-Filled Pore Space (WFPS) > 50% primarily cause denitrification driven N_2O emissions (Ussiri and Lal, 2013). However under oxygen rich conditions, nitrification of NH_4^+ to NO_3^- may produce N_2O (Firestone and Davidson, 1989; Ussiri and Lal, 2013). In dry and well-aerated soil, the oxidative process of nitrification dominates and the more oxidized gas, NO, is the most common nitrogen oxide emitted from the soil. Because the diffusivity of gases is high in dry soils, much of the NO can diffuse out of the soil before it is consumed. The water filled pore space (%WFPS) is therefore important as it impacts the soil diffusivity. Soil type is another important factor. In wet soils, where gas diffusivity is lower and aeration is poorer, much of the NO is reduced before escaping the soil, and the more reduced oxide, N_2O (Figure 2.1), is therefore the dominant end product. When the soil is even more water-saturated and mostly anaerobic, N_2O can be reduced to N_2 by denitrifiers before it escapes the soil.

2.3. Agricultural N_2O Emission

In the U. S., the crop lands constitute only 49% of agricultural land; however, these contribute to about 69% of direct N_2O emissions (University of Missouri, 2010). Whereas, grass lands constitute about 51% of agricultural land area and only contribute ~29% of direct N_2O emissions (University of Missouri, 2010). Figure 2.2 shows Agricultural N_2O Emissions.

Agriculture related anthropogenic activities such as deforestation, land use change, raising animals, application of nitrogenous fertilizers, and burning of biomass are all responsible for the increasing concentration of atmospheric N_2O (Hillel, 1998).

Among major crop lands, corn and soybean crops account for the highest N_2O emissions in the U.S. (Del Grosso et al., 2005). The adaptation of efficient agricultural practices can increase carbon sequestration (McLaughlin and Kszos 2005; Schlesinger 1999; Smith et al, 2008), reduce GHG emissions (Lal 2004a; Lal 2004b), and improve air and water quality (Schahczenski and Hill 2009). Owing to spatial and temporal variability associated with contributing factors, soil emissions of N_2O exhibit significant spatial (Folorunso and Rolston 1984; Mathieu et al, 2006) and temporal variability (Smith et al, 2010; Schelde et al, 2012) even on field scales. Moreover, soil microbial communities vary greatly in space (Saetre and Bååth, 2000) and time (Lauber, 2013) within and across the ecosystems. These variations pose major challenges in the quantification of soil emissions of N_2O.

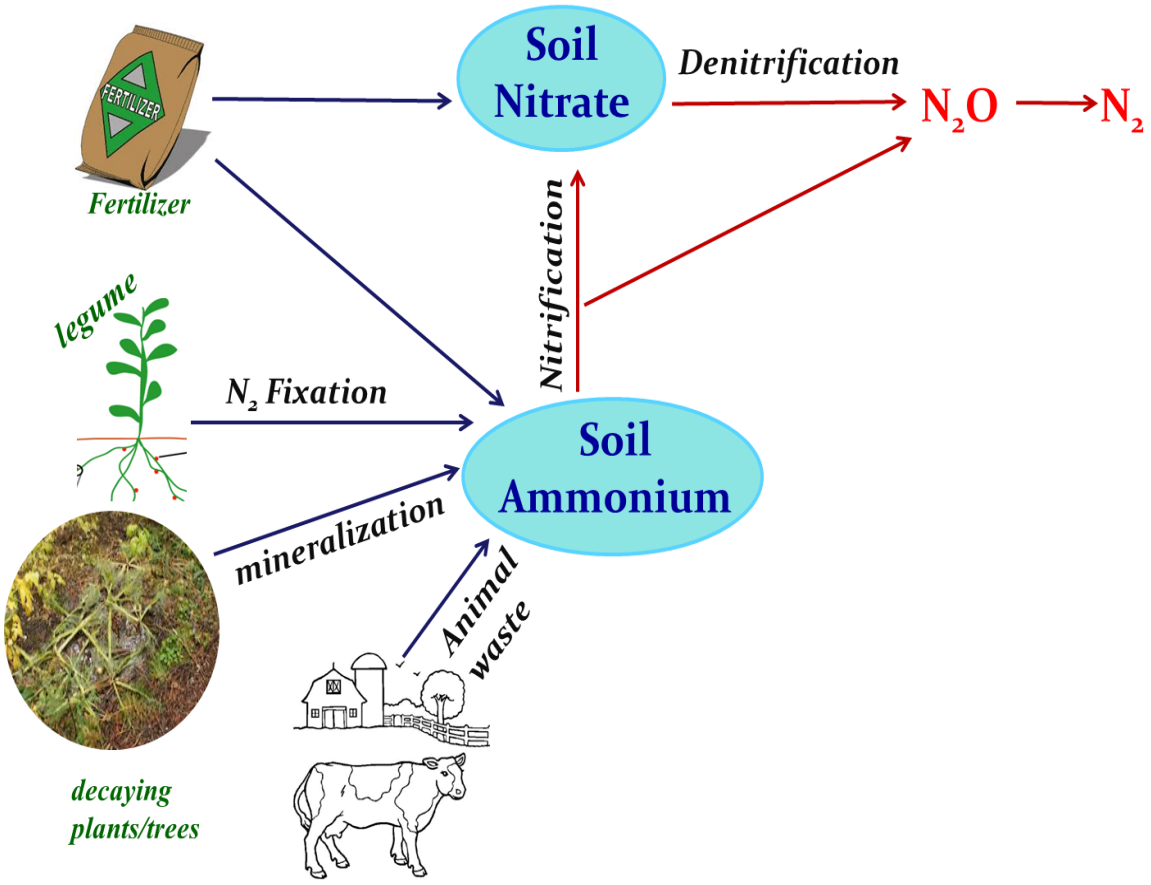

Figure 2.2. Important pathways associated with agricultural N_2O Emissions

In the United States, the agriculture sector accounts for the largest source of N_2O emissions (263.7 MMT CO_2 Eq. in 2013) of which agricultural soil management activities (e.g. fertilizer application, organic amendments, crop residues) make the highest contributions (US EPA, 2015). In the United States, for both direct and indirect emissions, crop lands account for the most N_2O emissions (~85% of the 263 MMT CO_2 Eq. in 2013) followed by grazing land (US EPA, 2015).

On a global scale, the majority of N_2O emissions come from agricultural soils (Del Grasso et al., 2005) and best management practices must be developed and implemented to minimize the environmental effects of biofuel production. In the U.S., agricultural soil management accounted for ~74% of total N_2O emissions in 2013 (U.S. EPA, 2015). Corn, a major food crop, is the current major crop for biofuel production. In the U.S., approximately 40% of the total annual corn production is being converted to bio-ethanol (Song et al, 2015). Growing energy demands in combination with its role as a widely used food and fuel crop enhance the competition between food and fuel from corn. A study by Foley et al (2005) on different land use regimes illustrated that intensively managed croplands were able to produce food in abundance but at the cost of several beneficial ecosystem services, including carbon sequestration, regional climate and air quality regulation, preserving habitats and biodiversity, water quality regulation etc.

As previously mentioned, the soil microbial communities in combination with other soil physical and chemical characteristics are responsible for N_2O emissions. The contributions of N_2O emissions from these factors have reasonably been addressed (Berthrong et al, 2014; Matson et al, 2002; Ramirez et al, 2010). Response to amount of N input is different across ecosystems. N-fertilizer as a substrate for soil microbial activities either through nitrification or denitrification contribute significantly to the soil N_2O (Smith et al., 2003). In N-limited temperate soils, addition of N enhances plant growth, at least initially; however, long term fertilization practices revealed enhanced emissions of N_2O (Ramirez et al, 2010) in the eastern United States. A study by Sehy et al in 2003 in a corn field showed that pulsed emissions of N_2O were observed following fertilization, rainfall, harvest, and tillage practices. Davidson in 1992 reported that N_2O emissions began within minutes in response to wetting of relatively dry soil. The cumulative flux of N_2O was about two times greater (8.7 kg N_2O-N ha^{-1}) in the high yield region (where relative abundance of water and nutrient supply was higher) compared to the low yield region (3.9 kg N_2O-N ha^{-1}) of the experimental site. The same study also demonstrated that, for low yield areas, lowering the fertilization rate from 150 to 120 kg N fertilizer ha^{-1} resulted in a 34% reduction of the quantity of N_2O released into the atmosphere. Zhou et al (2013) reported that N_2O fluxes for different fertilization rates (0 N, 150 kg N ha^{-1}, and 250 kg N ha^{-1}) applied to a wheat-corn rotation in the Sichuan basin in China resulted in the emission of 1.9 to 6.7 kg N ha^{-1} yr^{-1}. Mosier et al in 1991 showed that direct N input to the soil (through agricultural management practice) resulted in the net production of N_2O. A study by Sänger et al, 2011 revealed that irrespective of the differences in the rate

of fertilizer application, a 10 ^{0}C increase in soil temperature resulted in a slightly less than four-fold increase in the N_2O emission. The N-fertilization rates for switchgrass recommended by previous studies exhibit significant variability.

Soil N_2O emissions are therefore expected to vary as a function of the amount of N-fertilizer applied, time since fertilization, soil temperature, and soil volumetric water. For example, when fertilizer was placed closer to the plant roots at the early stages of plants, N_2O emission was low compared to different treatment methods applied. However, in this case the plant growth was not as enhanced as compared to the treatment in which fertilizer was premixed with the soil before planting (Council for Agricultural Science and Technology (CAST), 2004). The adoption of an optimized fertilization practice could potentially lead to a reduction in N_2O emission (Mosier and Kroeze, 2000) by 30-40% (CAST, 2004).

REFERENCES

Berthrong, S.T., Yeager, C.M., Gallegos-Graves, L., Steven, B., Eichorst, S.A., Jackson, R.B. and Kuske, C.R., 2014. Nitrogen Fertilization Has a Stronger Effect on Soil Nitrogen-Fixing Bacterial Communities than Elevated Atmospheric CO_2. *Applied and environmental microbiology*, *80*(10), pp.3103-3112.

CAST, 2004. Climate Change and Greenhouse Gas Mitigation: Challenges and Opportunities for Agriculture. *Council for Agricultural Science and Technology (CAST)*, Ames, Iowa, USA

Davidson, E. A. 1992. Sources of nitric oxide and nitrous oxide following wetting of dry soil. *Soil Science Society of America Journal*, *56*, 95–102.

Del Grosso, S.J., Mosier, A.R., Parton, W.J. and Ojima, D.S., 2005. DAYCENT model analysis of past and contemporary soil N_2O and net greenhouse gas flux for major crops in the USA. *Soil Tillage Res., 83*, 9–24.

Firestone, M.K. and Davidson, E.A., 1989. Microbiological basis of NO and N_2O production and consumption in soil. p. 7–21. Andreae, M.O and Schimel, D.S., (ed.) *Exchange of trace gases between terrestrial ecosystems and the atmosphere*. John Wiley & Sons, New York.

Foley, J.A., DeFries, R., Asner, G.P., Barford, C., Bonan, G., Carpenter, S.R., Chapin, F.S., Coe, M.T., Daily, G.C., Gibbs, H.K. and Helkowski, J.H., 2005. Global consequences of land use. *Science*, *309*(5734), pp.570-574.

Folorunso, O.A. and Rolston, D.E., 1984. Spatial variability of field-measured denitrification gas fluxes. *Soil Science Society of America Journal*, *48*(6), pp.1214-1219.

Hillel, D., 1998. Environmental Soil Physics, *Academic Press*, San Diego.

Lal, R., 2004a. Soil carbon sequestration impacts on global climate change and food security. S*cience, 304*(5677), pp.1623-1627.

Lal, R., 2004b. Soil carbon sequestration to mitigate climate change. *Geoderma*, *123*(1), pp.1-22.

Lauber, C.L., Ramirez, K.S., Aanderud, Z., Lennon, J. and Fierer, N., 2013. Temporal variability in soil microbial communities across land-use types. *The ISME journal*, *7*(8), pp.1641-1650.

Mathieu, O., Lévêque, J., Hénault, C., Milloux, M.J., Bizouard, F. and Andreux, F., 2006. Emissions and spatial variability of N_2O, N_2 and nitrous oxide mole fraction at the field

scale, revealed with 15N isotopic techniques. *Soil Biology and Biochemistry*, *38*(5), pp.941-951.

Matson, P., Lohse, K.A. and Hall, S.J., 2002. The globalization of nitrogen deposition: consequences for terrestrial ecosystems. *AMBIO: A Journal of the Human Environment*, *31*(2), pp.113-119.

Mosier, A. and Kroeze, C., 2000. Potential impact on the global atmospheric N_2O budget of the increased nitrogen input required to meet future global food demands. *Chemosphere-Global Change Science*, *2*(3), pp.465-473.

Mosier, A., Schimel, D., Valentine, D., Bronson, K. and Parton, W., 1991. Methane and nitrous oxide fluxes in native, fertilized and cultivated grasslands. *Nature*, *350*(6316), pp.330-332.

Ramirez, K.S., Lauber, C.L., Knight, R., Bradford, M.A. and Fierer, N., 2010. Consistent effects of nitrogen fertilization on soil bacterial communities in contrasting systems. *Ecology*, *91*(12), pp.3463-3470.

Rosswall, T., 1981. The biogeochemical nitrogen cycle. In *Some perspectives of the major biogeochemical cycles*, *17*, pp. 25-49). John Wiley & Sons.

Russow, R., Sich, I. and Neue, H-U., 2000. The formation of the trace gases NO and N_2O in soils by the coupled processes of nitrification and denitrification: Results of kinetic ^{15}N tracer investigations. *Chemosphere-Global Change Sci., 2,* pp.359–366.

Saetre, P. and Bååth, E., 2000. Spatial variation and patterns of soil microbial community structure in a mixed spruce–birch stand. *Soil Biology and Biochemistry*, *32*(7), pp.909-917.

Sänger, A., Geisseler, D. and Ludwig, B., 2011. Effects of moisture and temperature on greenhouse gas emissions and C and N leaching losses in soil treated with biogas slurry. *Biology and Fertility of Soils*, *47*(3), pp.249-259.

Schahczenski, J. and Hill, H., 2009. Agriculture, Climate Change and Carbon Sequestration. National Sustainable Agriculture Information Service (ATTRA). *National Center for Appropriate Technology (NCAT), and United States Department of Agriculture (USDA), Washington, DC*.

Schelde, K., Cellier, P., Bertolini, T., Dalgaard, T., Weidinger, T., Theobald, M.R. and Olesen, J.E., 2012. Spatial and temporal variability of nitrous oxide emissions in a mixed farming landscape of Denmark. *Biogeosciences*, *9*(8), pp.2989-3002.

Schlesinger, W.H., 1999. Carbon sequestration in soils. *Science, 284*(5423), pp.2095-2095.

Sehy, U., Ruser, R. and Munch, J.C., 2003. Nitrous oxide fluxes from maize fields: relationship to yield, site-specific fertilization, and soil conditions. *Agriculture, Ecosystems & Environment, 99*(1), pp.97-111.

Smith, J., Wagner-Riddle, C. and Dunfield, K., 2010. Season and management related changes in the diversity of nitrifying and denitrifying bacteria over winter and spring. *Applied Soil Ecology 44*(2), pp.138-146.

Smith, K. A., Ball, T., Conen, F., Dobbie, K. E., Massheder, J., and Rey, A., 2003. Exchange of greenhouse gases between soil and atmosphere: interactions of soil physical factors and biological processes, *European Journal of Soil Science, 54*, 779–791.

Smith, P., Martino, D., Cai, Z., Gwary, D., Janzen, H., Kumar, P., McCarl, B., Ogle, S., O'Mara, F., Rice, C. and Scholes, B., 2008. Greenhouse gas mitigation in agriculture. *Philosophical Transactions of the Royal Society B: Biological Sciences, 363*(1492), pp.789-813.

Song, Y., Jain, A.K., Landuyt, W., Kheshgi, H.S. and Khanna, M., 2015. Estimates of biomass yield for perennial bioenergy grasses in the USA. *BioEnergy Research*, *8*(2), pp.688-715.

University of Missouri. 2010. Agriculture and U.S. greenhouse gas emissions, http://extension.missouri.edu/explorepdf/agguides/agecon/g00310.pdf

U.S. EPA, 2015. Inventory of U.S. Greenhouse Gas Emissions and Sinks: 1990-2013. *U.S. Environmental Protection Agency*, Washington, D.C. www3.epa.gov/climatechange/Downloads/ghgemissions/USGHG-Inventory-2015-Main-Text.pdf

Ussiri, D. and Lal, R., 2013. Soil Emission of Nitrous Oxide and Its Mitigation. Springer, *Dordrecht*, 378 pp.

Warneck, P., 2000, Chemistry of the Natural Atmosphere, Academic Press, San Diego.

Zhou, M., Zhu, B., Butterbach-Bahl, K., Zheng, X., Wang, T. and Wang, Y., 2013. Nitrous oxide emissions and nitrate leaching from a rain-fed wheat-maize rotation in the Sichuan Basin, China. *Plant and soil*, *362*(1-2), pp.149-159.

Chapter 3

3. N_2O EMISSIONS FROM BIOFUEL CROPS

In North Carolina, switchgrass has the potential to become a favorable (smaller N to dry matter ratio) lignocellulosic bio-energy feedstock (Palmer et al, 2014a; McLaughlin and Kszos, 2005). Switchgrass seeds can germinate in a fairly wide range of soil acidity in warm soils. The pH range of 5 to 8 and soil temperature range of 25 – 35^0C were observed to be the optimum for germination (Hanson and Johnson, 2005). A study in the northern Great Plains showed a three-fold increase, from control (0 N ha^{-1} yr^{-1}) to 60 kg N ha^{-1} yr^{-1} treatment, in the N_2O emissions from switchgrass (Schmer et. al., 2012). Another study conducted in eastern Nebraska (Follet et. al., 2012) pointed out that there were significant improvements in the soil C credits associated with 60 kg N ha^{-1} yr^{-1} treatment compared to the control treatment (0 kg N ha^{-1} yr^{-1}). These improvements were observed in the 0-150 cm soil layer where > 50% C-sequestration occurred in layers deeper than 30 cm. In their study (Follet et. al., 2012), found that the greatest total biomass yield (11.4 Mg ha^{-1} yr^{-1}) for switchgrass was associated with 120 kg N ha^{-1} yr^{-1}. In our study we attempted to quantify the N_2O emissions, from corn and switchgrass, as a function of management practices and environmental variables. The inference drawn from our study warrants the urgent need for additional region specific studies to fill the large information gaps in the GHG emissions and biomass production from biofuel crops. Moreover, the huge spatial

and temporal variations in the GHG emissions associated with biofuel production additionally demands a well updated emission inventory and accurate life cycle assessment (LCA) of crops relevant to bio-energy production. The preparation of a regionally specific, accurate emission inventory therefore is crucial in the LCA studies attempting to fill the information gaps regarding the environmental impacts of crops (including but not limited to crop variety, regional adaptability, land use change, response to N-fertilization rate and other management practices) associated with biofuel production

There have been relatively few studies conducted in the southeastern United States to quantify the regional adaptability and the crop yield from switchgrass. McLaughlin and Kszos (2005) estimated a 25% reduction in the production cost of switchgrass through a 50% increase in the crop yield. This increase in switchgrass productivity in conventional agroecosystems was achieved through the selection of the best regionally adapted crop variety and through the adaptation of optimum management practices. Palmer et al, (2014b) studied the crop yield for two ecotypes (mountainous and coastal low land) for different N-fertilizer application rates and their study revealed no considerable variation in the biomass production. A study by Wullschleger et al, (2010) showed a biomass yield of 12.9 ± 5.9 Mg ha^{-1} for low lands. Modeling study by Ogle et al, (2008) suggested that about 2 – 2.5% of N-fertilizer added to the cropland may emit as N_2O. The IPCC 2006 (De Klein et al., 2006) guidelines suggest an emission factor of 1.0% for synthetic fertilizer application. Following this, Syakila and Kroeze, (2011) created a new emission inventory for global N_2O emissions by adding two new terms, a new ocean source term

and an uptake of N_2O at the earth's surface term, to the IPCC 2006 guidelines. This new inventory reported an emission factor of 0.9% for direct N_2O emissions associated with synthetic fertilizer application. Studies by Follet et al, (2012) and Hartman et al, (2011) suggested improved soil quality associated with switchgrass soils. A study conducted in Edinburgh, Scotland by Jones et al, 2011 found that the cumulative flux emitted from grasslands ranged between 0.03 to 2.89 kg N ha^{-1}. Studies by Monti et al, (2011) and Wile et al, (2014), found switchgrass was a modest crop in the context of biofuel production with relatively low GHG emissions. In a study by Wile et al, (2014) conducted in Nova Scotia, Canada, the cumulative N_2O flux remained significantly lower than the current direct emission factor of 1%. In a field scale study conducted in south-central Wisconsin, the N_2O emissions from switchgrass corresponding to an ammonium nitrate, $(NH_4)NO_3$ fertilizer applied plot (56 kg N ha^{-1}) were 3 times greater when compared to unfertilized plots (Duran et al, 2016). The same study also showed the N_2O emission factor for switchgrass as 2.4% in 2011 and 1.5% in 2012.

Table 3.1. Previous switchgrass studies addressing nitrogen fertilizer application for different regions of the US listed by state, the major parameters evaluated, and references for each study.

Study Objectives	Area	Reference
The roles of harvest periods and N- fertilization rates (0, 60, 120, 180, 240, and 300 kg N ha^{-1}) were investigated on the upland variety switchgrass. Biomass yields with 120 kg N ha^{-1} were identified as optimum (10.5 - 11.2 Mg ha^{-1} at NE; 11.6 - 12.6 Mg ha^{-1} at IA). Higher fertilization than this rate was associated with elevated inorganic N in the soil.	Iowa and Nebraska, U.S.	Vogel et al., 2002
Examined the production potential of upland (Cave-in-Rock and Shelter) and lowland (Alamo and Kanlow) varieties of switchgrass to identify the optimum variety for higher biomass production.	North Carolina, Tennessee, Virginia, West Virginia, and Kentucky U.S.	Fike et al., 2006
Crop yield and C-sequestration in corn and switchgrass as a function of N-fertilization and management practices	Nebraska, U.S.	Follet et al, 2012
Crop yield, methane and N_2O emissions from switchgrass and Reed Canarygrass as a function of N-fertilization (0, 40, and 120 kg N ha^{-1} yr^{-1})	Nova Scotia, Canada	Wile et al, 2014
The regional adaptability of switchgrass in North Carolina was examined among other perennial bio-energy grasses. Due to low nutrient removal and high crop yield, switchgrass was suggested as one of the more productive bio-energy crops suitable for North Carolina	North Carolina U.S.	Palmer et al, 2014a
N_2O emissions from switchgrass were examined as a function of fertilization (0 and 56 kg N ha^{-1} yr^{-1})	Wisconsin, U.S.	Duran et al, 2016
Crop yield, N_2O emissions were examined as a function of fertilization rates (0, 28, 56, 84, 112, 140, 168, and 196 kg N ha^{-1} yr^{-1})	Southwest Michigan	Ruan et al, 2016
N_2O emissions as a function of fertilization (0, 60, 120, and 180 kg N ha^{-1} yr^{-1}) rate, soil volumetric water, and soil temperature were examined for switchgrass and corn. The role of N-fertilization on soil inorganic N (NO_3^- and NH_4^+) was also investigated in both the crops for the 0 – 30 cm soil depth.	North Carolina, U.S.	Present study

These aforementioned studies emphasize the importance of variables such as the type of fertilizer, fertilizer application rate, timing of fertilization, irrigation amount and timing, crop type, and soil characteristics with respect to soil emissions of GHGs. Moreover, these studies reinstate the importance of the adoption of sustainable, but at the same time efficient and productive, agricultural practices specific to the region and the crop. A study by Edwards (2007) concluded that, despite its ability to grow in soils containing minimal nutrients, switchgrass showed increases in the variability among soil micro-organisms and subsequent microbial activity over time. Moreover, the deep fibrous root systems in switchgrass make it able to withstand soil conditions that are unfavorable for row crops. A recent 2-year field scale study (Duran et al, 2016) conducted in south-central Wisconsin showed switchgrass was associated with greater losses of N while having no productivity gain in response to fertilization. Model simulations by Ogle et al, 2008 showed the southeastern states in the US are associated with lowest soil N_2O emissions in connection with crop production. The same study also pointed out the need for additional studies to evaluate scenarios of lowest N_2O emissions in the context of GHG mitigation associated with biofuel production in the southeastern U.S. Ruan et al in 2016 emphasized that application of N-fertilizer at a rate greater than that needed by the crop may not bring the expected outcome of the usage of cellulosic biofuels as a greener alternative to fossil fuels or grain-based biofuels. Therefore, quantifying the optimal fertilizer application rate relevant to the crop and the region is of primary importance in achieving both economic and environmental benefits associated with the production of cellulosic biofuel.

The objectives of this study are to (i) quantify the soil N_2O emissions, as a function of three different N-fertilizer application rates, from a potential biofuel crop of high N-uptake capacity, switchgrass; (ii) at the same N-fertilizer application rates, compare with N_2O emission from the current major biofuel crop, corn; and (iii) analyze the complex interactive influences of nitrogen fertilization, soil moisture, and soil temperature on soil N_2O fluxes. The current study therefore attempts to establish an improved understanding on the adaptation of switchgrass as a potential biofuel crop in the southeastern US.

3.1. Methods and Materials

3.1.1. Study Site

This study was conducted at the BASF research farm in Holly Springs (35°36'29" N, 78°50'43" W), North Carolina. Switchgrass (*Panicum virgatum* L.) was Alamo variety established in December, 2008, seeded at a rate of 9.2 lbs per acre and planted on 16" row spacing. Alamo varieties are lowland ecotype switchgrass and are suitable to grow in warm and moist regions. The crop was cut annually and fertilized once in spring. Corn (*Zea mays*) was DeKalb C6805 variety planted at a density of 28,000 seeds per acre on 40" row spacing (in-row of 5.5"). Switchgrass and corn plots were maintained according to the standard protocols for production in North Carolina (Fike et al., 2006; Mitchell et. al., 2008).

Figure 3.1. Alamo variety switchgrass established in December, 2008.

Switchgrass treatments included three N fertilization rates, 60, 120, 180 kg N ha^{-1} yr^{-1}, and a control treatment receiving no N fertilization. 100% of fertilizer treatment was applied at one time at the beginning of each growing season. Corn treatments consisted of three N rates, 60, 120, and 180 kg N per ha^{-1} yr^{-1}, and did not include the control treatment as zero

N application is not a standard practice for corn. For corn, in years 2011 and 2013, 25% of the total nitrogen application was applied at planting and the remaining 75% was applied when the corn reached a height of approximately 30”. In 2012, 100% of the N treatment was applied at the time of planting. Fertilizer was granular ammonium sulfate, $(NH_4)_2SO_4$, and was broadcast applied by hand. Counter insecticide was applied at planting at 4.9 lbs per acre applied in a t-band.

A complete randomized block design consisting of four replicates of each N treatment level was established in each crop. The experiment was blocked in order to account for the slight north/south slope of the field. Individual experimental plots (replicates) were 6.7' x 15' (2 rows) within which four permanent soil collars were randomly located for flux measurements. There was an untreated row between each plot and a 5' alley at the end of each plot. Measurements were conducted from April, 2011 to September, 2013.

Figure 3.2. DeKalb C6805 variety corn planted on May 5, 2011. Rows are on a 16" spacing.

Soils at the site are Appling sandy loam (Fine, kaolinitic, thermic Typic Kanhapludults) consisting of 58% sand, 26% silt, and 16% clay in corn and 70% sand, 22% silt, and 8% clay in switchgrass in the upper 10 cm. Other soil chemical and physical characteristics, provide by the BASF research farm, are summarized in Table 3.2.

Table 3.2. Summary of soil physical and chemical properties (0 – 10 cm depth) for switchgrass and corn plots.

	Soil Texture						
Crop	**Sand**	**Silt**	**Clay**	**Organic content**	**pH**	**Cation Exchange Coefficient**	**Bulk density**
Switchgrass	70%	22%	8%	1.9%	6.1	4.5 meq/100	1.48 g cm^{-3}
Corn	58%	26%	16 %	1.1%	6.4	3.7 meq/100	1.48 g cm^{-3}

Additional measurements of soil extractable NO_3^- and NH_4^+ were conducted in 2011 and 2013 post-harvest. Triplicate soil samples were collected in each experimental plot and composited. Cores of 10 cm depth were collected from three layers 0-10 cm, 10-20 cm and 20-30 cm. Soils were extracted in 1 M KCl (1:5 soil/extract) and extracts were analyzed by colorimetry by the Analytical Service Laboratory at North Carolina State University, Department of Soil Science.

3.1.2. N_2O Chamber Sampling Procedures

3.1.2.1. Chamber Sampling

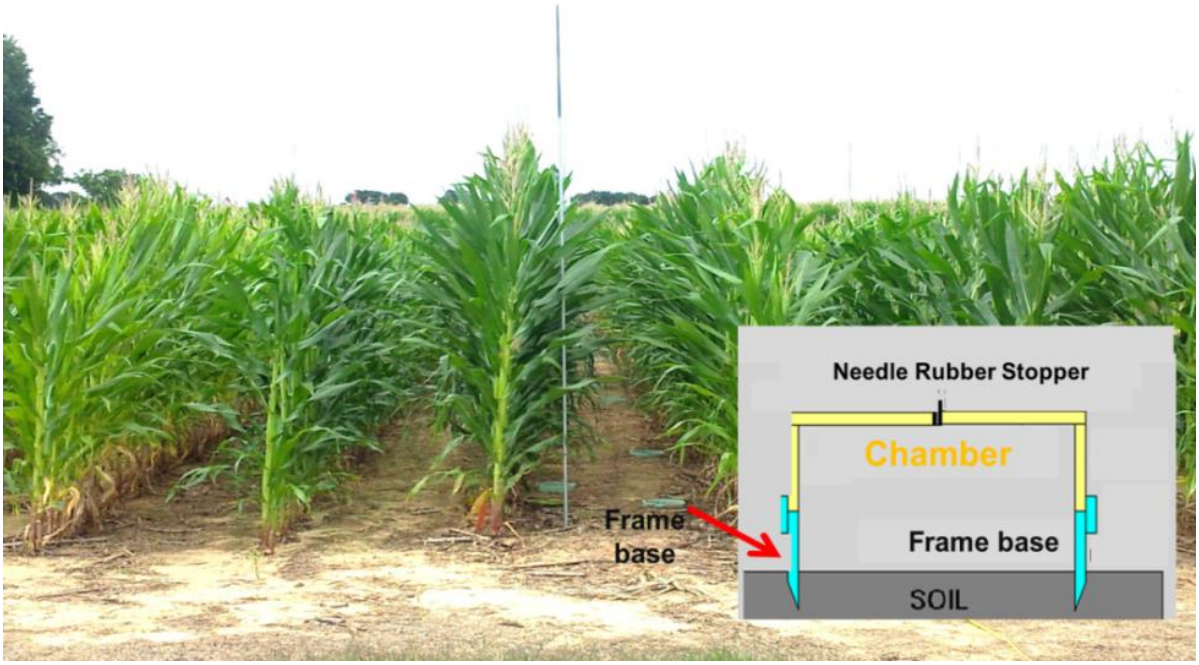

Figure 3.3. Experimental setup in a corn plot showing the permanently inserted PVC collars along with the schematic of the PVC end cap (chamber).

N_2O fluxes were measured using vented static chambers following the GRACENet protocol (Parkin et al., 2010, Livingston and Hutchinson, 1995). Four PVC collars (surface area ~314 cm^2; total volume ~3900 cm^3; V/A ratio = 12) were permanently inserted randomly in the soil in each switchgrass and corn plot. The PVC collars facilitated a gas tight seal with an overlying PVC end cap (~13 cm long with a beveled edge on one end) to create the chamber. The pressure vent dimensions on the end caps

followed the recommendations of Hutchinson and Mosier (1981) for wind speeds < 2 m sec^{-1} and ~4 L volume (vent tube length 7 cm; vent tube diameter 2 mm). The sampling port consisted of a Swagelok ¼ inch bulkhead fitting with 11 mm septa. Figure 3.3 shows the experimental setup at the corn plot. The PVC collars along with the schematic of the PVC end cap are also shown in Figure 3.3.

During N_2O sampling, the PVC chamber was inserted over the soil collar and 15 mL gas samples were drawn at 10, 20, and 30 minutes using a 60 ml polypropylene syringe (BD, Franklin Lakes, NJ) inserted into the chamber through a rubber septum. At each sampling interval, a total of 60 ml samples were collected by combining 15 mL samples drawn from each of the four rings within each plot. This approach yields a spatially integrated composite sample at each sampling interval. All plots within both crops were sampled on the same day at a frequency of twice per week following fertilization, for approximately three weeks, then weekly for the remainder of the growing season.

After collection from the soil chamber, syringe samples were stored for up to 48 hours (typically less than 24 hours) prior to analysis. To account for diffusive losses of N_2O from the syringe during storage, loss rates were developed for syringes filled with a range of standard concentrations (400 to 4000 ppb N_2O) and stored for a period of 72 hours. Field samples were corrected for storage losses based on time of storage and concentration in the syringe at time of analysis. This resulted in corrections of approximately 10 – 15% at storage times of 24 – 48 hours.

3.1.2.2. N_2O Sample Processing

Concentrations of N_2O in the chamber headspace are determined by gas chromatography (GC) /electron capture detection (ECD). The GC employs a backflush system controlled by a 10 port valve (Model 090-0025V; Vici Valco Instruments; Houston, TX) and is configured with a 6' Hayesep D precolumn (Supelco, Inc.; Bellafonte, PA) and 12' Poropak Q analytical column (Supelco, Inc.; Bellafonte, PA). The instrument is equipped with a 5 mCi ^{63}Ni electron capture detector (Model N-1001; SRI Instruments, Inc., Las Vegas, NV). The makeup gas was argon/10% methane (P10) (Airgas National Welders; Raleigh, NC). Air samples were analyzed by direct injection onto the sample loop.

Analytical accuracy was controlled by calibrating the GC with certified N_2O standards prepared by Scott Marrin, Inc., Riverside, CA and analyzed by the NOAA Earth Systems Laboratory. Prior to the analysis of each batch of samples, the GC was calibrated using the following standard mixtures:

Calibration 1: 10 mL of 999.8 ppb N_2O standard = 999.8 ppb N_2O
Calibration 2: 8 mL of 999.8 ppb N_2O standard + 2 mL of He = 799.9 ppb N_2O
Calibration 3: 6 mL of 999.8 ppb N_2O standard + 4 mL of He = 599.9 ppb N_2O
Calibration 4: 4 mL of 999.8 ppb N_2O standard + 6 mL of He = 399.9 ppb N_2O
Calibration 5: 3 mL of 999.8 ppb N_2O standard + 7 mL of He = 299.9 ppb N_2O

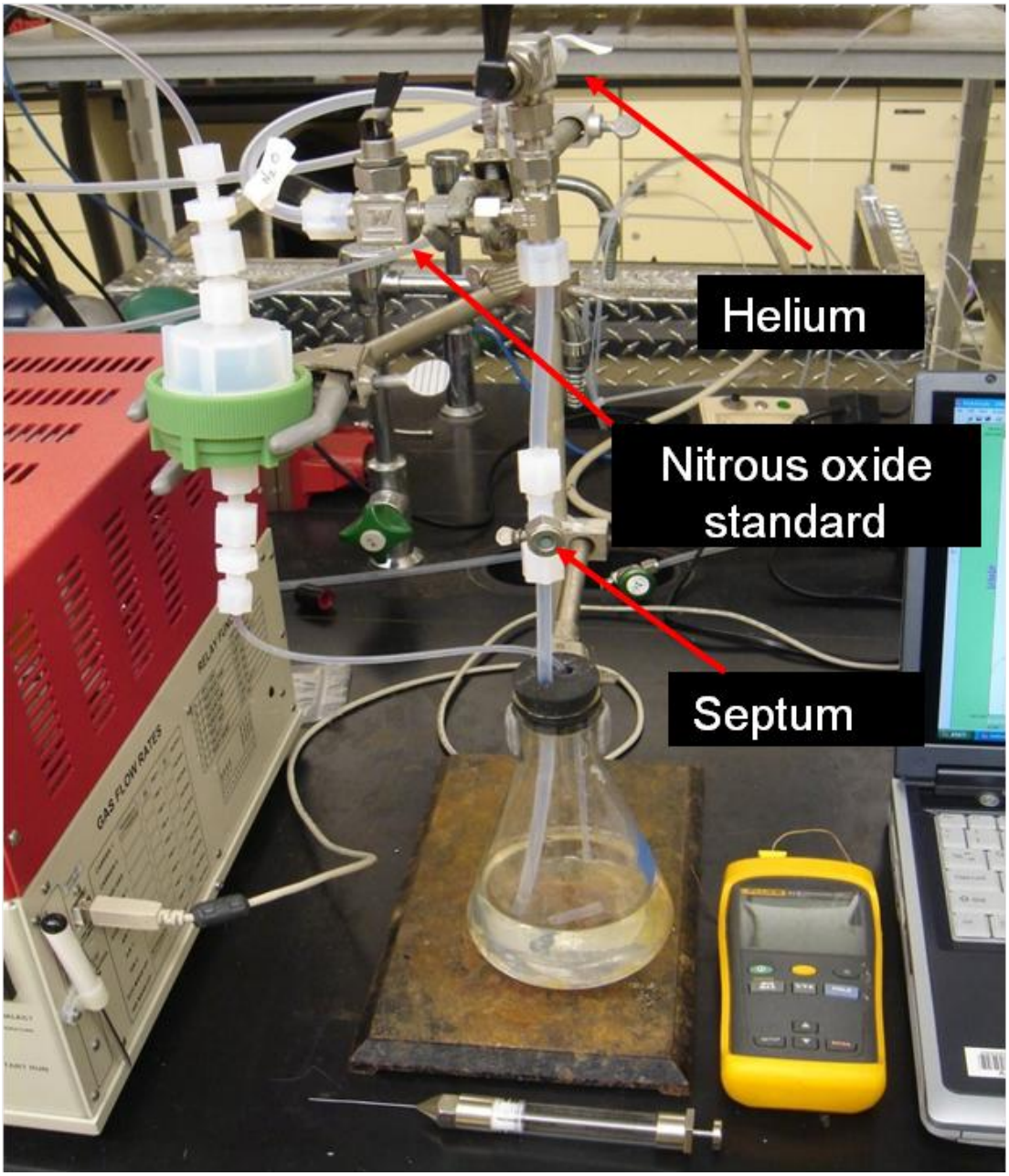

Figure 3.4. Gas bubbler used for generating calibration standards

Standards were introduced to the GC by direct injection from a 10 mL gastight syringe (Hamilton Company, Reno, NV). In some cases it was necessary to calibrate with a wider range of concentrations (up to 4000 ppb N_2O) to account for large N_2O concentrations experienced immediately following fertilization. All 10 mL are used to flush the loop, then the final 1 mL was retained in the loop for injection onto the analytical column. For dilutions, standard and diluent gases were drawn into the syringe, one at a time, at the corresponding volumes specified above. This method of gas dilution was compared to a TEI Model 146 mass flow controlled gas dilution system and the two methods agreed within 0.5%. The 999.8 ppb and the 333.53 ppb N_2O standards were prepared for by Scott Marrin, Inc. (Riverside, CA) and analyzed by the NOAA Earth System Research Laboratory (333.53 ppb N_2O, NOAA 2006 scale; 999.8 ppb N_2O, provisional scale). The reported accuracy of these standards is 0.2% and 1%, respectively. The peak areas for each of these standards along with their values in ppb were then entered into a calibration table provided in the PeakSimple software. The software generates a quadratic regression curve against which the N_2O concentrations in the samples were calculated.

Accuracy of the calibration curve was quantified as the standard error of the residuals of the curve expressed as a % according to:

$$\%\ RSE = 100\sqrt{\frac{\sum_{i=1}^{n}\left(\frac{y_{i(pred)}-y_{i(st)}}{y_{i(st)}}\right)^2}{n-p}} \qquad (3.1)$$

where $y_{i(pred)}$ and $y_{i(st)}$ are values of the response (ppb) and standard injected (ppb) of calibration point i, n is the number of non-zero calibration points, and p is the number of coefficients in the regression equation. If $\%\ RSE$ is > 10, the GC was recalibrated. If the second calibration did not meet this criterion, trouble shooting procedures were conducted to identify the cause of the poor calibration. The corrective actions taken against poor calibration included but were not limited to: testing for non-airtight syringes, confirmation of proper GC settings (carrier flow rate, column over temperature, detector temperature and gain), testing for instability in baseline resulting from drift in carrier flow rate, column over temperature, detector temperature and gain, improper 10 port valve operation. A quality check standard (333.53 ppb) was run immediately following calibration and after every 10^{th} sample. If duplicate analyses of the quality check standard were not within 10% of the calibration point, the instrument was recalibrated and all samples following the previous acceptable quality standard check were reanalyzed. Analytical precision was

quantified as the batch wise % relative standard deviation of the quality check standards. The sampling and analytical methods along with the data quality are shown in Table 3.3

3.1.2.3. N_2O Flux Calculation

Trace gas fluxes were measured using the static chamber approach (Livingston and Hutchinson, 1995) by which the emission flux of N_2O was calculated as a function of the rate of accumulation inside the chamber according to

$$F = (V/A)(\Delta C/\Delta t) \qquad (3.2)$$

where F is the emission rate (ng N m^{-2} s^{-1}), V is chamber volume (3900 cm^3), A is the soil surface area enclosed by the chamber (314 cm^2), and $\Delta C/\Delta t$ is the change in concentration per unit time within the chamber (ng N m^{-2} s^{-1}). After placement onto the soil collar, N_2O air samples were collected from the chamber at 10 minutes intervals over a period of 30 minutes. Change in concentration was calculated by fitting a linear regression model to C and t (Wagner et al., 1997)

$$C = a + bt \qquad (3.3)$$

where $\Delta C/\Delta t$ in equation (3.2) is equal to regression coefficient b in equation (3.3).

Closed chambers often suppress the soil/atmosphere concentration gradient, thereby resulting in an underestimation of the actual soil emission flux (Venterea, 2010). In order to overcome this limitation, the flux calculated from equations (3.2) and (3.3) were corrected by accounting for the effects of soil properties and chamber geometry on soil gas diffusion characteristics. The method of Venterea (2010) was used to quantify and correct for the theoretical flux underestimation (TFU), which consists of two terms, E_1 and E_2, described below.

The term E_1 (units of cm^6 gas cm^{-4} soil h^{-1}) takes into account the effects of soil and trace gas physical properties on chamber dynamics:

$$E_1 = [\phi + \theta\,(\beta K - 1)] D \phi^2 \left[1 - \frac{\theta}{\phi}\right]^{\left[2+\frac{3}{P_{dp}}\right]} \qquad (3.4)$$

where ϕ is total soil porosity (cm^3 pores cm^{-3} soil) determined from $(1 - \rho/\rho_p)$ where ρ and ρ_p are soil bulk density and particle density, respectively, θ is soil volumetric water (cm^3 H_2O cm^{-3} soil), β is a correction factor for pH that is set to 1 for N_2O, K (cm^3 gas cm^{-3} H_2O) is the trace gas Henry's Law gas-liquid partitioning coefficient, D (cm^2 gas h^{-1}) is the trace gas diffusivity in free air, and P_{dp} is the Campbell soil pore-size distribution parameter, which can be estimated from $P_{dp} = 13.6\,CF + 3.5$ where CF is the clay fraction of the soil (Rolston and Moldrup, 2002). Appropriate values of K and D and their

temperature dependencies are described by Venterea (2010) and references therein. The term E_2 in equation (3.5) accounts for the interaction between the variables in E_1, chamber geometry, and deployment time:

$$E_2 = ln\left[\frac{{H_c}^2}{E_1 T_d}\right] \qquad (3.5)$$

where H_c (cm^{-3} gas cm^2 soil) is the ratio of the chamber internal volume to surface area of the soil and T_d is the total chamber deployment time (h). The theoretical flux underestimation is then calculated as:

$$TFU = \frac{a+bE_2}{1+cE_2+d{E_2}^2} \qquad (3.6)$$

Note that the terms a, b, and c in equation (3.6) are different than the regression coefficients a, b, and c in equation (3.3). The actual "pre-deployment" flux (F_o), adjusted for chamber effects, is then calculated from equations (3.6) and (3.3) as:

$$F_o = \frac{F}{1-TFU/100} \qquad (3.7)$$

Flux detection limit was assessed following Parkin et al. (2012). Based on replicate measurements of ambient air, the analytical precision of the GC/ECD was 0.9%.

Assuming three measurements taken over 30 minutes to calculate fluxes using linear regression, this translated to a flux detection limit of ± 0.49 ng N m^{-2} s^{-1}.

3.1.3. Soil Moisture and Temperature

As discussed previously, the soil emissions of N_2O depended on soil microbial activities which are a function of soil temperature and soil volumetric water. It is important to understand the N_2O emissions as a function of soil temperature and soil moisture from both corn and switch grass. Thus soil temperature and soil water content were measured adjacent to each flux ring at the time of the flux measurement. Soil temperature (0 – 10 cm) was measured using an Oakton Acorn Temp6 RTD Thermometer and probe (WD-08117-20, Oakton Instruments, Vernon Hills, IL) and soil volumetric water (0 – 12 cm) was measured using the soil water content probe (CS658, Campbell Scientific, Logan, UT). Hourly rainfall was measured using a tipping bucket rain gauge and CR10X datalogger (Campbell Scientific, Logan UT).

Accuracy of the soil volumetric water sensor was assessed by comparison to soil moisture determined gravimetrically by weight loss after heating 25 g of soil for 24 hours at 105 °C. Once per weekly sampling event, the volumetric water probe was inserted into the soil and a 0-12 cm coil core was extracted at 10 – 15 cm horizontal distance to the north, south, east, and west of the probe. These 4 samples were composited and analyzed gravimetrically for water content. Using this approach, a working calibration curve for the

volumetric water sensor was developed over time and accuracy was assessed at the end of each 6 month interval. Precision was assessed every 6 months by repeated sampling (N = 10 measurements) of a homogenized soil sample.

Table 3.3. Sampling and analytical methods along with data quality objectives

Measurement	Sampling Method	Analytical Method	Quantity	Time Scale	Precision Goal	Accuracy Goal
Nitrous oxide/air	Syringe/ glass vial	GC/ECD	15 mL	Grab sample	±5% @ 333 ppb	±10%
Soil temperature	In-situ probe		-	Instantaneous	±0.1°C (-300 to 300°C)	±0.25%
Soil volumetric water	In-situ probe		-	Instantaneous	±1%	±3%

3.1.4. Crop Yields

Switchgrass yields were determined by cutting a swath 1.36 m wide across each experimental plot (width = 204 cm, cut area = 2.78 m^2). Cutting height was approximately 10 cm. Cut biomass was weighed onsite and a subsample was dried for 72 hours at 60 °C and reweighed to determine moisture content. Yields are expressed as Mg dry biomass per hectare (Mg ha^{-1}). Corn yields and kernel moisture content were determined by combine. Yields are expressed in bushels per acre standardized to 15.5% moisture (bu ac^{-1}).

3.1.4. Statistical Analysis

The experiment was designed as randomized complete blocks. Corn and switchgrass plots were blocked four groups each to account for the slope of the field. Effects of fertilizer treatment and blocks on N_2O emissions from crops were examined by performing a 2-way Analysis of Variance (ANOVA) model using matlab statistical software. The ANOVA models were run for each year for three fertilization rates for corn and for three fertilizations plus the control treatment for switchgrass. In accordance with the hypothesis of normal distribution and equal variance in ANOVA models, N_2O fluxes were transformed to their natural logarithms. The annual and entire-study-period statistics of N_2O fluxes were calculated as a function of fertilizations and crops. In order to identify the correlations between N_2O emissions and soil volumetric water, soil temperature, and fertilizer application rates, linear regression analyses were also performed.

3.2. Results and discussions

3.2.1. Environmental Soil Parameters

Within each crop, there were no significant differences in soil temperatures observed between years. However, a difference in the average soil temperature was observed between the two crop types. For switchgrass plots, the average annual soil temperature for 2011, 2012, and 2013 was 24.27 ± 1.03 ^{o}C, 21.96 ± 0.72 ^{o}C, and 21.96 ± 2.45 ^{o}C, respectively. For corn, these values were 27.74 ± 0.4 ^{o}C, 25.53 ± 0.51 ^{o}C, and 25.93 ± 0.42 ^{o}C. The year 2013 received higher rainfall as compared to 2011, and 2012. The annual rainfall received in Holly Springs in inches was 27.97 (2011), 39.20 (2012), and 42.57 (2013). Percentage of total rainfall received between June and August was ~ 33%, 24%, and 53% in 2011, 2012, and 2013, respectively. Corn plots were irrigated three times in 2011 and 2012. Switchgrass plots were irrigated three times in 2011 and once in 2012. The average soil volumetric water for switchgrass for 2011, 2012, and 2013 was 11.79 ± 1.23%, 14.91 ± 0.63%, 18.09 ± 0.64%, respectively, during the growing season. For corn, corresponding average soil volumetric water was 8.39 ± 1.8 %, 12.08 ± 1.13 %, and 12.59 ± 0.62 %. Although the environmental parameters showed variation with respect to crop type and study period, there were no significant variations in soil volumetric water or temperature among treatments within crops.

3.2.2 N_2O Flux

Planting, fertilization, irrigation and harvest dates are summarized in Table 3.4. Note that for corn, 100% of fertilizer was applied at time of planting in 2012, as opposed to 25% in other years.

Table 3.4. Summary of planting, fertilization, irrigation, and harvest dates for switchgrass and corn plots.

Crop	Irrigated on (depth eq. to rainfall in cm)			Planted on	Harvested on	Fertilized on
Switchgrass						
2011	6/17 (2.54)	6/21 (2.54)	7/21 (1.91)	18/12/08	10/17/11	05/06 (100%)
2012	-	6/21 (2.54)	-	18/12/08	11/14/12	04/23 (100%)
2013	-	-	-	18/12/08	11/04/13	05/20 (100%)
Corn						
2011	6/17 (2.54)	6/21 (2.54)	7/21 (1.91)	5/06/11	9/15/11	5/6 (25%); 6/22 (75%)
2012	4/09 (1.91)	6/21 (2.54)	7/05 (3.08)	4/04/12	9/14/12	4/23/12 (100%)
2013	-	-	-	4/10/13	9/05/13	5/20 (25%); 6/11(75%)

The overall statistics of the flux detection limit are summarized in Table 3.5. In total, 71% of the switchgrass and 92% of corn N_2O flux observations were larger than the flux detection limit (± 0.49 ng N m^{-2} s^{-1}). The lower percentage observed for switchgrass is in agreement with the lower N_2O flux from switchgrass. In general, for both the crops, the percentage of data greater than the detection limit increased with increasing rate of fertilization.

Table 3.5. Percentage of fluxes greater than the N_2O flux detection limit (± 0.49 ng N m^{-2} s^{-1}).

Switchgrass	Fertilization kg N ha^{-1}	# of data within the detection limit	Total # of observations	% data > detection limit
2011	0	27	90	70.97%
	60	42	90	53.33%
	120	31	89	65.17%
	180	30	94	68.09%
2012	0	36	130	72.31%
	60	52	130	60.00%
	120	34	129	73.64%
	180	18	130	86.15%
2013	0	30	79	62.03%
	60	22	79	72.15%
	120	17	79	78.48%
	180	11	79	86.08%
Switchgrass (All data)		**350**	**1198**	**71%**
Corn				
2011	60	26	90	71.11%
	120	12	90	86.67%
	180	7	90	92.22%
2012	60	6	103	94.17%
	120	1	103	99.03%
	180	8	104	92.31%
2013	60	3	97	96.91%
	120	1	97	98.97%
	180	0	97	100%
Corn (All data)		**64**	**869**	**93%**

Flux statistics are summarized by crop, treatment and year in Table 3.6. The average N_2O fluxes for switchgrass during fertilization to harvest (growing season) ranged between 0.6 ± 0.89 ng N m^{-2} s^{-1} (2013 control treatment) and 26.1 ± 60.3 ng N m^{-2} s^{-1} (2013, 180 kg N ha^{-1} yr^{-1}). For corn, the lowest N_2O flux observed is 2.93 ± 3.57 ng N m^{-2} s^{-1} (2011, 60 kg N ha^{-1} yr^{-1}) and the highest average flux observed is 114.2 ± 152.7 ng N m^{-2} s^{-1} (2013, 180 kg N ha^{-1} yr^{-1}). When averaged from fertilization to harvest, in both corn and switchgrass, the maximum of the average N_2O emission was associated with highest (180 kg N ha^{-1} yr^{-1}) N-treatment and minimum of the average N_2O emission was associated with lowest (i.e., control treatment for switchgrass and 60 kg N ha^{-1} yr^{-1} for corn) N-treatment. The strongest relationship between N application rate and N_2O emission was observed in 2013, while in other years the relationships is less clear. Averaged over the entire study (Figure 3.5), fluxes increase with N application rates in both switchgrass and corn. Furthermore, average fluxes from switchgrass are significantly lower than fluxes from corn at all treatment levels.

Table 3.6. The average, minimum, mean, median, maximum, and cumulative N_2O emissions for corn and switchgrass along with their direct emission factors (EF) are shown as a function of fertilization rate for each year. The statistics are computed based on N_2O fluxes measured from fertilization to harvest (± 1 standard deviation is indicated).

Switchgrass	kg N ha^{-1} yr^{-1}	N_2O Flux (ng N m^{-2} s^{-1})				Cumulative Flux	EF
		Min	Max	Average	Median	Kg N ha^{-1}	(%)
2011	0	-	5.48	0.99 ± 0.77	0.77	0.167	-
	60	-	50.47	4.93 ± 14.35	0.24	0.255	0.43
	120	-	28.27	2.35 ± 6.63	0.46	0.897	0.75
	180	-	93.19	6.24 ± 20.20	0.57	1.784	0.99
2012	0	-	35.33	1.66 ± 3.09	1.03	0.29	-
	60	-	33.15	1.07 ± 2.95	0.21	0.02	0.03
	120	-	46.45	1.80 ± 4.03	0.50	0.06	0.05
	180	-	55.40	3.10 ± 5.37	0.97	0.38	0.21
2013	0	-	13.83	0.60 ± 0.89	0.54	0.31	-
	60	-	38.28	3.74 ± 6.78	1.41	0.57	0.95
	120	-	238.8	11.59 ± 23.73	1.75	1.30	1.08
	180	-	536.2	26.10 ± 60.28	8.82	3.14	1.74
Corn							
2011	60	-0.64	23.41	2.93 ± 3.57	1.55	0.425	0.71
	120	-1.0	30.45	3.93 ± 4.13	2.44	0.701	0.59
	180	0.21	45.54	8.24 ± 6.08	7.88	0.935	0.52
2012	60	-3.65	212.58	17.83 ± 29.2	3.85	2.33	3.88
	120	-0.80	134.84	14.33 ± 16.65	6.85	2.60	2.16
	180	-0.79	285.88	18.02 ± 27.58	5.71	2.79	1.55
2013	60	-2.54	314.89	28.11 ± 43.21	11.81	2.20	3.67
	120	0.44	461.40	63.4 ± 92.43	18.521	4.81	4.01
	180	4.39	1194.47	114 ± 152.74	48.088	9.25	5.13

ANOVA indicated that corn and switchgrass N_2O emissions showed different responses to the effects of block and fertilizer application rates. In the first year of measurements, in corn, the individual main effects of blocks were significant (Table 3.7). During the rest of the measurement periods, ANOVA indicated no significant effect of blocks on corn N_2O emissions (Tables 3.9 and 3.11). In 2011, switchgrass showed no significant effect of blocks on soil N_2O emissions (Table 3.8). However, during the rest of the measurement period the individual main effect of the slope of switchgrass plots becomes significant. In switchgrass, throughout the measurement period, ANOVA indicated a significant effect of fertilizer application rate on soil N_2O emissions (Tables 3.8, 3.10, and 3.12). In corn, except in 2012 (Table 3.9), there was also statistically significant effect of fertilizer application rates on N_2O emissions. Linear regression analysis indicated that corn was the only crop and 2012 was the only year when there was significant correlation observed between N_2O emissions and soil temperature.

Table 3.7. ANOVA Table for N_2O emissions from corn in 2011

Source of variation	***SS***	***df***	***MS***	***F***	***Prob> F***
Fertilization	9.66	2	4.83	18.82	<0.0001
Block	3.19	3	1.06	4.14	0.0069
Error	63.14	246	0.26	-	-
Total	75.99	251	-	-	-

Table 3.8. ANOVA Table for N_2O emissions from switchgrass in 2011

Source of variation	***SS***	***df***	***MS***	***F***	***Prob> F***
Fertilization	3.55	3	1.18	3.19	0.0239
Block	0.23	3	0.08	0.21	0.8895
Error	123.99	334	0.37	-	-
Total	127.77	340	-	-	-

Table 3.9. ANOVA Table for N_2O emissions from corn in 2012

Source of variation	***SS***	***df***	***MS***	***F***	***Prob> F***
Fertilization	2.49	2	1.25	1.24	0.291
Block	7.07	3	2.36	2.35	0.0727
Error	280.63	280	1	-	-
Total	290.19	285	-	-	-

Table 3.10. ANOVA Table for N_2O emissions from switchgrass in 2012

Source of variation	***SS***	***df***	***MS***	***F***	***Prob> F***
Fertilization	5.48	3	1.83	9.28	<0.0001
Block	5.91	3	1.97	10.01	<0.0001
Error	101.39	515	0.20	-	-
Total	112.78	521	-	-	-

Table 3.11. ANOVA Table for N_2O emissions from corn in 2013

Source of variation	***SS***	***df***	***MS***	***F***	***Prob> F***
Fertilization	59.01	2	29.51	22.26	<0.0001
Block	4.07	3	1.36	1.02	0.3842
Error	355.24	268	1.33	-	-
Total	418.32	273	-	-	-

Table. 3.12. ANOVA Table for N_2O emissions from SG in 2013

Source of variation	***SS***	***df***	***MS***	***F***	***Prob> F***
Fertilization	34.35	3	11.45	19.98	<0.0001
Block	8.71	3	2.90	5.07	0.0020
Error	165.03	288	0.57	-	-
Total	208.09	294	-	-	-

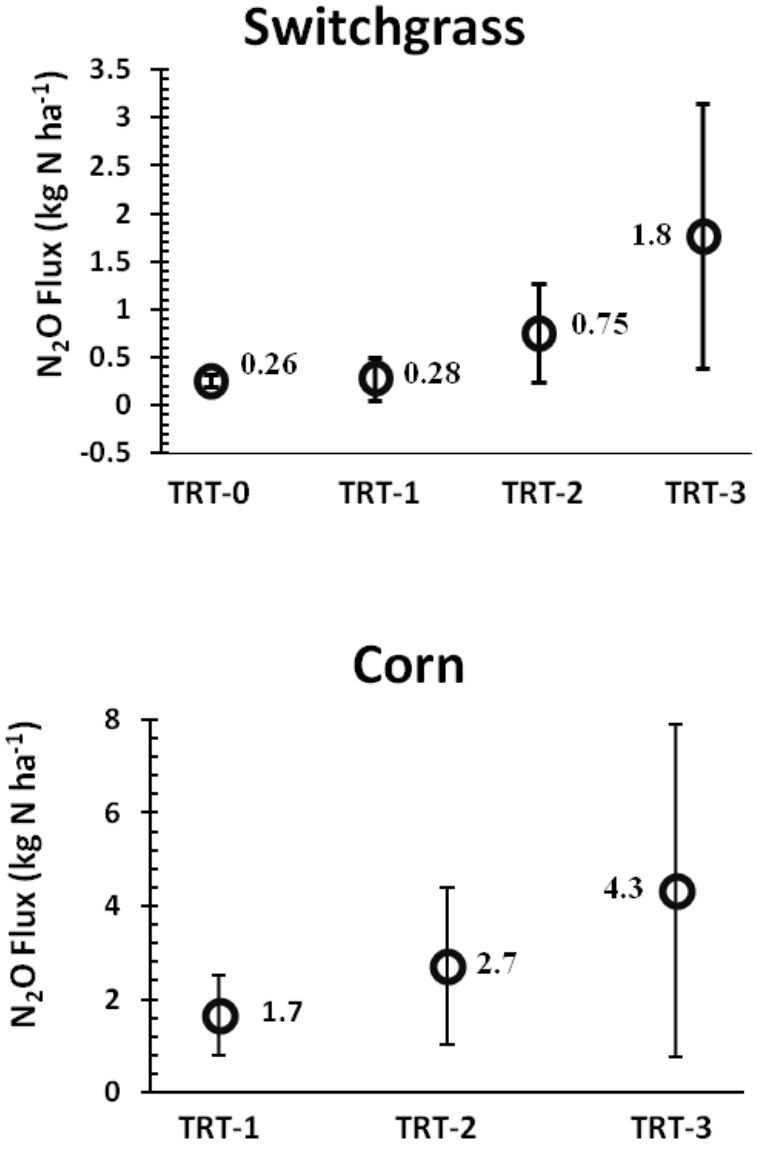

Figure 3.5. Cumulative N_2O flux during fertilization to harvest averaged over the entire study (2011 – 2013), along with the standard error, as a function of fertilization treatment level (TRT-0 = 0 kg N ha^{-1}, TRT-1 = 60 kg N ha^{-1}, TRT-2 = 120 kg N ha^{-1}, TRT-3 = 180 kg N ha^{-1}).

3.2.3. Cumulative N_2O Emissions

Cumulative N_2O emissions were estimated for both corn and switchgrass as a function of fertilization rate. The sampling frequency was twice per week following fertilization, for a period of approximately three weeks, then weekly. Therefore, to fill data gaps, it was assumed that the observed flux represent the daily mean fluxes. Linear interpolation was then performed to fill the data gaps. Cumulative flux was then calculated as the sum of daily mean N_2O fluxes for all the days from fertilization to harvest. The direct emission factor (EF) of N_2O-N was estimated, for corn and switchgrass, as the ratio of the cumulative flux to the total N-fertilizer applied, expressed as a percentage. For switchgrass, the cumulative flux of N_2O generally increased with increasing fertilization: the lowest flux (0.02 kg N_2O-N ha^{-1}) was observed for TRT-1 (60 kg N ha^{-1}) in 2012 and the highest flux (3.14 kg N_2O-N ha^{-1}) observed for treatment-3 in 2013 (Table 3.6). However, there is large variability across years and within years among treatments. In corn, the patterns of cumulative flux versus N application were more consistent, with the lowest flux (0.42 kg N_2O-N ha^{-1}) observed for TRT-1 in 2011 and the highest flux (9.25 kg N_2O-N ha^{-1}) observed for TRT-3 in 2013 (Table 3.6). Moreover, in corn, the cumulative flux of N_2O increased over the years from 2011 to 2013 for all treatments. The reason for this increasing trend is not clear but may reflect a combination of meteorological and soil conditions or perhaps adaptation of the soil to our study conditions. Averaged over the entire study, cumulative emissions from switchgrass ranged from as low as 0.26 kg N ha^{-1} in the 0 N control plots to 1.77 kg N ha^{-1} in the 180 kg N ha^{-}

^{1} treatment (Figure 3.5). In comparison, cumulative emissions from corn, averaged over the entire study (Figure 3.5), ranged from as low as 1.65 kg N ha^{-1} in the 60 Kg N ha^{-1} treatment to 4.33 kg N ha^{-1} in the 180 kg N ha^{-1} treatment.

Table 3. 13. The cumulative N_2O flux for corn and switchgrass are shown as function of fertilization rate averaged over the entire measurement period during fertilization to harvest. The corresponding emission factor (EF, %) is also shown.

Crop	Fertilization kg N ha^{-1} yr^{-1}	N2O Cumulative flux Kg N ha^{-1}	Direct EF %
Switchgrass	0	0.26 ± 0.06	-
	60	0.28 ± 0.23	0.47 ± 0.38
	120	0.46 ± 0.59	0.63 ± 0.43
	180	1.77 ± 1.13	0.98 ± 0.63
Corn			
	60	1.65 ± 0.87	2.75 ± 1.45
	120	2.70 ± 1.68	2.25 ± 1.4
	180	4.33 ± 3.56	2.40 ± 1.98

In switchgrass, the EF is dependent on the rate of fertilizer application during all years. The cumulative flux and corresponding EF are shown in Table 3.13 as function fertilization for corn and switchgrass. Averaged over the study, the switchgrass EF ranges from 0.47% in the 60 Kg N ha^{-1} TRT-1 to 0.98% in the 180 kg N ha^{-1} TRT-3. Ruan et al, (2016), based on a three years study, reported that the EF for upland Cave-in-Rock variety switchgrass increased from 0.6% to 2.1% as a response to 28 kg ha^{-1} to 198 kg ha^{-1} of N-added. Their study revealed that the IPPC 2006 constant emission factor (DeKlein et al., 2006) is underestimated in switchgrass by about 30% for 28 kg ha^{-1} and 107% for 198 kg ha^{-1} N fertilization. On the other hand, for corn, such linear dependency was observed

only in 2013. For corn, EF shows an increasing trend over time in which, for all the treatment types, the highest emission factor was observed in latest year, i.e., 2013, of the experiment. In corn, the EF exceeded the IPCC suggested 1% direct emission factor (DeKlein et al., 2006) in 2012 and 2013. The study wide average EF for corn was 2.47± 1.1 %, which is larger than the IPCC suggested factor but within the range of uncertainty of the IPCC value (0.3 – 3%) and typical values observed for corn in the U.S. (Griffis et al., 2013 and references therein).

3.2.4. Temporal Variability of N_2O Emissions

Time series of N_2O emissions from switchgrass and corn are shown in Figures 3.6 and 3.7, respectively. Results from our work are consistent with previous studies in which large pulses of N_2O are observed immediately following fertilization ((Bouwman et al. (2002); Mosier et al. (2000); Ramirez et al. (2010)) particularly in combination with rainfall. For example, the soil volumetric water measured in the switchgrass plots on 5/9/11 was approximately 15%, increasing to 20 % on 5/16/2011 following 0.01 inches of rainfall the previous day. The highest pulsed N_2O emission from switchgrass was observed following this rainfall event. Davidson in 1992 showed that the wetting of dry soil resulted in significant N_2O emissions. Based on a study conducted in potatoes, the highest N_2O emissions during the growing season were associated with post-fertilization heavy rainfall events (Burton et al in 2008).

Wetting of dry soils were associated particularly with stimulation of nitrification driven N_2O emissions. However, prolonged soil saturation limits oxygen leading to anaerobic (denitrification) production of N_2O (Sprent, 1987; Dobbie and Smith, 2001). Past studies investigating the relationship between N_2O fluxes and soil moisture therefore exhibited strong variability. For example, a study by Pinto et al, (2002) showed no significant role of soil moisture on the soil emissions of N_2O. In 2012, for switchgrass, another short lived N_2O pulse emission was observed post-fertilization. From 5/3/2012 to 5/7/2012, increases in both soil temperature (23^0C to 26.7^0C) and soil volumetric water (~9.5% to 14%) were associated with an N_2O emission pulse in which the flux increased from 4.2 ng N m^{-2} s^{-1} to 55.3 ng N m^{-2} s^{-1}. The soil volumetric water continued to increase throughout 05/2012 and was associated with large N_2O net fluxes. Similar patterns were observed in the corn plots. In 2011, the pulsed emissions following fertilization were observed with higher than average soil volumetric water (~14%). The study site received ~8" of rainfall in the first two weeks of June, 2013. This increase in soil water content in combination with the application of the remaining 75% of the fertilization, amplified post-fertilization emissions from corn.

Post-harvest emissions also differed between crops. Normally, following the corn harvest, for all fertilizer treatments, the N_2O emissions began to decline. However, for switchgrass, even though the N_2O net flux was significantly low for all the treatments, these patterns of post-harvest decrease were not observed.

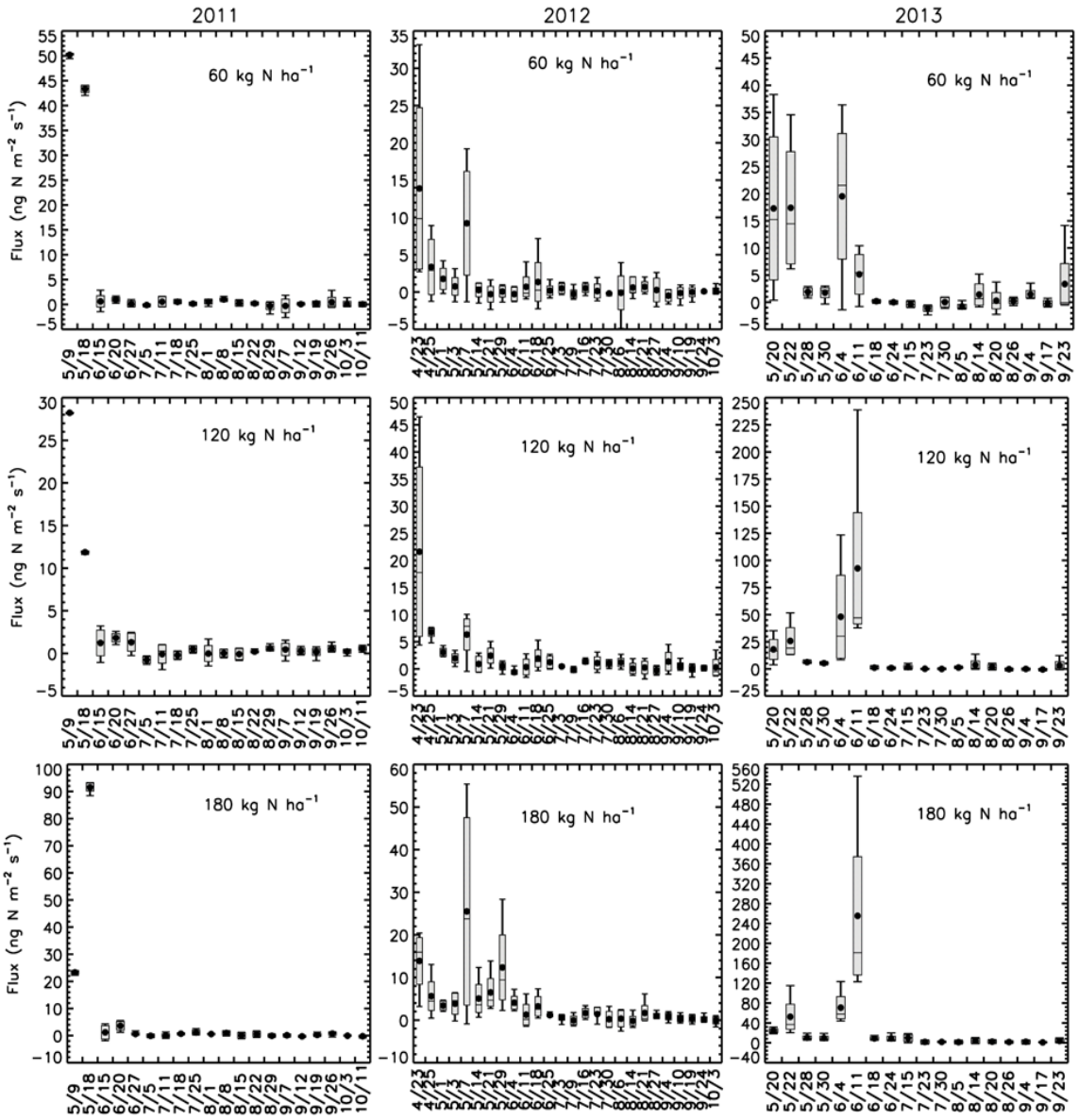

Figure 3.6. Soil N_2O emissions from switchgrass for selected fertilization rates (60, 120, and 180 kg N ha^{-1} yr^{-1}) from 2011 to 2013.

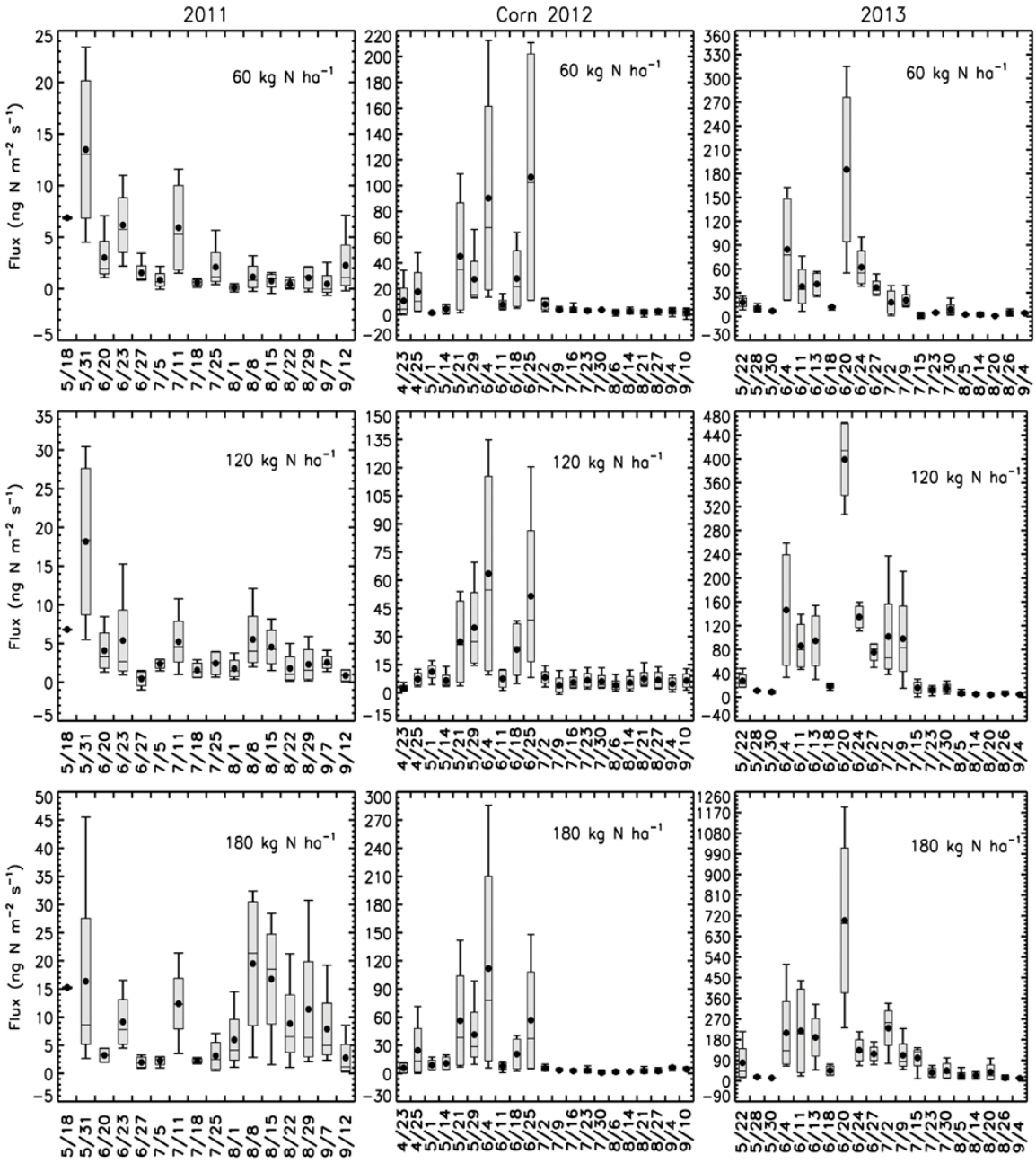

Figure 3.7. Soil N_2O emissions from corn are shown for selected fertilization rates (60, 120, and 180 kg N ha^{-1} yr^{-1}) from 2011 to 2013.

As described above, studies show that soil moisture regulates the oxygen availability to soil microbes and thus acts as a major driving force on N_2O emission. Relationships between soil volumetric water and N_2O fluxes are shown in Figures 3.8 & 3.9. Irrespective of crop type and fertilization rate, a positive correlation between N_2O flux and soil moisture was observed. During May to mid-August, when the soil volumetric water was low (< 15%), N_2O flux and soil moisture showed a strong correlation, especially at higher fertilization rates, indicating a more pronounced effect of soil moisture on N_2O emissions under relatively drier soil conditions. This pattern was observed for all cases of fertilization in both crop types (Figures 3.6 & 3.7). However, when the soil volumetric water was generally high (mid-August to December), an impact of wetting the soil on the N_2O flux was not observed except TRT-2 and TRT-3 for corn in 2011. Though positive correlations between N_2O emissions and soil volumetric water were observed (Figures 3.8 & 3.9), the expected pattern of increasing emissions with soil temperature was not observed. This may have been due to the confounding effects of fertilization and soil water content.

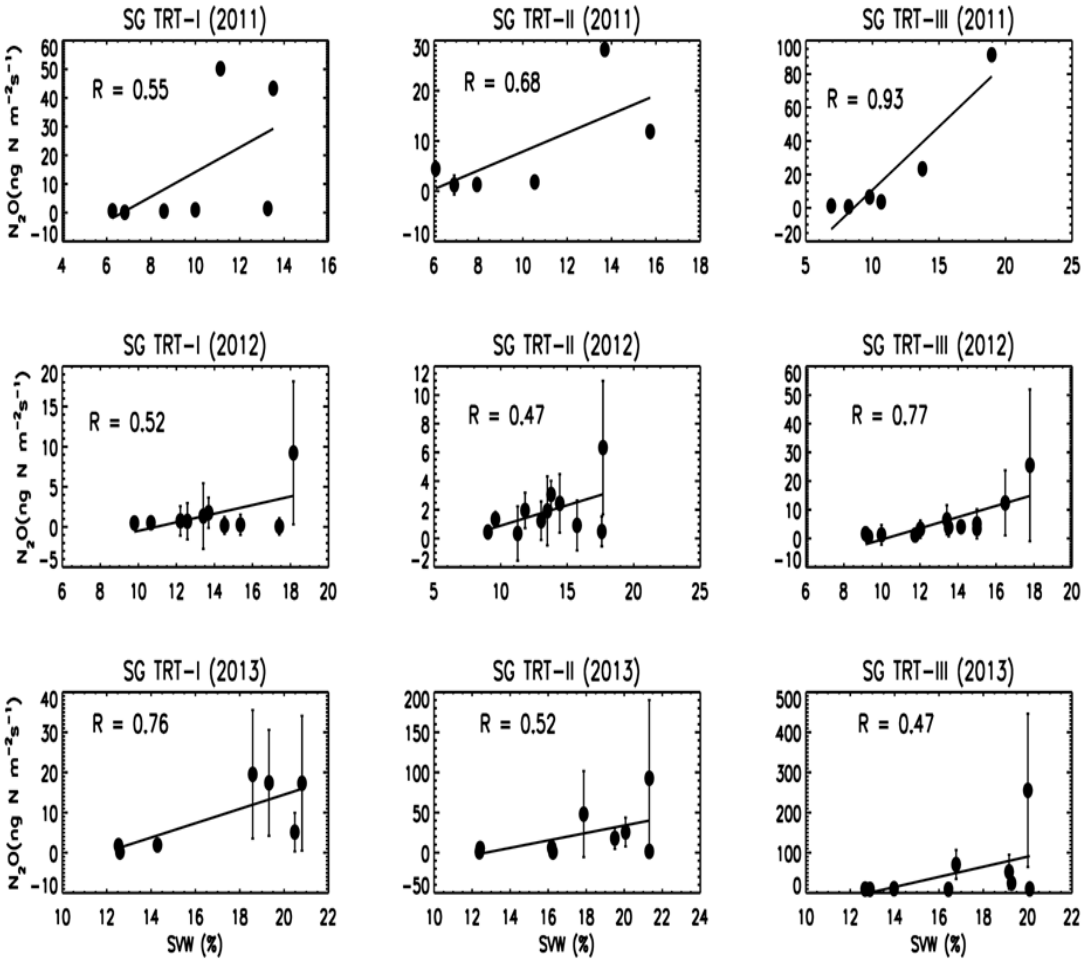

Figure 3.8. The correlation between N_2O fluxes and soil volumetric water (SVW, %) for switchgrass for selected fertilization rates (60, 120, and 180 kg N ha^{-1} yr^{-1}) during 2011 to 2013.

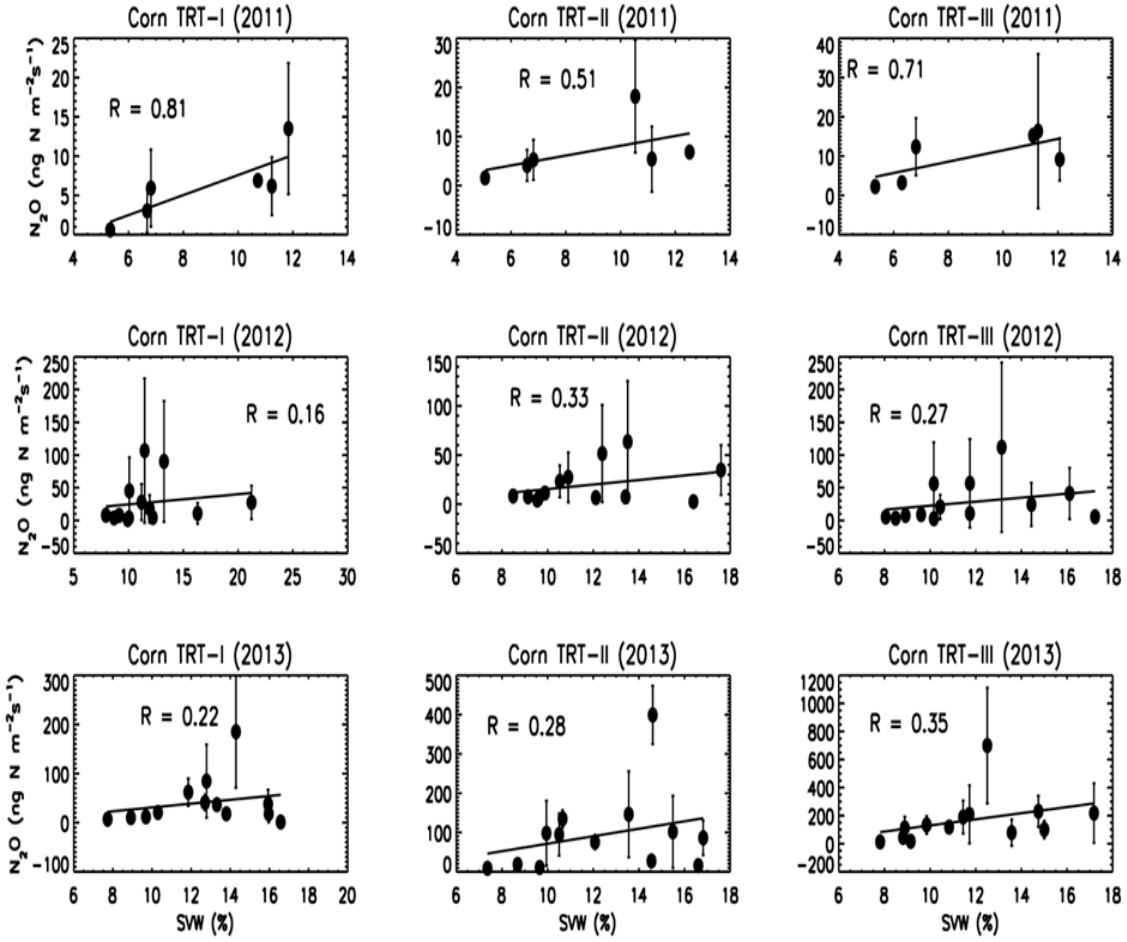

Figure 3.9. The correlation between N_2O fluxes and soil volumetric water (SVW, %) for corn for selected fertilization rates (60, 120, and 180 kg N ha^{-1} yr^{-1}) during 2011 to 2013.

3.2.5. Soil Inorganic Nitrogen (NH_4^+ and NO_3^-)

Soil inorganic nitrogen (NH_4^+ and NO_3^-) concentrations are summarized in Figure 3.10. Soil samples were collected in the fall and therefore characterize the residual soil nitrogen pool post-harvest. NH_4^+ concentrations are lower in the corn soil relative to switchgrass, though there is no clear relationship with N treatment level in either crop. The most distinctive pattern of NH_4^+ concentrations is a decrease in concentrations with depth, which is observed in both crops. While the NH_4^+ pools are similar among crops, NO_3^- concentrations are more than 10X larger in the corn soil relative to switchgrass. In contrast to NH_4^+, NO_3^- concentrations increase with N treatment level in the 0-10 cm and 0-20 cm layers in switchgrass and at all depths in the corn soil. NO_3^- concentrations increase with depth at all N treatment levels in corn, though the same pattern is not observed in switchgrass.

The pattern of much lower soil NO_3^- under switchgrass relative to corn is consistent with the findings of Ahlschwede (2013), who also found lower N_2O emissions from switchgrass relative to corn at the same N fertilization rates. The lack of accumulation of NO_3^- in the switchgrass soil may reflect uptake of NH_4^+ and subsequent low rates of mineralization, leading to a small NO_3^- pool or, more likely, efficient plant uptake of NO_3^- produced via nitrification of fertilizer NH_4^+. The much larger disparity in NO_3^- concentrations between crops compared to NH_4^+ supports the latter hypothesis. High rates of N uptake are consistent with the more extensive rooting system and greater root

biomass of the switchgrass relative to corn. The ability of perennial grasses to efficiently take up nitrogen and prevent its accumulation in the rooting zone is well established (Schimel, 1986; McIsaac et al., 2010).

Burton et. al., (2008) showed that the impacts of soil NO_3^- on N_2O emissions were directly connected to the duration of the exposure of soil microbial population to NO_3^-. Assuming nitrification is not limited in either crop, the much lower N_2O emissions from switchgrass are likely related to differences in denitrification derived N_2O, which would be much smaller in switchgrass due to less available substrate (i.e., NO_3^-). Thus, N_2O emissions from switchgrass may primarily reflect nitrification whereas emissions from corn reflect a combination of nitrification and denitrification. An alternative possibility is that the soil NO_3^- pool in switchgrass was low due to depletion by denitrification (McIsaac et al., 2010). However, consideration of the inorganic N mass balance suggests that such large rates of denitrification would presumably lead to N_2O production and emissions larger than were observed for corn.

Application of N-fertilizer in excess of plant requirements leads to a greater potential for loss from the plant/soil system (Heggenstaller et. al., 2009; McIsaac et al., 2010). For both crops, as N-fertilization increased, NO_3^- concentrations increased as well. The much larger concentrations in corn reflect a much greater potential for loss not only as N_2O emissions but also NO_3^- leaching.

From figure 3.10, it is clear that the ratio between ammonium losses and NO_3^- leaching is greater in switchgrass compared to corn. This behavior was consistent with the findings by McIsaac et al, 2010 for the Midwestern U.S. As discussed earlier, switchgrass plots were associated with stronger correlation between soil volumetric water and N_2O emissions as compared to corn plots. The higher soil moisture for a prolonged period may increase denitrification while reducing nitrification in switchgrass. This may partly explain the lower NO_3^- concentrations in switchgrass.

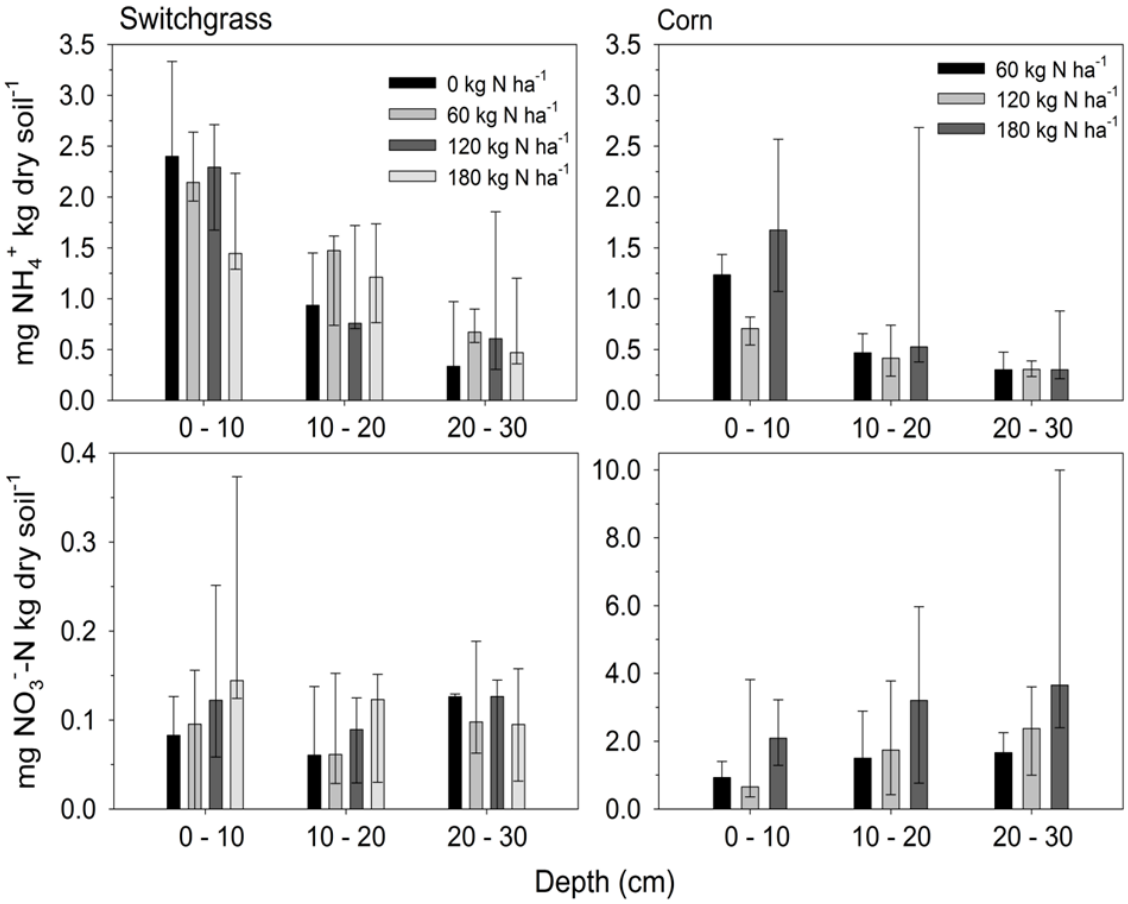

Figure 3.10. Inorganic soil N (NH_4^+ and NO_3^-) is shown for three different soil depths (0 - 10 cm, 10 – 20 cm, and 20 - 30 cm) for corn and switchgrass. Median concentrations are shown along with inter-quartile range.

3.2.6. Crop Yield

Study average yields for switchgrass and corn are shown in Figure 3.11. The overall average yield across all treatments and years was 13.3 Mg ha^{-1} y^{-1}, which is on the lower end of the range of previously published yields of Alamo variety in North Carolina (13.4 – 21.6 Mg ha^{-1} y^{-1}, McLaughlin and Kszos, 2005; Palmer et al., 2014a) and within the range of average yields (12 – 19 Mg ha^{-1} y^{-1}) for mid-latitude and southern sites in the U.S. (McLaughlin and Kszos, 2015). Aside from year 1 of the study (2011), switchgrass yields did not show a clear relationship with N application rate. This is consistent with the findings of Palmer et al. (2014a), which showed that N application rate (0 – 134 kg N ha^{-1} y^{-1} ammonium nitrate) did not significantly influence the amount of biomass produced. The average crop yield showed a stronger relationship with rate of fertilization in the case of corn (Figure 3.11). Average yields for our 120 and 180 kg N ha^{-1} treatments were slightly higher than the North Carolina statewide average corn yield for 2011 – 2013 (114 bu ac^{-1}, USDA National Agricultural Statistics Service, 2016).

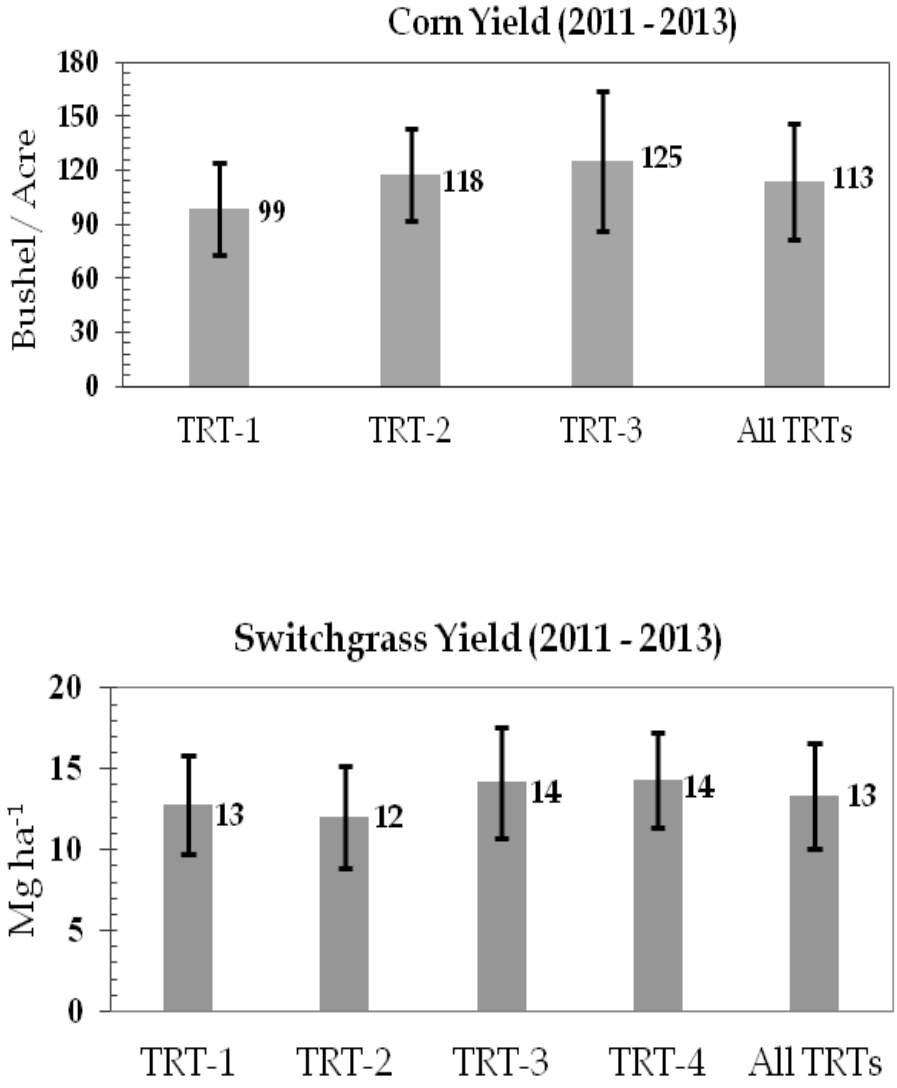

Figure 3.11. The crop yield for corn (top panel) and switchgrass (bottom panel) (with ± 1 standard deviation) are shown averaged across all the years (2011 to 2013) as function of the selected N-fertilizer treatments (60, 120, and 180 kg N ha-1 yr-1 . The 3-year average crop yield is also shown for both crops.

3.3. Conclusions

In this study, the N_2O emissions from switchgrass and corn biofuel crops were investigated as a function of fertilization (60, 120, and 180 kg N ha^{-1} yr^{-1}) rate over three growing seasons (2011 to 2013). The soil volumetric water and soil temperature feedbacks on these emissions were analyzed for both crops. For both corn and switchgrass, in general, the N_2O emission increased as a function of fertilization rate. In both the crops, the cumulative emission increased from 2011 to 2013 during the experiment. Despite the increase in N_2O emissions as a function of fertilization, the average as well as the cumulative, N_2O fluxes from switchgrass plots were much lower than that from corn. During May to mid-August, when the soil volumetric water was relatively low, the N_2O flux and the soil moisture showed a strong correlation, especially at higher fertilization rates, indicating a more pronounced effect of soil moisture on N_2O emissions under relatively drier soil conditions.

Except for treatment-3 (180 kg N ha^{-1} yr^{-1}), the cumulative emissions from switchgrass were well below the IPCC emission factor of 1%. The cumulative N_2O flux from corn was about 3 to 6 times greater than that from switchgrass crops. This is consistent with the findings by Duran et al, 2016 (south-central Wisconsin) and Wile et al, 2014 (Nova Scotia, Canada) on the impact of N fertilization on N_2O emissions from switchgrass. The cumulative N_2O flux from switchgrass ranges between 0.02 to 3.14 kg N ha^{-1}. The observed range comparable to the cumulative flux reported for a grassland (0.03 to 2.89 kg N ha^{-1}) in Edinburgh, Scotland (Jones et al, 2011).

Also consistent with other studies (Palmer et al, 2014b; Monti et al, 2011; Wile et al, 2014), the differences in cumulative emissions of N_2O between switchgrass and corn may be attributed to the greater nitrogen use efficiency of switchgrass. Observation of much lower NO_3^- concentrations in the shallow soil profile of the switchgrass supported this assertion, and further suggests lesser potential for soil NO_3^- leaching as an additional environmental benefit of producing switchgrass rather than corn for biofuel production. Moreover, for both crop types, the increase in fertilization rates was associated with increases in the cumulative N_2O flux. As discussed earlier, the rate of fertilization showed only modest increase in switchgrass yield. These findings suggest the importance in the selection of the crop type, N-application rate, and adaptation of efficient management practices to meet the increasing energy demands through biofuel production but not at the cost of N_2O greenhouse gas emissions. Additional studies involving field scale biogeochemical models may complement the inferences drawn from our studies. The combination of long term observations and model studies are warranted to understand and quantify N_2O emissions as a contribution from each N-loss pathways.

REFERENCES

Ahlschwede, C.M., 2013. Microbial Ecology, Nitrogen, and Nitrous Oxide Trends in Marginal Soils Used for Cellulosic Biofuel Production in Eastern Nebraska.

Bouwman, A. F.: Direct emission of nitrous oxide from agricultural soils, Nutr. Cycl. Agroecosys., 46, 53–70, 1996. Bouwman, A. F., Boumans, L. J. M., and Batjes, N. H.: Emissions of N2O and NO from fertilized fields: summary of available measurement data, Global Biogeochem. Cy., 16, 1–13, 2002.

Burton, D.L., Zebarth, B.J., Gillam, K.M. and MacLeod, J.A., 2008. Effect of split application of fertilizer nitrogen on N~ 2O emissions from potatoes. *Canadian Journal of Soil Science*, 88(2), p.229.

Davidson, E. A. 1992. Sources of nitric oxide and nitrous oxide following wetting of dry soil. *Soil Science Society of America Journal*, 56 95–102.

De Klein, C., Novoa, R.S.A., Ogle, S., Smith, K.A., Rochette, P., Wirth, T.C., McConkey, B.G., Mosier, A. and Rypdal, K., 2006. N_2O emissions from managed soils and CO_2 emissions from lime and urea application. p. 11.1–11.54. *S. Eggelson et al.(ed.)*, pp.11-1.

Dobbie, K.E. and Smith, K.A., 2001. The effects of temperature, water-filled pore space and land use on N2O emissions from an imperfectly drained gleysol. European Journal of Soil Science, 52(4), pp.667-673.

Duran, B.E., Duncan, D.S., Oates, L.G., Kucharik, C.J. and Jackson, R.D., 2016. Nitrogen Fertilization Effects on Productivity and Nitrogen Loss in Three Grass-Based Perennial Bioenergy Cropping Systems. *PloS one*, 11(3), p.e0151919.

Edwards, L., 2007. Enhancing the ability of Panicum virgatum to survive flooding and its effects on soil activity when used for lakeshore stabilization. *All Dissertations.* Paper 146. http://tigerprints.clemson.edu/all_dissertations/146

Fike, J.H., Parrish, D. J., Wolf, D. D., Balasko, J. A., Green Jr., J. T., Rasnake, M., Reynolds, J. H., 2006. Switchgrass production for the upper southeastern USA: influence of cultivar and cutting frequency on biomass yields. *Biomass and Bioenergy*, 30:207-213.

Follett, R.F., Vogel, K.P., Varvel, G.E., Mitchell, R.B. and Kimble, J., 2012. Soil carbon sequestration by switchgrass and no-till maize grown for bioenergy. *BioEnergy Research*, *5*(4), pp.866-875.

Griffis, T.J., Lee, X., Baker, J.M., Russelle, M.P., Zhang, X., Venterea, R. and Millet, D.B., 2013. Reconciling the differences between top-down and bottom-up estimates of nitrous oxide emissions for the US Corn Belt. *Global Biogeochemical Cycles*, *27*(3), pp.746-754.

Hanson, J.D. and Johnson, H.A., 2005. Germination of switchgrass under various temperature and pH regimes. *Seed Technology*, pp.203-210.

Hartman, J.C., Nippert, J.B., Orozco, R.A. and Springer, C.J., 2011. Potential ecological impacts of switchgrass (Panicum virgatum L.) biofuel cultivation in the Central Great Plains, USA. *biomass and bioenergy*, *35*(8), pp.3415-3421

Heggenstaller, A.H., Moore, K.J., Liebman, M. and Anex, R.P., 2009. Nitrogen influences biomass and nutrient partitioning by perennial, warm-season grasses. *Agronomy Journal*, 101(6), pp.1363-1371.

Hutchinson, G.L., Mosier. A.R., 1981. Improved soil cover method for field measurement of nitrous oxide fluxes. *Soil Sci. Soc. Am. J.*, 45:311–316.

Jones, S.K., Famulari, D., Di Marco, C.F., Nemitz, E., Skiba, U.M., Rees, R.M. and Sutton, M.A., 2011. Nitrous oxide emissions from managed grassland: a comparison of eddy covariance and static chamber measurements. *Atmospheric Measurement Techniques*, 4(10), pp.2179-2194.

Livingston, G.P., Hutchinson, G. L., 1995. Enclosure-based measurement of trace gas exchange: Applications and sources of error. p. 14-51. *In* P.A. Matson, and R.C. Harriss (Eds.).
Biogenic Trace Gases: Measuring Emissions from Soil and Water. Blackwell Sci. Ltd., London.

McIsaac, G.F., David, M.B. and Mitchell, C.A., 2010. Miscanthus and Switchgrass Production in Central Illinois: Impacts on Hydrology and Inorganic Nitrogen Leaching. *Journal of Environmental Quality*, 39(5), pp.1790-1799.

Mitchell, R., Vogel, K.P. and Sarath, G., 2008. Managing and enhancing switchgrass as a bioenergy feedstock. *Biofuels, Bioproducts and Biorefining*, 2(6), pp.530-539.

Monti, A., Barbanti, L., Zatta, A. and Zegada-Lizarazu, W., 2012. The contribution of switchgrass in reducing GHG emissions. *GCB Bioenergy*,*4*(4), pp.420-434.

Mosier, A. and Kroeze, C., 2000. Potential impact on the global atmospheric N 2 O budget of the increased nitrogen input required to meet future global food demands. *Chemosphere-Global Change Science*, 2(3), pp.465-473.

Ogle, S.M., Del Grosso, S.J., Adler, P.R. and Parton, W.J., 2008. Soil nitrous oxide emissions with crop production for biofuel: implications for greenhouse gas mitigation. *The Lifecycle Carbon Footprint of Biofuels*, pp.11-18.

Palmer, I.E., Gehl, R.J., Ranney, T.G., Touchell, D. and George, N., 2014a. Biomass yield, nitrogen response, and nutrient uptake of perennial bioenergy grasses in North Carolina. *Biomass and Bioenergy*, 63, pp.218-228.

Palmer, N.A., Saathoff, A.J., Tobias, C.M., Twigg, P., Xia, Y., Vogel, K.P., Madhavan, S., Sattler, S.E. and Sarath, G., 2014b. Contrasting metabolism in perenniating structures of upland and lowland switchgrass plants late in the growing season. *PloS one*, 9(8), p.e105138.

Parkin, T.B. and Venterea, R.T. 2010. Sampling Protocols. Chapter 3. Chamber-Based Trace Gas Flux Measurements. IN *Sampling Protocols*. R.F. Follett, editor. p. 3-1 to 3-39. Available at: www.ars.usda.gov/research/GRACEnet

Pinto, A.D.S., Bustamante, M., Kisselle, K., Burke, R., Zepp, R., Viana, L.T., Varella, R.F. and Molina, M., 2002. Soil emissions of N2O, NO, and CO2 in Brazilian Savannas: Effects of vegetation type, seasonality, and prescribed fires. *Journal of Geophysical Research: Atmospheres*, 107(D20).

Ramirez, K.S., Lauber, C.L., Knight, R., Bradford, M.A. and Fierer, N., 2010. Consistent effects of nitrogen fertilization on soil bacterial communities in contrasting systems. *Ecology*, *91*(12), pp.3463-3470.

Rolston, D.E., Moldrup, P., 2002. Gas diff usivity. p. 1113–1139. *In* J.H. Dane and G.C. Topp (ed.) Methods of soil analysis. Part 4. SSSA Book Ser. 5. SSSA, Madison, WI.

Ruan, L., Bhardwaj, A.K., Hamilton, S.K. and Robertson, G.P., 2016. Nitrogen fertilization challenges the climate benefit of cellulosic biofuels. *Environmental Research Letters*, 11(6), p.064007.

Schimel, D.S., 1986. Carbon and nitrogen turnover in adjacent grassland and cropland ecosystems. *Biogeochemistry*, *2*(4), pp.345-357.

Schmer, M.R., Liebig, M.A., Hendrickson, J.R., Tanaka, D.L. and Phillips, R.L., 2012. Growing season greenhouse gas flux from switchgrass in the northern great plains. *biomass and bioenergy*, 45, pp.315-319.

Sprent, J.I., 1987. The ecology of the nitrogen cycle. *Cambridge University Press*.

Syakila, A. and Kroeze, C., 2011. The global nitrous oxide budget revisited.*Greenhouse Gas Measurement and Management*, *1*(1), pp.17-26.

USDA, 2016. Research and Applications Division, *National Agricultural Statistics Service (NASS)*. U.S. Department of Agriculture, Washington, D.C.

Venterea, R.T., 2010. Simplified method for quantifying theoretical underestimation of chamber-based trace gas fluxes. *J. Environ. Quality*. 39:126-135.

Vogel K.P., Brejda J.J., Walters D.T., Buxton D.R., 2002. Switchgrass biomass production in the Midwest USA: harvest and nitrogen management. *Agronomy Journal*, 94:413-420.

Wagner, S.W., Reicosky, D.C., Alessi. R.S., 1997. Regression models for calculating gas fluxes measured with a closed chamber. *Agron. J.* 89:279–284.

Wile, A., Burton, D.L., Sharifi, M., Lynch, D., Main, M. and Papadopoulos, Y.A., 2014. Effect of nitrogen fertilizer application rate on yield, methane and nitrous oxide emissions from switchgrass (Panicum virgatum L.) and reed canarygrass (Phalaris arundinacea L.). *Canadian Journal of Soil Science*,*94*(2), pp.129-137.

Wullschleger, S.D., Davis, E.B., Borsuk, M.E., Gunderson, C.A. and Lynd, L.R., 2010. Biomass production in switchgrass across the United States: database description and determinants of yield. *Agronomy Journal*, 102(4), pp.1158-1168.

Atmospheric Aerosols over the Southeastern US: Associations in Air Quality and Regional Climate

Chapter 4

4. REGIONAL NUCLEATION EVENTS OVER A FOREST SITE IN THE SOUTHEAST U.S.

4.1. Background

Atmospheric aerosols have adverse effects on human health (Nel, 2005; Pope et al., 2009) and the environment (Ramanathan et al., 2001). Aerosols modify the earth's energy budget directly through interactions with incoming solar radiation and outgoing terrestrial radiation. Aerosols as cloud condensation nuclei modify the cloud optical and micro-physical properties to consequently interact indirectly with the shortwave solar and longwave terrestrial radiation (Ramanathan et al., 2001). Size distributions of aerosols in the ambient atmosphere depend on local sources (primary emissions), reaction conditions (meteorological and chemical conditions and the oxidizing capacity of the atmosphere), and transport (Zhuang et al., 1999). Nucleation involves the formation of initial nuclei in the atmosphere from gaseous precursors through gas-to-particle conversion and growth to larger sizes primarily through condensation. Therefore, nucleation is an important mechanism responsible for maintaining the atmospheric aerosol concentrations (Yu et al., 2008) and the abundance of cloud condensation nuclei (Spracklen et al., 2008). For the aforementioned reasons, for a given location, the geographical features, atmospheric chemical conditions, meteorological conditions, and biospheric interactions may play

significant roles in new particle formation and subsequently in the evolution of aerosol size distributions.

A large number of studies have conducted around the world to identify new particle formation under various environmental conditions and to discern the responsible mechanisms (Kulmala et al., 2004).These studies reported frequent occurrences of nucleation events at sites from sub-arctic, suburban, urban, industrialized agricultural, forests, to coastal regions (Kulmala et al., 2004 and references therein). The theories that attempt to explain aerosol nucleation in the boundary layer include binary (Kulmala and Laaksonen, 1990), ternary (Korhonen et al., 1999; Kulmala et al., 2002; Merikanto et al., 2007), organic vapor mediated (Marti et al., 1997) and ion induced (Yu and Turco, 2000). The fact that most of the observed nucleation events occurred during daytime suggests the important role of photochemistry on nucleation events (Kulmala et al., 2004; Pillai et al., 2013). Depending on the meteorological and chemical conditions, newly formed particles can grow to 60 nm or greater to act as cloud condensation nuclei, and the particles that grow to and beyond 100 nm can interact directly with the incoming solar radiation. In both cases, these newly formed particles may alter the earth's radiative balance (Stratmann et al., 2003). The uncertainties in the estimation aerosol radiative forcing arise mainly from their sources, vertical distribution, optical properties, and their interactions with background aerosols (IPCC, 2014). Studies conducted in the past investigated the

correlation between surface-based fine particulate matter and the satellite based AOD (Engel-Cox et. al., 2004; Gupta et al., 2006; Mei et al., 2011). Aerosol vertical distribution varies as a function of aerosol chemical composition. For example, in the case of sulfate-rich aerosols, the concentration is largest near the surface and decreases exponentially with height (Torres et al., 2007). Liu et al. (2011) concluded that in areas dominated by sulfate aerosols, under well-developed boundary layer conditions, satellite-derived AOD can be used effectively to predict sulfate aerosol concentrations.

We have conducted long term (November 2005 to September 2007) aerosol particle size distribution, particulate matter (PM) organic and elemental carbon, trace gas, and meteorology observations over a loblolly pine plantation at the Duke Forest. Pillai et al. (2013) showed that new particle formation is frequent in the Duke Forest region. Moreover, a modeling study by Yu et al., (2012) showed that the AOD over this region is dominated by secondary aerosols. Based on aerosol size distribution measurements at Duke Forest, Chapel Hill, NC, Stroud et al. (2007) identified that aerosols at this site are influenced by both anthropogenic and biogenic sources. At this site, ~69% of the total observation days are associated with new particle formation, of which 36% of the total observation days showed the characteristics of regional nucleation (Pillai et al., 2013).Yu and Luo (2009) and Luo and Yu (2011) showed that, over the Duke Forest area, the secondary particles formed via nucleation can contribute to approximately 80-90% of the cloud condensation nuclei (CCN). Poor characterization of aerosols in climate models

poses one of the greatest uncertainties in climate simulations (Ramanathan et al., 2001). For these reasons, it is important to study the role of these frequent and strong regional aerosol nucleation events in the radiative forcing at this site.

Boucher and Theodore (1995) defined the forcing efficiency as the ratio between direct radiative forcing and the aerosol column burden. For a particular wavelength, Satheesh and Ramanathan (2000) estimated aerosol forcing efficiency at the TOA as the rate of change in TOA net irradiance with respect to unit change in aerosol optical depth. Estimation of the wavelength-dependent aerosol forcing efficiency may provide improved parameterization of aerosol forcing for use in climate models (Meywerk and Ramanathan, 1999). For a given location, the local aerosol radiative forcing depends on a number of factors, including incoming solar radiation, surface albedo, local anthropogenic aerosol species, aerosol column burden, altitude of the aerosol layer, and ambient relative humidity if the aerosol species is hygroscopic (Haywood and Boucher, 2000).

In this study, we investigated the role of frequent new particle formation events on the radiative balance over a forest site. We combined ground-based particle size distribution and total particle number concentration with the spatially and temporally coincident aerosol and cloud property retrievals from Moderate Resolution Infrared Spectro-radiometer (MODIS) and Top of the Atmosphere (TOA) upward shortwave flux from Clouds and Earth's Radiant Energy System (CERES) sensor onboard the Earth Observing System (EOS) Terra satellite to estimate the TOA shortwave aerosol direct radiative

forcing owing to atmospheric new particle formation. The present study is unique because this study incorporates multi-year observations (November, 2005, to September, 2007) of particle size distribution (10.2 nm < D_p < 250 nm) and total particle number concentration of nucleation mode (NM, < 25nm) and fine mode (FM, 25 < D_p < 250 nm) particles to identify new particle formation event days at the Duke Forest. To our knowledge, there are no studies conducted in the past in the United States to identify the role of regional nucleation events in direct shortwave aerosol radiative forcing. For nucleation day radiative forcing calculations, we also included certain non-nucleation days if that particular day's particle size distribution is affected mainly by particles derived from the previous day's regional nucleation event. Hereafter in this manuscript, the "nucleation day aerosol radiative forcing" calculations include both regional nucleation days and non-nucleation days contributed by particles from the previous day's regional nucleation event. The lack of clear association between oxides of nitrogen and particle number concentration on selected nucleation days confirms the regional characteristics of these nucleation events (Qian et al., 2007). These stringent criteria followed for the selection of new particle formation event days brings an additional confidence in the radiative forcing estimation as the particles formed during regional nucleation show steady growth characteristics and are extended over a larger area as compared to local nucleation events.

Chapter 5

5. SATELLITE-BASED ESTIMATION OF SHORTWAVE AEROSOL RADIATIVE FORCING BY REGIONAL NUCLEATION EVENTS OVER A FOREST SITE IN THE SOUTHEAST U.S.

5.1. Experimental

The study was conducted over a suburban forest site, the Duke Forest near Chapel Hill, NC (Figure 5.1). Duke Forest comprises 7052 acres of land spread across Durham, Orange, and Alamance counties in North Carolina and is surrounded by the cities of Chapel Hill (7 km to the south-southeast), Durham (17 km to the east-northeast), Raleigh (40 km to the southeast), and Burlington (33 km to the west-northwest).

Even though Interstate-40 passes ~ 2.4 km to the northeast of the study area, Pillai et al. (2013) showed no significant impact of traffic on the diurnal profiles of nucleation day NM or FM particle number concentration by separating the observation days into week days and weekends. A detailed description of the site can be found in Geron (2009) and at the website http://dukeforest.duke.edu.

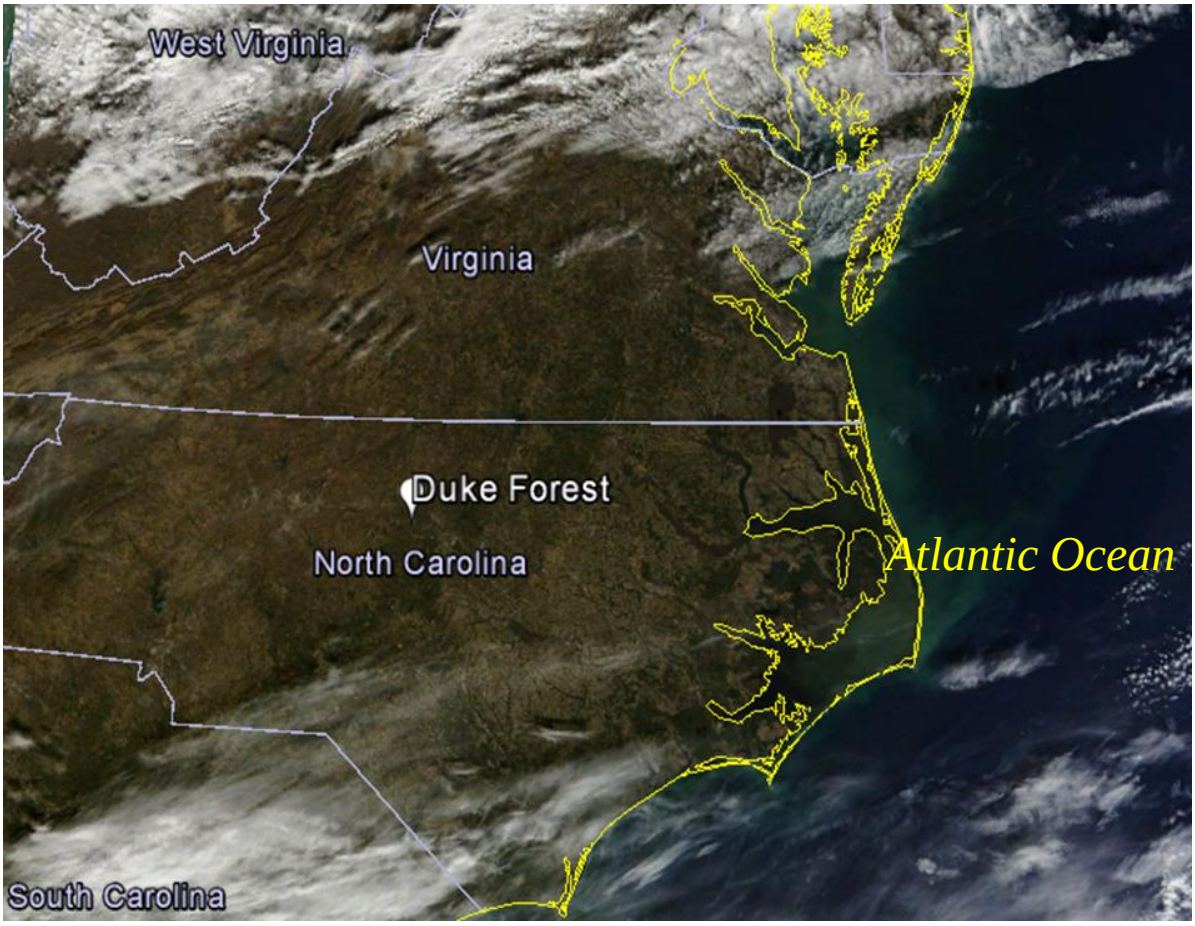

Figure 5.1. The observations of particle size distributions, meteorology and chemistry are conducted in Duke Forest, Chapel Hill, NC. The MODIS three band overlay file projected on Google Earth was obtained from http://ge.ssec.wisc.edu/.

5.1.1. Particle Size Distribution and Meteorology

Particle Size Distribution measurements were conducted over the Duke Forest Loblolly pine plantation (35^0 55' 45'' N, 79^0 05' 33'' W) with an approximate tree height of 18 m. Duke Forest observations used in this research include particle size distribution in the size range 10.2 nm < Dp < 250 nm and the corresponding total particle number concentration (Pillai et al., 2013). The airborne particle size distributions during November, 2005, to September, 2007, were measured using a Scanning Mobility Particle Sizer (SMPS, TSI, Shoreview, MN, USA). The SMPS used in this study incorporates a TSI series 3080 Electrostatic Classifier coupled with a 3081 Differential Mobility Analyzer (DMA), and a 3010 Condensation Particle Counter (CPC). For a brief period, a TSI Model 3025 CPC was used. The DMA classified the aerosol particles based on their mobility in an electric field. Particles within a narrow mobility range are allowed to enter the CPC to derive the particle number concentration at that particular mobility diameter. The instrument is operated with a 0.0457 cm impactor inlet at a particle free sheath flow of 10 Lpm and an aerosol air flow of 1 Lpm. This experimental setup established an effective particle size range of 7 to 305 nm. The observations are then adjusted for multiple charge and diffusion loss corrections. For detailed information on the aerosol observations used in this manuscript, readers are referred to Pillai et al. (2013). In addition, we have used the optically corrected mass concentrations of Organic (OC) and Elemental Carbon (EC) obtained from Geron (2009) for this study.

Meteorological data at the Duke Forest site are compiled from the measurements conducted by the Brookhaven National Laboratory (BNL) and Free-Air Carbon Enrichment (FACE) science teams. These data are 30-minute averages and include the above-canopy air temperature (°C), relative humidity, wind speed (m s^{-1}), wind direction, and Photosynthetically Active Radiation (PAR, millimol $m^{-2} \cdot s^{-1}$). Meteorology, including above-canopy air temperature (T), relative humidity (RH), wind speed, wind direction and PAR, at the site are used to categorize the observations into different groups of near-uniform meteorology and radiation conditions.

5.1.2. Satellite Data

In this study, we used the Terra CERES Edition 3A single scanner footprint (SSF) product that provides TOA shortwave flux and the MODIS aerosol and cloud properties. The CERES instrument onboard Terra is a scanning broadband radiometer with a spatial resolution of 20 km at nadir. The CERES instrument is deployed to provide accurate long term estimates of surface and top of the atmosphere radiative fluxes (Wielicki et al., 1996). The CERES instrument measures filtered radiances in three different spectral regions, the reflected shortwave (SW, 0.3 to 5 μm), infrared window (WN, 8 to 12 μm), and total (0.3 to 200 μm) spectral regions (Wielicki et al., 1996). These filtered radiances are corrected for imperfect spectral responses of the instrument by converting the filtered radiances to the unfiltered radiances (Loeb et al., 2001) and are further converted to fluxes using the global Angular Distribution Models (ADMS) (Wielicki et al. 1996). In the CERES SSF Edition-2 and Edition-3 products, radiances are converted into fluxes based

on very comprehensive ADMs developed from Terra observations (Loeb et al., 2005). Two CERES instruments are on board the Terra satellite, one with a fixed cross-track scan mode and the other with a Rotating Azimuth Plane (RAP) or an along track Programmable Azimuth Plane (PAP) scan mode. The RAP mode is designed to capture radiance information from a wide range of viewing configurations, whereas the PAP mode is designed for only specific viewing geometries (Loeb et al., 2005).

The CERES SSF product combines the CERES instrument-derived surface and TOA radiance and fluxes within the three aforementioned broadband spectral ranges with the high spectral and spatial resolution MODIS aerosol and cloud information within the larger CERES footprint. Only CERES pixels containing one or more MODIS imager pixels are included in the SSF product.

5.2. Methodology

5.2.1. Nucleation event identification and classification

Observations at the Duke Forest site are classified into nucleation days and non-nucleation days based on the particle number concentration, characteristics of the particle size distribution and particle growth rate. A log-normal fit is applied to the data to identify the particle size distribution peaks at each instant of time, and the diameters corresponding to these peaks are used to calculate the particle growth rate. During a nucleation event, we expect an increase in the particle number concentration and the diameter corresponding to these peaks. The nucleation events are further classified into different event classes (A, B, or C) based on the nucleation event classification scheme by Dal Maso et al., 2005; Boy et al., 2008; and Pryor et al., 2010 based on the two-dimensional aerosol size distribution plots. The particle number concentration for each size bins (N_i) and for each observation days were plotted as a function of particle diameter and time. The periods of increasing N_i were assessed to identify potential nucleation event classes A, B, C, or to categorize the day as non-nucleation (non-event) day.

The condensation sink (CS) and growth rate of the particles were also examined in classifying the observation days into different event classes. Condensation sink quantifies the loss rate of molecules in the entire size spectrum due to condensation of condensable vapors on pre-existing aerosols (Dal Maso et al., 2002; Kulmala et al., 2001). It is calculated as the integration of condensational loss of condensable vapors onto existing

aerosols and is dependent on the molecular properties such as vapor phase diffusion and mean free path. The CS (cm^{-2}) is calculated as follows

$$CS = \int_{10\ nm}^{250\ nm} D_p\ \beta(D_p)\ n(D_p)\ dlog(D_p) \qquad (5.1)$$

where β is the transitional correction factor [30, 31], D_p is the mid-point diameter, and $n(D_p)$ is the number distribution of particles corresponding to different size classes with mid-point diameter (D_p) between the size range 10 nm and 250 nm.

The accommodation coefficient of unity was used to calculate β. Since we use 10 nm to 250 nm diameter range for quantitative analysis, the calculated value is an underestimation of the actual CS, though the contribution of particles with sizes outside the measured range is expected to be relatively small.

Growth rate indicates size changes of nucleated particles with time. A log-normal fit is applied to the data to identify the peaks in each size distribution. GR in nm hr^{-1} was calculated from the difference between midpoint diameters corresponding to the peaks in particle number concentration for each instant of time (ΔD_{Peak}) by dividing it with the corresponding differences in time (Δt).

$$\mathrm{GR} = \frac{\Delta D_{Peak}}{\Delta t} \qquad (5.2)$$

Particle growth rate is a function of the condensable vapor concentration and the CS. GR increases significantly when the condensable vapor concentration is large and the CS is low (Kulmala et al., 2004).

The event classes that are interrupted or that do not fit into the aforementioned categories are identified as unclassified events and are excluded from further analysis. The typical size distribution behavior for each of these event classes are shown in Figure 5.2.

Class A: Increased concentrations of nucleation mode (NM) particles ($D_p \leq 25$nm) are found and these particles exhibit well defined and uninterrupted growth to about 100 nm or greater.

Class B: Increased NM particle concentrations are observed and followed by particle growth to about 100 nm however, the highest concentrations of new particles are found not at the lowest size bins of NM but at diameters greater than 10nm. Such a growth pattern indicates the occurrence of nucleation upwind of the site followed by transport of

NM particles larger than 10nm and subsequent local growth due to condensation of vapors to less volatile forms. On some days these events exhibited fluctuations in growth rate.

Class C: Increased NM particles at lower size bins with consequent particle growth that does not exceed generally 40 nm. This event class was observed frequently with a discontinuous growth rate and is not included in the quantitative analysis of particle growth rate and Condensation Sink.

Non-Nucleation: Observation days with particle size distributions devoid of increased NM concentration and their subsequent growth to larger particles.

Unclassified: Days that do not fit into the described event classes or that had an interrupted size distribution data due to inclement weather or instrument outage or for which the growth rates are extremely fluctuating.

During Class A nucleation events, we observed the highest particle number concentrations in the lowest size bins followed by uninterrupted and steady growth to larger diameters spanning an average time period of three or more hours.

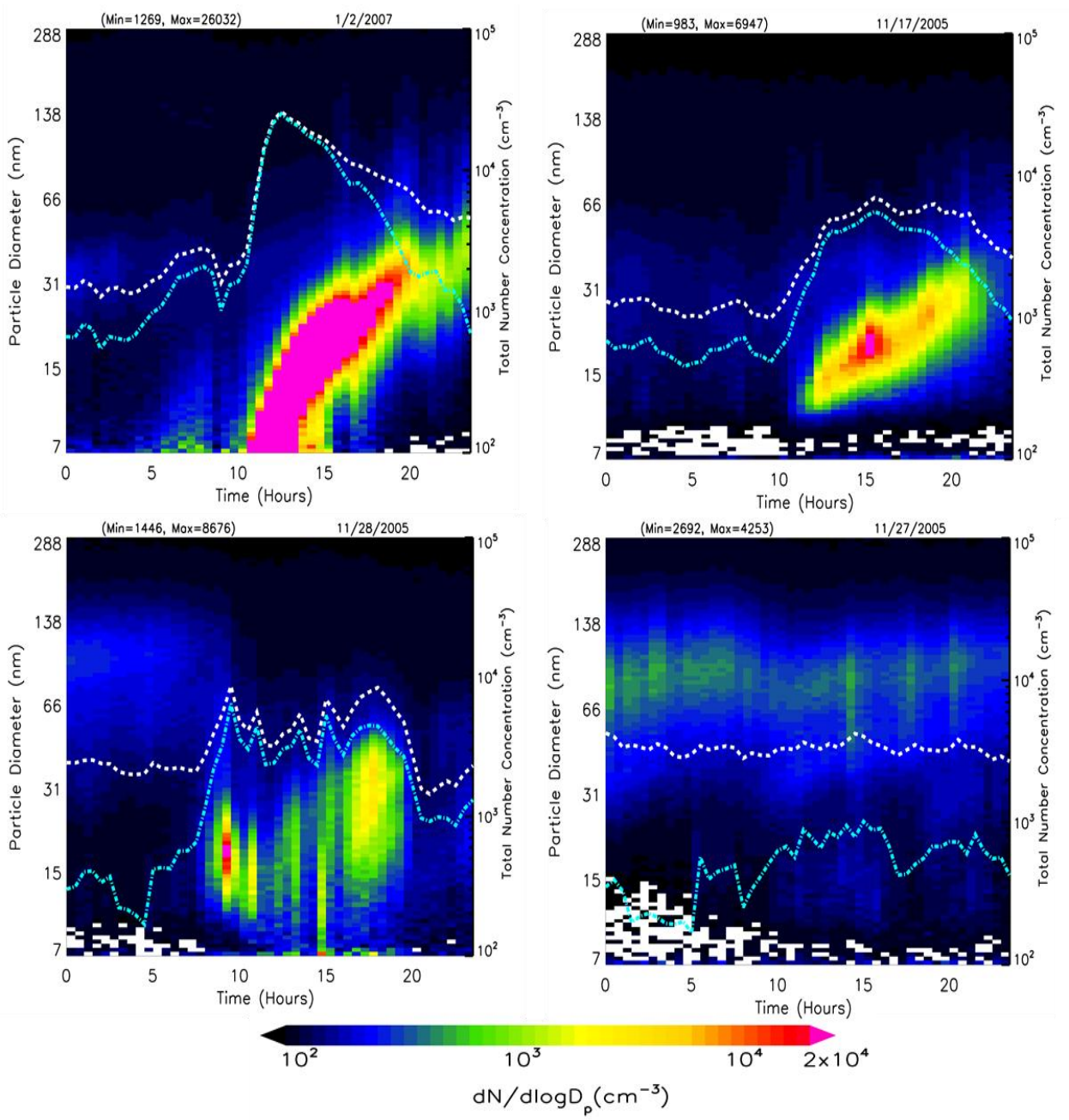

Figure 5.2. Examples aerosol size distributions for A (top left), B (top right), C (bottom left), and Non Nucleation (bottom right) event classes are shown along with total particle number concentration (white) and nucleation mode particle number concentration (cyan). (Source: Pillai et al, 2013)

Class B events follow a growth pattern similar to Class A. However, in Class B events, the highest particle number concentrations are observed at a diameter larger than the lowest size bin. In both cases, particles grow larger than 60 nm and often beyond 100 nm in diameter. Class C events exhibit short-lived random peaks in the particle size distribution instead of the steady growth of particles. Therefore, Class A and Class B events are identified to possess the regional nucleation characteristics as explained in Seinfeld and Pandis (2006) compared to the local random outbursts of particles in the case of Class C. The classification methods and the characteristics of these different event classes are explained in detail in Pillai et al. (2013).

Based on our observations, nucleation events are frequent at the Duke Forest site except during September and October. Figure 5.3 shows nucleation events observed for four consecutive days from 8 – 11 April, 2007, and 24 -27 November, 2005. Strong and uninterrupted nucleation occurred during these two entirely different meteorological and atmospheric radiation and chemical conditions. From the close examination of Figure 5.3, we can see that the April, nucleation events are Class A events in which, at the beginning of each nucleation event, we observe the highest particle number concentration in the lowest diameter bin (10.2 nm to 10.6 nm) in the 10.2 nm to 250.3 nm (89 bins) size range. However, for the November nucleation events, we can see that the lowest size bin does not correspond to the highest particle concentration at the beginning of the nucleation event. Therefore these nucleation events are classified as Class B events. On 11th April, 2007, and 27th November, 2005, we did not observe nucleation events (Figure 5.2).

However, from Figure 5.3 we identify that the peaks in the fine mode particle concentration existing beyond ~60 nm at the site on both these days are the contribution from the previous day's nucleation event at the site. Therefore, these days are also grouped under nucleation events for the estimation of nucleation day aerosol radiative forcing.

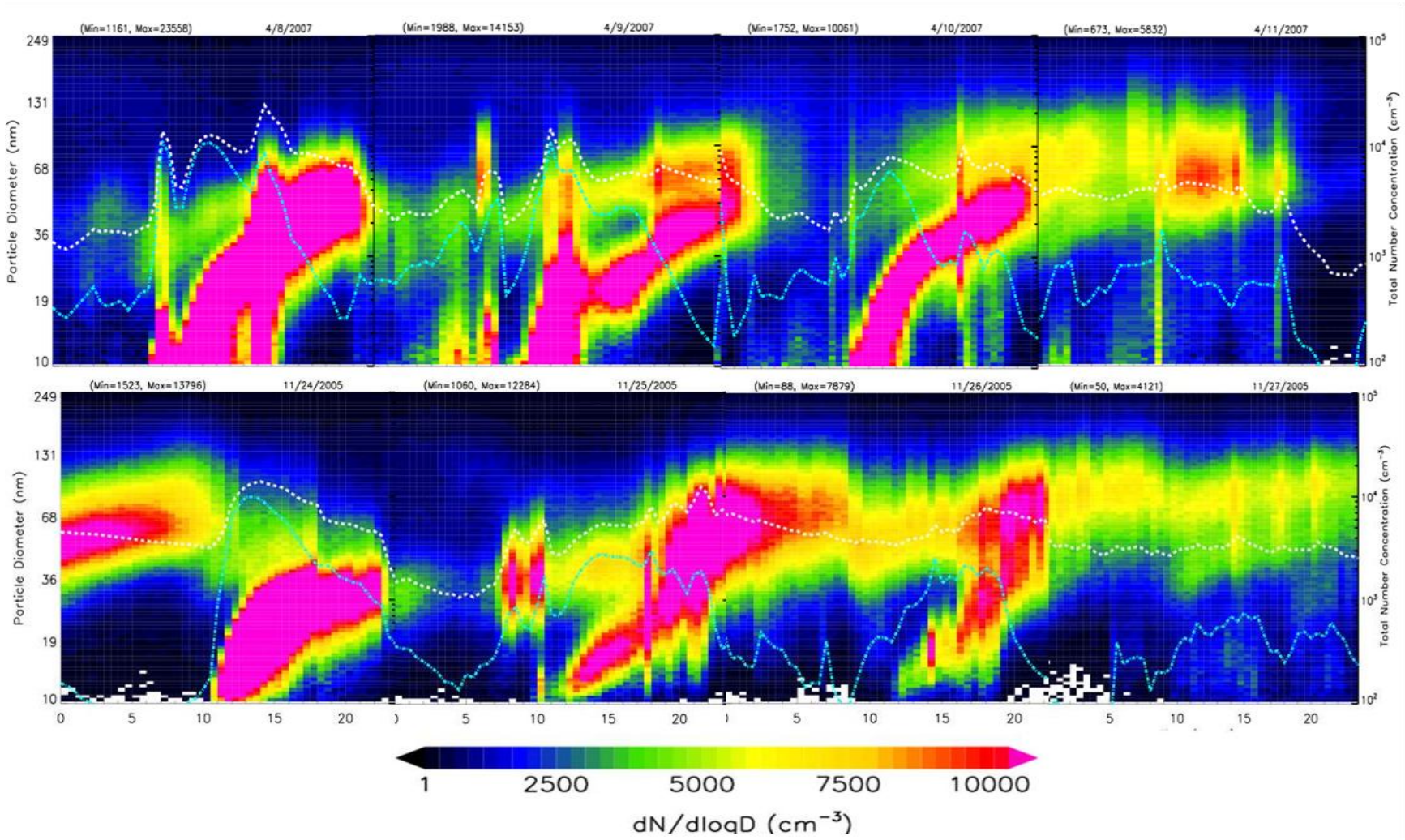

Figure 5.3. Aerosol nucleation events observed at the Duke Forest site during warm period (8 – 11 April, 2006) and cold period (24 – 27 November, 2005) are shown, respectively, in the top panel and the bottom panel. The fine mode (white line) and nucleation mode (cyan line) particle number concentration is also shown on the secondary Y-axis

Furthermore, in the estimation of the nucleation day aerosol radiative forcing, we incorporated only the days that showed regional nucleation characteristics and excluded regional nucleation days that are affected, at the time of satellite overpass, by transported fine mode particles. In our radiative forcing calculations, by selecting only the nucleation event days that showed regional particle formation characteristics (Seinfeld and Pandis, 2006), it is reasonable to assume that the particle formation has happened over a relatively larger area as compared to local nucleation events.

Photosynthetically Active Radiation (PAR) is used as a surrogate to examine the radiation conditions at this site. Monthly mean daytime PAR along with the minimum and maximum values during the time window from 8:30 am to 5:30 pm are shown in Figure 5.4a along with the monthly mean day time air temperature and RH (Figure 5.4b), wind speed and wind direction (Figure 5.4c). In this study, prior to categorizing different months into seasons, we also examined the monthly mean PAR, air temperature, RH, and wind speed and direction. The time of nucleation onset, average mean particle growth rate, nucleation event types, and also fine and nucleation mode particle number concentration were examined along with the site's radiation and meteorological conditions to group the observation days into different seasons. June, July, and August are grouped as summer, and March, April, and May are grouped into spring.

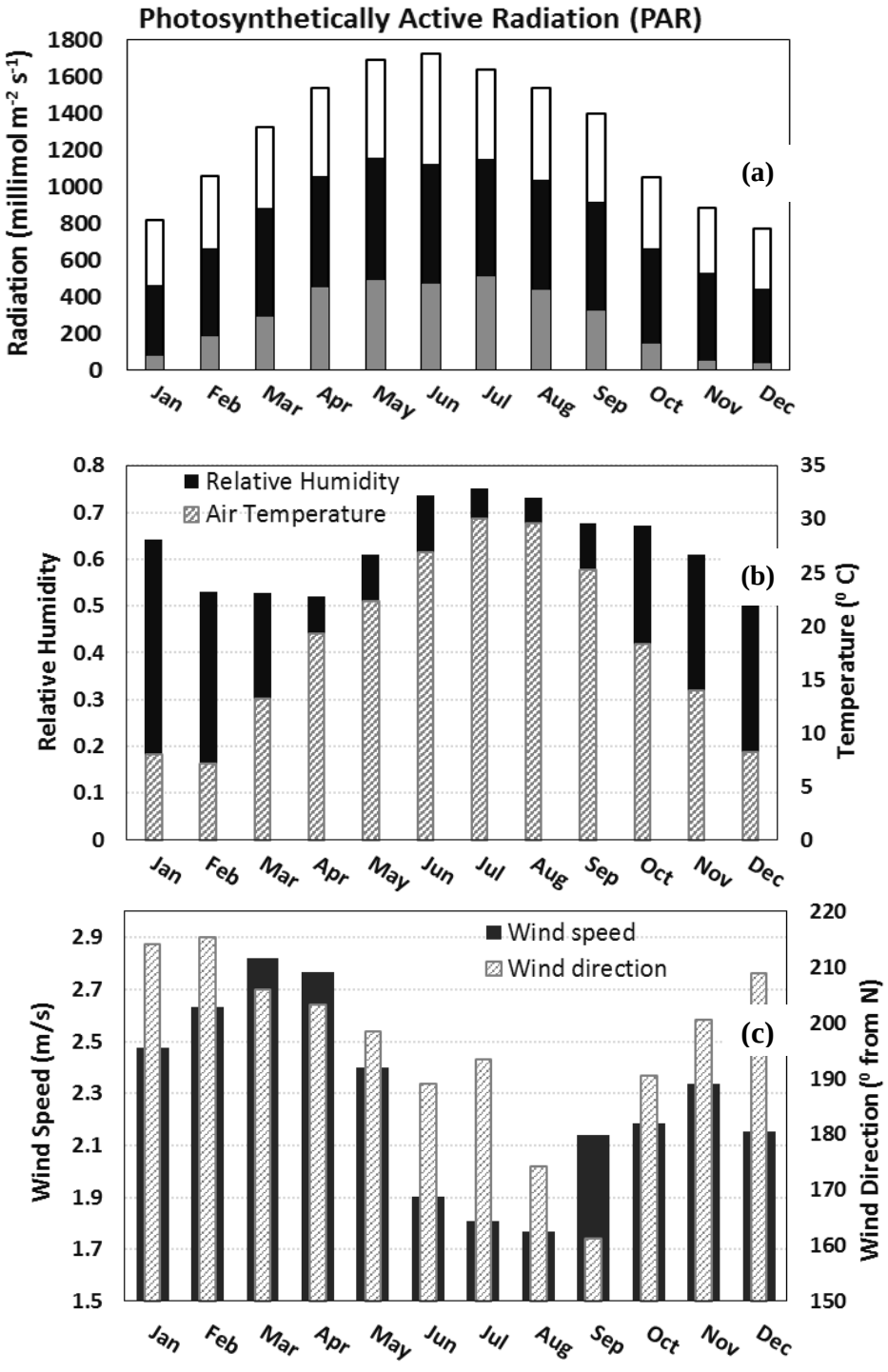

Figure 5.4. Monthly mean daytime (a) Photosynthetically Active Radiation (PAR) is shown along with the monthly mean; (b) relative humidity and air temperature; and (c) wind speed and wind direction. Based on these parameters, the observation days are classified into different groups in which these parameters did not vary significantly.

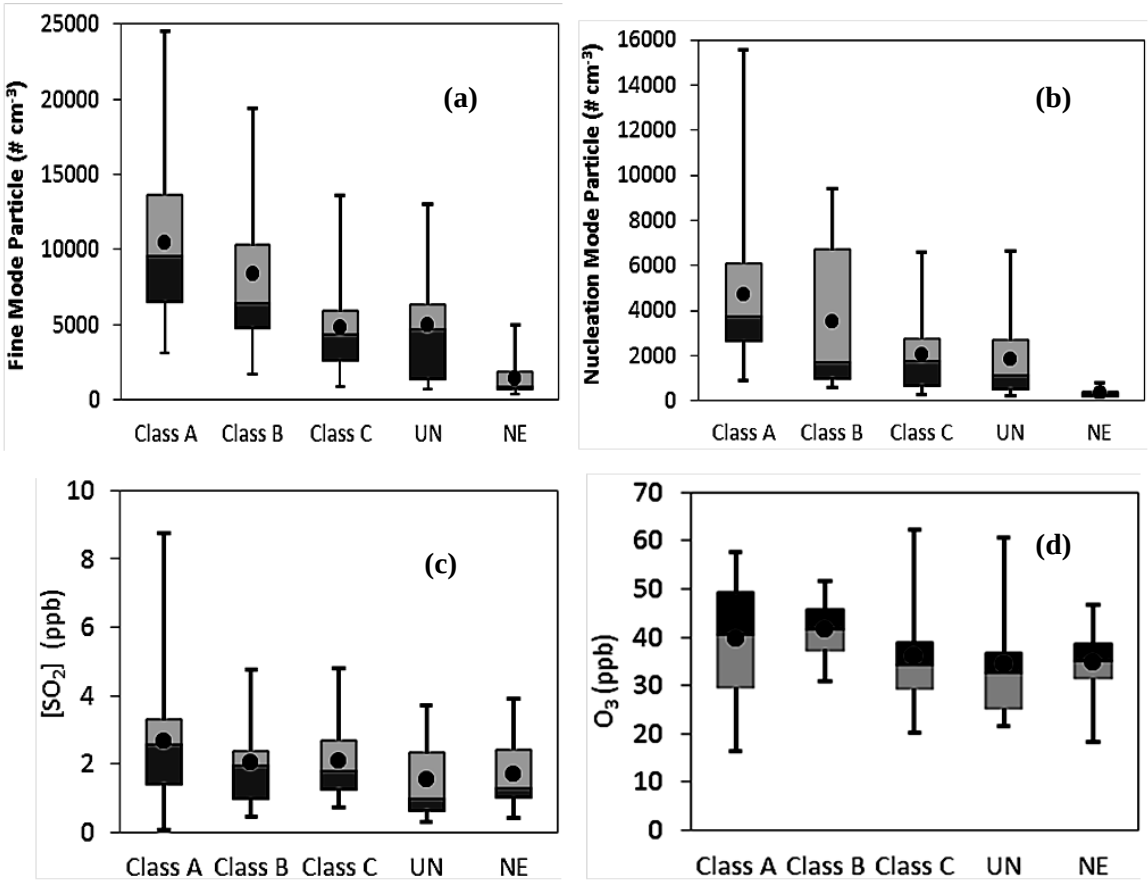

Figure 5.5. The box plots show median (the line separating gray and black boxes), 25th (bottom of gray box) and 75th percentiles (top of black box), minimum and maximum (whiskers), and mean (filled circles) for (a) fine mode (b) nucleation mode particles (c) SO_2 and (d) O_3 from July, 2006, to September, 2007. The days that exhibited particle formation characteristics but do not show the characteristics of A, B, or C events are categorized as unidentified (UN), and days with no nucleation events (NEs) are also shown.

The mean and standard deviation of the fine mode and nucleation mode particle number concentrations along with SO_2 and O_3 concentrations are shown for each nucleation event class (Figure 5.5). The total particle number concentrations in the NM and FM are highest for Class A events followed by Class B events. Even though both the Class A and Class B events exhibited regional nucleation characteristics, the Class A events are associated with highest particle number concentration followed by Class B events. The highest average SO_2 (2.65 ppb) and second highest O_3 (40 ppb) concentrations are observed during Class A events. The highest O_3 (~43 ppb) concentration is observed during Class B events. Class C events are associated with increased cloud cover and precipitation. Class C events have the second highest SO_2 (2.08 ppb). However, increased cloud cover on Class C event days lowers the photochemical reactivity and atmospheric oxidizing capacity by reducing incoming solar radiation. Precipitation may cause the nucleated particles to wet deposit before being grown to detectable size. In estimating the TOA clear sky fluxes, the correlation between SW flux and AOD increased significantly when we excluded the Class C nucleation days.

For the radiative forcing calculation, we assumed that the surface reflectance remained constant within the selected seasons in that particular year. The highest seasonal mean particle growth rate is observed during summer when the average wind speed is lowest. The second highest seasonal average particle growth rate is observed during spring. Although strong nucleation events are observed in winter, they are excluded from the

forcing calculations because, in these periods, lower correlations between upward SW flux at the top of the atmosphere and MODIS AOD were observed. The particle growth rate is lowest in winter. In addition, during winter months, the nucleation onset is observed later in the day and therefore at the time of satellite overpass, the particles have not grown sufficiently to interact directly with the incoming solar radiation. For these reasons, the radiative forcing estimation is conducted only for summer and spring.

5.2.2. Shortwave Aerosol Direct Radiative Flux

Estimation of shortwave aerosol radiative forcing may involve the incorporation of observed or simulated aerosol properties into a radiative transfer model (Satheesh et al., 2002). Other methods attempt to quantify the TOA aerosol direct radiative effect by combining satellite retrievals with ground-based observations (Patadia et al., 2008; Sena et al., 2013). In this study, we integrate satellite data with ground-based observations to estimate the aerosol radiative forcing due to regionally nucleated aerosols.

CERES SSF data are collocated in space and time with the particle size distribution measurements at the Duke Forest site. CERES SSF data that fall within our particle size distribution sampling period are grouped into two categories: regional nucleation event day and non-nucleation day. To estimate the shortwave radiative forcing solely by aerosols, cloud contaminated pixels in the SSF data are eliminated. The MODIS cloud fraction provided in the CERES SSF data product is used to eliminate the cloud-contaminated pixels. For pixels with a sub-pixel clear area greater than 99.9%, we have

considered only those pixels for which the MODIS cloud fraction is zero. Patadia et al. (2008) reported the uncertainties associated with sub-pixel cloud contamination as the change in diurnal average SW radiative forcing (~0.5 Wm^{-2}) when the percentage cloud cover is relaxed from 1% to 10%. Signals reaching the sensor are impacted by the geometric configuration of the illumination source as well as the viewing sensor (Bryant et al., 2003). Therefore, we have applied restrictions to the solar and viewing zenith angles to avoid large scan angles and to incorporate only highly accurate satellite retrievals. The viewing zenith angle is restricted to < 60°. Based on the relationship between radiative forcing and the solar zenith angle (Haywood and Shine, 1997), the forcing trend begins to decrease significantly at ~ 60°. (Table 5.1).

Table 5.1. The seasonal averages of upward shortwave flux at the TOA and the MODIS aerosol optical depth (mean ± 1 SD) at the Duke Forest site are calculated based on 2006 and 2007 data.

2006 and 2007	TOA SW Flux Upward (Wm^{-2})	AOD @ 550 nm
Winter	132.56 ± 19.53	0.06 ± 0.05
Spring	172.60 ± 22.29	0.16 ± 0.15
Summer	188.23 ± 21.86	0.38 ± 0.20
Annual	165 .97 ± 30.29	0.21 ± 0.19

To compare the AOD and SW flux for different seasons, the values reported in Table 5.1 are calculated for all cloud-free but aerosol days. The seasonal average flux is highest (188 ± 22 Wm^{-2}) in summer when the aerosol optical depth is highest (0.38 ± 0.20). The highest seasonal average flux also coincides with the period of highest particle growth rate (Pillai et al., 2013). The AOD (0.06 ± 0.05) is lowest during winter months when the particle growth rate is the lowest. For the estimation of SW direct aerosol radiative forcing, we first need to estimate the clear sky SW flux (F_{clr}) at the TOA. By definition, the clear sky SW flux is the SW flux exiting the TOA if a scene is aerosol- and cloud-free. Therefore, F_{clr} is a function of the scene type, and F_{clr} varies according to the surface albedo and insolation. The SW direct aerosol radiative forcing at the instant of the satellite overpass is calculated as Shortwave Aerosol Radiative Forcing = F_{clr} - F_{aer}, where F_{aer} is the TOA SW flux under cloud-free but aerosol conditions. To estimate F_{clr}, we plotted the CERES SW upward flux at the TOA as a function of 550 nm MODIS AOD for the selected cloud-free data. Previous studies estimated the radiative forcing by biomass burning aerosols over the Amazon forest region (Patadia et al., 2008; Sena et al., 2013). For the radiative forcing calculations, we have selected a 0.35° x 0.35° grid cell that covers the entire Duke Forest plantation (Figure 5.1). This grid cell selection helps us preserve the surface uniformity in radiative forcing calculations by restricting the pixel selection to the forested areas that also include our measurement site. Within this selected grid cell, the MODIS-derived surface reflectances over land at 470 nm are 0.127 ± 0.028 and 0.134 ± 0.029, respectively, during spring and summer. Following Patadia et al. (2008), we

estimated the uncertainties associated with F_{clr} as the product of TOA instantaneous shortwave radiative forcing efficiency and the maximum uncertainty associated with MODIS AOD. The estimated uncertainty of AOD is greater than or equal to ± 0.05 ± 15% (Levy et al., 2010) based on collection-5 MODIS data. The associated uncertainty of F_{clr} is -4.2 Wm^{-2} for an average shortwave efficiency of -73 Wm^{-2}.

As we have mentioned earlier, the selection of only nucleation events that showed regional event characteristics adds an additional confidence that the aerosol signal captured from within the selected grid cell is primarily due to new particle formation and growth at the site. On some nucleation days, particularly in summer in the early morning hours, we observed transport of particles larger than ~ 60 nm to the site. These transport event days are also excluded from the radiative forcing calculation to help resolve the relationship between regionally nucleated aerosols and radiative forcing.

5.3. RESULTS AND DISCUSSION

New particle formation events are frequent at the Duke Forest site and are generally observed on days without precipitation. For particles within the diameter (Dp) range 10.2 nm < Dp < 250 nm, the average mode diameter corresponding to all nucleation event days (28 nm) is significantly smaller compared to the average mode diameter on non-nucleation days (44.5 nm) (Pillai et al., 2013). The same study also showed a significant increase in the fine mode and nucleation mode particle number concentration at the Duke Forest site on nucleation days compared to non-nucleation days. Hereafter in this manuscript, total particles or fine mode (FM) particles implies particles in the size range of 10.2 nm < Dp < 250 nm, and nucleation mode (NM) implies particles in the size range 10.2 nm < Dp < 25 nm. Considering all the nucleation event days, the daily average number concentrations are 8,684 cm^{-3} for fine mode particles and 3,991 cm^{-3} for nucleation mode particles, and on non-nucleation days these values are, respectively, 2143 cm^{-3} and 615 cm^{-3} (Pillai et al., 2013). Further, these nucleation events are associated with strong photosynthetically active radiation (PAR), low relative humidity, and sparse or no cloud cover (Pillai et al., 2013). In general, the association between nucleation events and PAR indicate the significant role of photochemistry in new particle formation at the site. For all the events involved in this study during the estimation of nucleation day radiative forcing, the onset of nucleation occurred during the day time. Pillai et al. (2013) observed that, on nucleation days, a distinct peak in SO_2 concentrations between 8 am and 10 pm existed, and this peak in SO_2 concentration observed after sunrise is associated with

the downward mixing of SO_2 from aloft as the nocturnal boundary layer breaks down. The same study noted that in warmer months, these morning peaks in SO_2 concentrations coincide with the onset of nucleation. Particle number concentrations correlated well with SO_2 and PAR suggest sulfuric acid (H_2SO_4)-mediated nucleation at the Duke Forest, especially during mid-spring to summer.

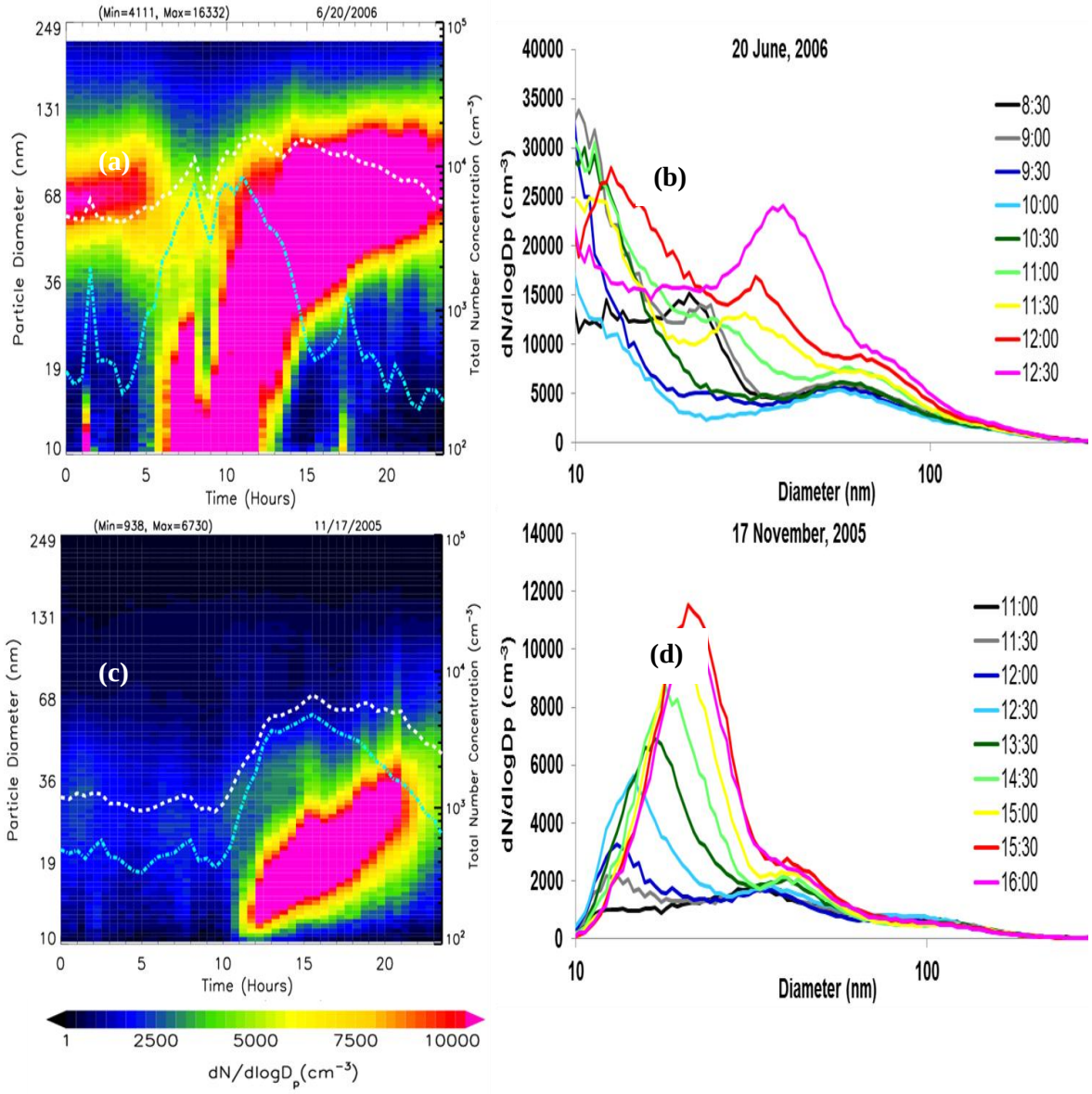

Figure 5.6. The particle size distributions are shown for (a) 20th June, 2006, and (c) 17th November, 2005, for nucleation event categories. The corresponding evolution of particles is shown in (b) and (d), respectively, in the right panel. Fine mode (white line) and nucleation mode (cyan line) particle number concentrations are also shown in the secondary Y-axis in # cm^{-3} as an overlay on the particle size distribution plot.

Figure 5.6 shows the particle size distribution along with the evolution of particles on 20th June, 2006, and 17th November, 2005. On 20th June, 2006, the onset of nucleation is early in the morning at ~6:30 am whereas on 17th November, the onset is later in the day at ~11:30 am. Minimum and maximum in total particle number concentrations are, respectively, 4111 cm^{-3} and 16332 cm^{-3} on 20th June and 938 cm^{-3} and 6730 cm^{-3} on 17th November. In the size distribution of the 20th June nucleation event, we can see larger particles of ~60 nm even before the onset of nucleation. After examining the previous day's size distribution data, we confirmed that these particles are not transported particles but the contribution from the previous day's nucleation event. During warmer months, the onset of nucleation is early in the morning, and particles are able to grow readily to larger sizes as indicated by the higher particle growth rates in summer and spring. Particle growth generally continues throughout the night. Therefore, by the time of satellite overpass at the site (equatorial crossing time of Terra is ~ 10:30 am), these nucleated particles are able to reach 100 nm or larger in diameter and subsequently interact with the incoming shortwave radiation. In late fall and winter months, the particle growth rate is lowest and subsequently leads to reduced impact of the freshly nucleated particles on the incoming shortwave radiation. The MODIS-derived aerosol optical depth and the average growth rate of particles are the lowest in winter. In winter months, the onset of nucleation is delayed due to delayed sunrise and less intense solar radiation. Therefore, at the time of the Terra satellite overpass (equatorial crossing time of ~10:30 am), the particles may not be grown large enough to interact directly with the solar radiation. The delayed nucleation onset in winter in combination with the requirement that newly formed particles must

grow to and beyond 100 nm to interact directly with the incoming solar radiation, therefore, explains the lowest correlation between SW flux and AOD in winter.

The seasonal average and standard deviation of TOA SW Flux and AOD on regional nucleation days during 2006 and 2007 are shown in Table 5.2. In spring, the nucleation day average SW fluxes are 158 ± 11 Wm^{-2} and 163 ± 22 Wm^{-2} and average AOD are 0.15 ± 0.09 and 0.16 ± 0.18, respectively, for 2006 and 2007. Due to the increased aerosol loading and the intense incoming shortwave radiation, the average summer SW flux is 187.70 ± 11.46 Wm^{-2} and AOD is 0.34 ± 0.15. The MODIS-derived mean surface reflectances over land at 470 nm are 0.127± 0.028 and 0.134 ± 0.029 during spring and summer, respectively.

Table 5.2. The TOA SW flux, AOD, and the instantaneous shortwave direct radiative forcing observed on regional nucleation days at the Duke Forest site during spring and summer for the years 2006 and 2007.

		TOA SW Flux (Wm^{-2})	**AOD @ 550 nm**	**SWRF (Wm^{-2})**
2006	**Spring**	157.95 ± 11.28	0.15 ± 0.09	-13.33 ± 11.28
	Summer	187.77 ± 12.19	0.29 ± 0.13	-28.29 ± 12.19
2007	**Spring**	163.05 ± 21.93	0.16 ± 0.18	-15.60 ± 21.93
	Summer	187.65 ± 10.90	0.38 ± 0.16	-21.81± 10.90

The TOA clear sky fluxes (cloud-free and aerosol-free) are estimated over the Duke Forest. Regression relationships are derived between the CERES upward shortwave flux at the top of the atmosphere and the MODIS sensor-retrieved total atmospheric column aerosol optical depth for spring and summer in 2006 and 2007. These parameters are shown averaged for a 0.35° x 0.35° grid (Figures 5.7 & 5.8), which includes the Duke Forest site. From the zero intercept of these regression relationships, the TOA SW clear sky fluxes (cloud-free and aerosol-free) are estimated for spring and summer 2006 and 2007. The average TOA shortwave clear sky fluxes for the spring and summer periods are 159.5 Wm^{-2} and 147.5 Wm^{-2}, respectively. As we have discussed earlier, for the radiative forcing calculations, we selected only the regional nucleation event days (days for which the new particle formation is happening over a relatively larger area around the Duke Forest site as compared to local nucleation events). Including only the regional nucleation days for deriving the clear sky flux therefore enables a better correlation between the SW flux exiting the TOA and the MODIS-derived aerosol optical depth.

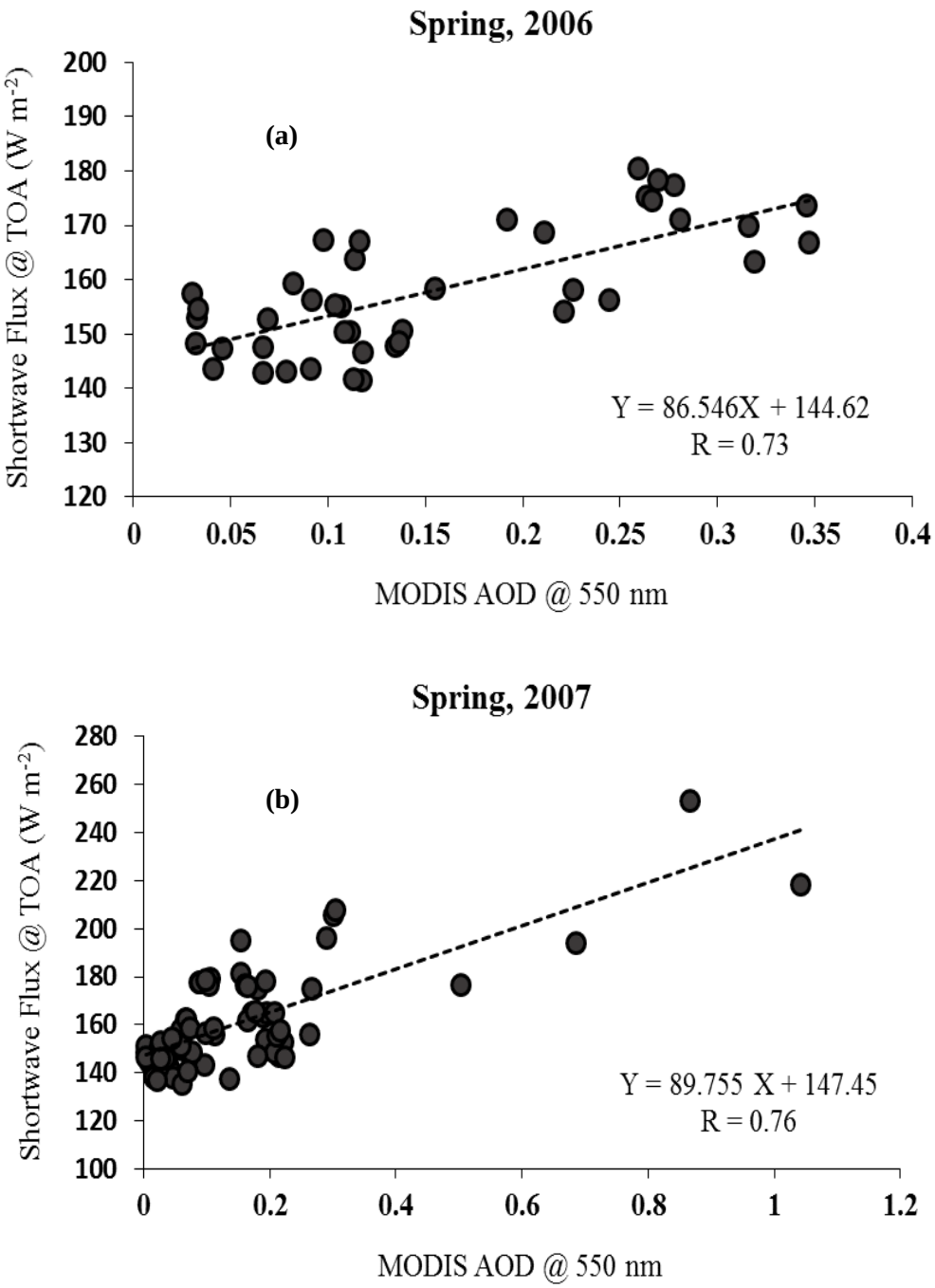

Figure 5.7. CERES shortwave flux at the top of the atmosphere and the MODIS sensor-retrieved total atmospheric column aerosol optical depth for nucleation days in (a) spring 2006 and (b) spring 2007 are shown averaged for the 0.35° x 0.35° grid box over the Duke Forest site.

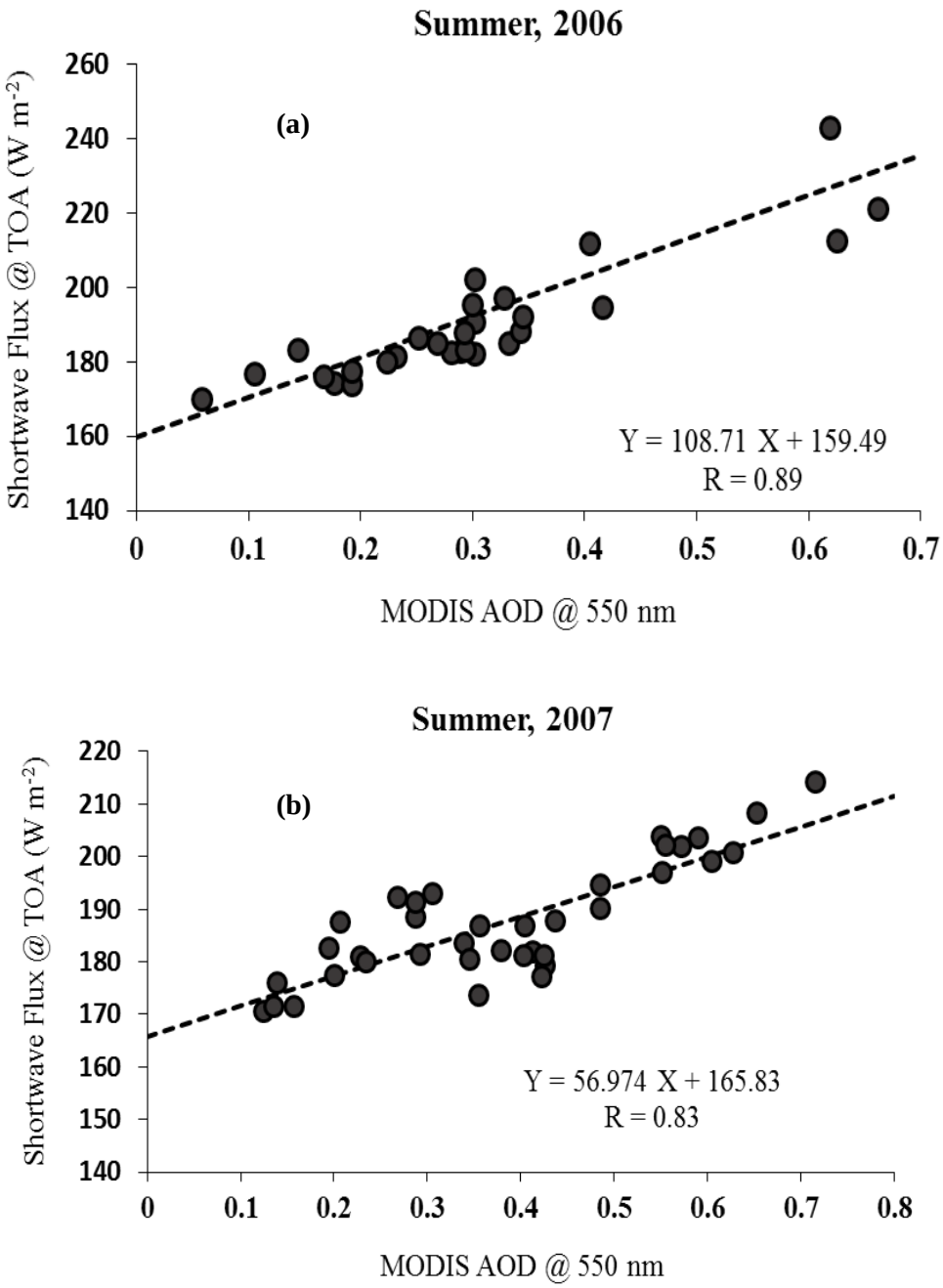

Figure 5.8. CERES shortwave flux at the top of the atmosphere and the MODIS sensor-retrieved total atmospheric column aerosol optical depth for nucleation days in (a) summer 2006 and (b) summer 2007 are shown averaged for the 0.35° x 0.35° grid box over the Duke Forest site.

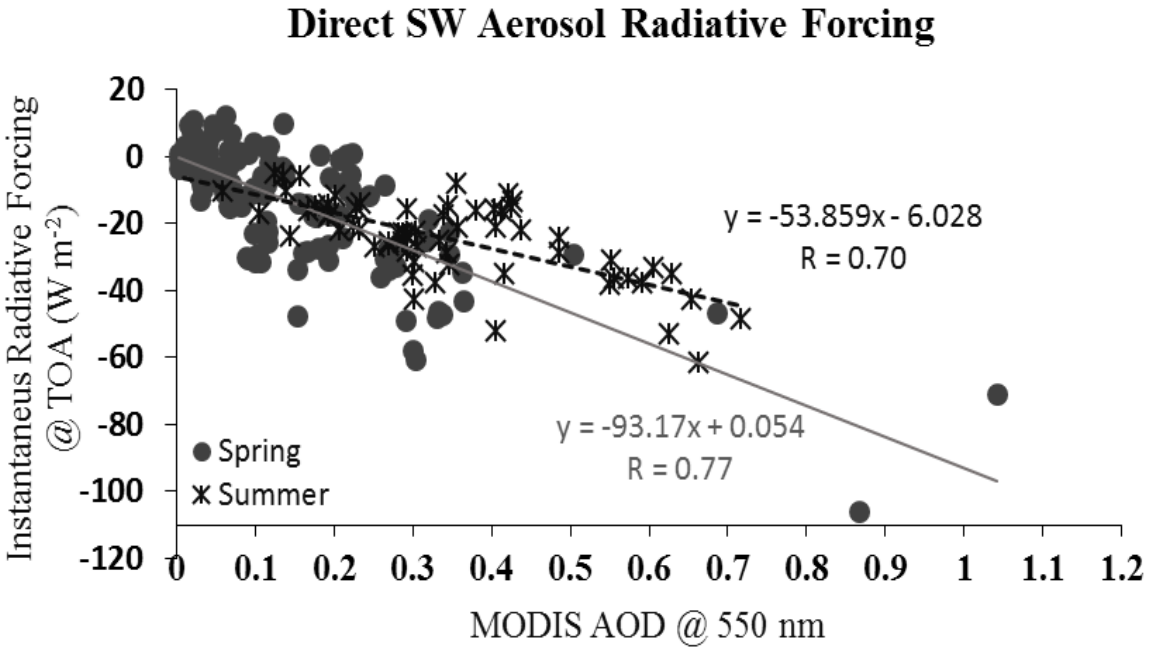

Figure 5.9. The estimated TOA shortwave aerosol radiative forcing as a function of MODIS sensor-retrieved total atmospheric column aerosol optical depth as observed on particle nucleation days during spring (filled gray circles) and summer (asterisks) are shown for a 0.35° x 0.35° grid which covers the Duke Forest site.

The shortwave aerosol direct radiative forcing at the TOA is shown in Figure 5.9 as a function of MODIS-derived AOD at 550 nm for summer and spring during 2006 and 2007. During summer, the seasonal average nucleation day instantaneous radiative forcing is -24 ± 11 Wm^{-2} and during spring, the estimated forcing is -15 ± 19 Wm^{-2}. Although the average aerosol optical depth in spring is lower than the average aerosol optical depth in the summer, a significant aerosol radiative forcing is estimated for spring. The

instantaneous direct shortwave aerosol radiative forcing efficiency of the nucleation day aerosol is -54 Wm^{-2} per unit per 550 nm AOD in summer and -93 Wm^{-2} per 550 nm AOD in spring. During this study period, the average forcing efficiency by particles formed during regional nucleation events is -73 Wm^{-2} per AOD. The higher forcing efficiency observed at our site during spring indicates more effectively scattering aerosols as compared to summer aerosols, pointing to differences in the extinction characteristics of the nucleated particles between spring and summer. These differences may be due to higher BVOC emissions during the summer months (Geron, 2011) when the foliage is well developed and PAR is the highest. Sena et al. (2013) studied the shortwave aerosol radiative budget in the Amazon region over the thick forested areas and over a deforested area in the Amazon region. They observed maximum daily shortwave direct radiative forcing as large as -20 Wm^{-2} locally for high biomass aerosol loadings. During their study, the biomass aerosol loading over the thick forested areas resulted in greater negative values for the average daily radiative forcing efficiencies (-15.7 ± 2.4 Wm^{-2} per 550 nm AOD) as compared to savannah-like areas (-9.3 ± 1.7 Wm^{-2} per 550 nm AOD).

The correlation of MODIS AOD at 550 nm with the ambient sulfur dioxide concentration and the particulate matter organic carbon for spring and summer is shown in Figure 5.10. During both spring and summer, we observed no clear association between AOD and nitric oxide or nitrogen dioxide. We observed a positive correlation between $PM_{2.5}$ (organic) and MODIS AOD in the summer months (R = 0.54). However, there is a negative correlation between SO_2 and AOD during both spring (R = 0.76) and summer (R

= 0.43). In the diurnal profile, the observed increase in SO_2 concentrations after sunrise is consistent with downward mixing of SO_2 from aloft, accompanied with the breakdown of the nocturnal boundary layer (Pillai et al., 2013). The early morning peaks in SO_2 concentration are observed prior to the onset of nucleation, particularly during warmer months when the oxidizing capacity of the atmosphere is favorable. The daily mean SO_2 concentrations are 1.80 ± 1.3 ppb and 2.6 ± 1.5 ppb in spring and summer, respectively. We also observed a positive correlation between nucleation mode particles and SO_2 in the initial couple of hours at the start of the nucleation events. As the particle number concentration increased, the concentration of SO_2 decreased. These patterns suggest H_2SO_4-mediated nucleation at the site during warmer months. In addition, warmer months are associated with the onset of nucleation in the early morning. Therefore, at the time of the satellite overpass, the particle number concentration increased significantly and ambient SO_2 concentration decreased significantly. In addition, in summer, the presence of gas phase organic compounds may promote intense growth of these H_2SO_4-nucleated particles, and therefore we observe a strong positive correlation between AOD and OC in the $PM_{2.5}$. However, during spring there is no clear association between OC and AOD, but a strong negative correlation (logarithmic) between SO_2 and AOD, suggesting a prominent role of SO_2 in nucleation as well as growth of particles during spring.

Laaksonen et al. (2008) suggested that an exponential relationship exists between the particle formation rates and temperature because the saturation vapor pressure of the condensing vapors is exponentially related to the temperatures. Limbeck et al. (2003)

showed the formation of secondary aerosol polymers owing to the heterogeneous reaction between the oxidation products of BVOCs (isoprene or terpenoids) and the acidic aerosols (sulfuric acid) in the continental atmosphere. Geron (2009) revealed the significant role of the oxidation products of biogenic volatile organic carbon in the organic $PM_{2.5}$ at the Duke Forest site. As compared to spring, during summer, the association between $PM_{2.5}$ (organic) and AOD further suggests the role of biogenic volatile organic species (BVOC) in the growth of the nucleated particles at the site.

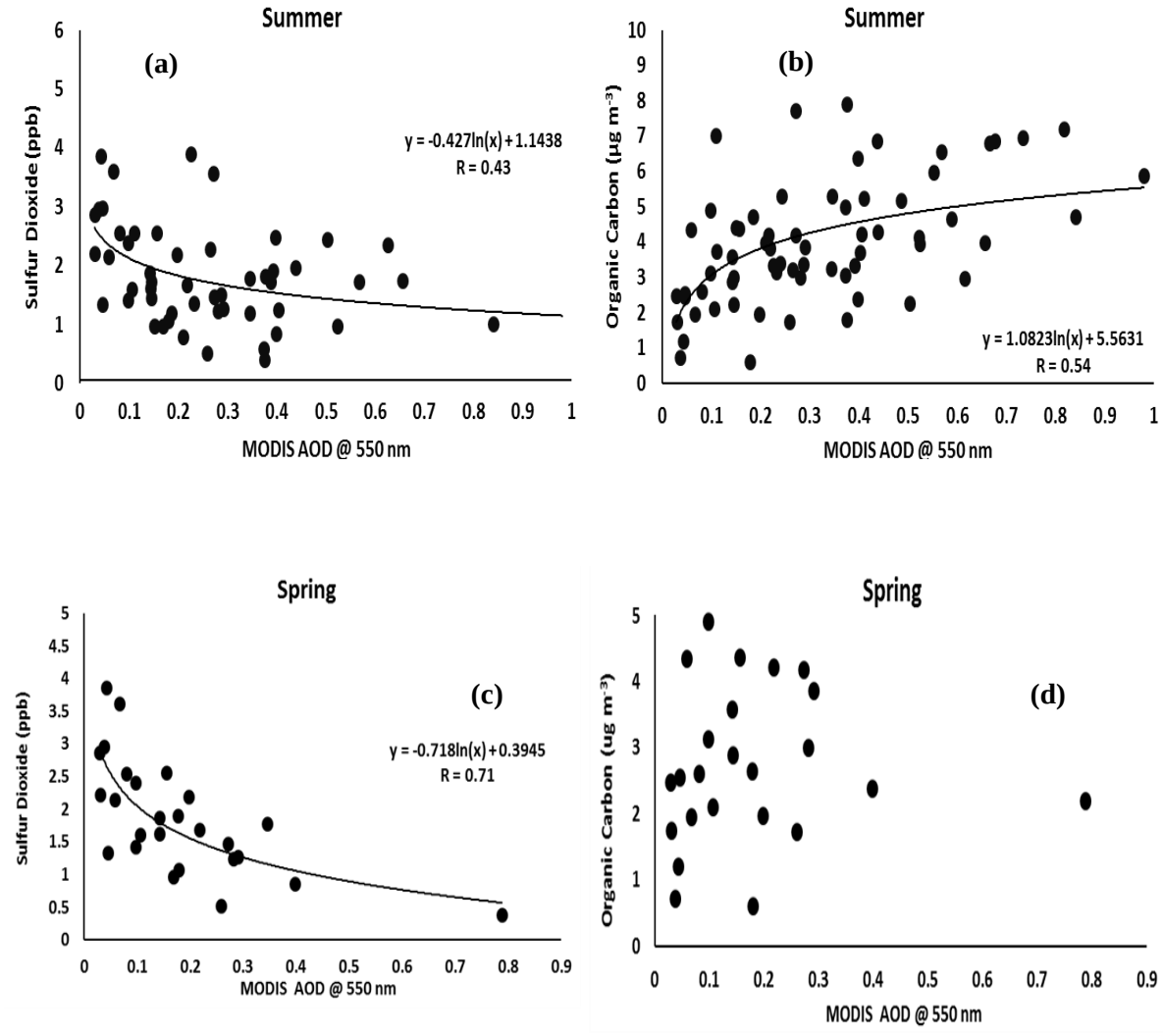

Figure 5.10. The relationship between ambient sulfur dioxide concentration and the particulate matter organic carbon with MODIS AOD at 550 nm during (a) summer, 2006, (b) summer, 2007, (c) spring, 2006, and (d) spring, 2007, are shown.

At the Duke Forest site, the regional nucleation events are observed on cloud-free days with intense photosynthetically active radiation. The role of photochemistry along with the morning peaks in SO_2 concentrations observed during these regional nucleation events points to the H_2SO_4-mediated nucleation at the Duke Forest site during spring and summer. In addition, BVOCs play a significant role in the organic $PM_{2.5}$ at the site, especially during summer months, as compared to spring. Based on MODIS land surface reflectance at 470 nm, we observed slightly lower surface reflectance in spring (0.127) than in summer (0.134). By combining these factors, we expect larger negative radiative forcing during spring than in summer. During the spring season when there is the strongest negative correlation between SO_2 and AOD, we estimated -93 Wm^{-2} radiative forcing efficiency at the site. However, in summer, when both SO_2 and BVOC species are abundant, the instantaneous shortwave radiative forcing efficiency is -54 Wm^{-2}. To our knowledge, this is the first study that attempts to derive the radiative forcing owing to particles formed during regional nucleation events over a forest canopy.

5.4. Conclusions

Multiyear observations of particle size distribution revealed frequent new particle formation at the Duke Forest site in Chapel Hill, NC. These nucleation events were observed to contribute significantly to the nucleation mode and fine mode particle number concentration at the site and therefore necessitate the estimation of the perturbation in radiation owing to the regional nucleation events. The focus of our study is to understand the role of these frequent nucleation events in the shortwave radiative balance at the Duke Forest site for different seasons. Therefore, we attempt to estimate the top of the atmosphere direct shortwave aerosol radiative forcing for spring and summer when the aerosol loading is high. By confining our radiative forcing calculations to each season, we are able to account for the effect of albedo changes over the forest canopy by assuming no changes in surface albedo over the selected forest canopy during that particular season in that particular year. To estimate the role of regional nucleation events on aerosol shortwave radiative forcing, in this study we excluded Class C nucleation events that showed local nucleation characteristics. Also, selecting only regional nucleation events in the radiative forcing calculation gave additional confidence in our assumption that only aerosol species with similar extinction properties are included in this calculation.

The top of the atmosphere SW flux is highest (188 ± 22 Wm^{-2}) in summer when the aerosol optical depth (0.38 ± 0.20) and the seasonal average particle growth rate are highest. The AOD (0.06 ± 0.05) is lowest during winter months when the particle growth

rate is the lowest. In winter months nucleation days are associated with delayed onset of nucleation. In winter, lower values of AOD and particle growth rate along with the delayed nucleation onset might have contributed to the observed poor correlation between TOA SW flux and AOD. In spring and summer months, we observed good correlation between TOA SW Flux and AOD for the estimation of clear sky flux. In spring, the nucleation day SW fluxes are 158 ± 11 Wm^{-2} and 163 ± 22 Wm^{-2} and AOD are 0.15 ± 0.09 and 0.16 ± 0.18, respectively, for 2006 and 2007. Due to the increased aerosol loading and the intense incoming shortwave radiation, average summer AOD is 0.34 ± 0.15 and SW flux is 187.70 ± 11.46 Wm^{-2}. In the spring, the instantaneous shortwave radiative forcing is -15 ± 19 Wm^{-2} and in the summer, the nucleation day instantaneous shortwave radiative forcing is -24 ± 11 Wm^{-2}. The photosynthetically active radiation along with the morning peaks in SO_2 concentrations observed during regional nucleation events suggests H_2SO_4-mediated nucleation at the Duke Forest site during spring and summer. The higher radiative forcing efficiency observed during the spring compared to the summer may be attributed to the following factors: (i) lower scattering efficiency in summer due to biogenic volatile organic carbon in the $PM_{2.5}$ and (ii) lower surface reflectance, i.e., MODIS-derived land surface reflectance at 470 nm is lower during spring (0.127) than in summer (0.134). The estimated 550 nm instantaneous radiative forcing efficiency over the Duke Forest site in spring is -93 Wm^{-2} and in summer is -54 Wm^{-2}. During spring and summer of 2006 and 2007, the estimated average instantaneous forcing efficiency at the Duke Forest site was -73 Wm^{-2}. From this study, it is evident that the frequent nucleation events at the Duke Forest site are associated with significant direct

shortwave negative radiative forcing. Furthermore, this study shows the potential of integrating global scale satellite retrievals with ground-based observations in quantifying the direct radiative impact of regional nucleation events. Even though the direct role of aerosols in radiative interactions are well characterized, aerosols continue to contribute the largest uncertainties to the estimation of total radiative forcing and these uncertainties arise from the poor characterization of aerosols in climate models (IPCC, 2014). Therefore, the current study should be extended to different regions of the globe where regional-scale new particle formation is frequent and contributes significantly to the atmospheric particle size distribution.

REFERENCES

Boy, M., T. Karl, A. Turnipseed, R. L. Mauldin, E. Kosciuch, J. Greenberg, J. Rathbone, J. Smith, A. Held, K. Barsanti, B. Wehner, S. Bauer, A. Wiedensohler, B. Bonn, M. Kulmala, and A. Guenther (2008), New particle formation in the front range of the Colorado Rocky Mountains, *Atmospheric Chemistry and Physics Discussions, 7,* 15581-15617, doi:10.5194/acp-8-1577-2008.

Boucher, O., and L. A. Theodore (1995), General circulation model assessment of the sensitivity of direct climate forcing by anthropogenic sulfate aerosols to aerosol size chemistry, *Journal of Geophysical Research*, 100, 26,117– 26,134.

Bryant, R., J. Qi, M. S. Moran, and W. Ni (2003), Comparison of BRDF models with a fuzzy inference system for correction of bidirectional effects. *Remote Sensing of the Environment, 88,* 221-232, doi: 10.1016/S0034-4257(03)00072-5

Dal Maso, M., M. Kulmala, I. Riipinen, R. Wagner, T. Hussein, P. P. Aalto, and K. E. J. Lehtinen (2005), Formation and growth rates of fresh atmospheric aerosols: eight years of aerosol size distribution data from SMEARII, Hyytiala, Finland, *Boreal Environmental Research, 10,* 323–336, doi: doi: 10.1029/2001JD001053.

Engel-Cox J. A., C. H. Holloman, B. W. Coutant, and R.M. Hoff (2004), Qualitative and quantitative evaluation of MODIS satellite sensor data for regional and urban scale air quality, *Atmospheric Environment* , 38, 2495–2509, doi:10.1016/j.atmosenv.2004.01.039.

Geron, C. (2009), Carbonaceous aerosol over a pinus taeda forest in central North Carolina, USA, *Atmospheric Environment, 43,* pp. 659-969, doi: 10.1016/j.atmosenv.2008.10.053.

Geron, C. (2011), Carbonaceous aerosol characteristics over a Pinus taeda plantation: Results from the CELTIC experiment, *Atmospheric Environment, 45,* 794–801, doi: 10.1016/j.atmosenv.2010.07.015.

Gupta, P., S.A. Christopher, J. Wang, R. Gehrig, Y. Leed, and N. Kumar (2006), Satellite remote sensing of particulate matter and air quality assessment over global cities, *Atmospheric Environment* , 40, 5880 – 5892, doi: 10.1016/j.atmosenv.2006.03.016

Haywood, J. M. and O. Boucher (2000), Estimates of the direct and indirect radiative forcing due to tropospheric aerosols: A review, *Reviews of Geophysics, 38,* 513–543, doi: 10.1029/1999RG000078.

Haywood, J. M., and K.P. Shine (1997), Multi-spectral calculations of the radiative forcing of tropospheric sulphate and soot aerosols using a column model, *Q. Journal of the Royal Meteorological Society., 123,* 1907–1930, doi: 10.1002/qj.49712354307.

IPCC (2014), Summary for Policymakers. In: Climate Change (2014), Impacts, Adaptation, and Vulnerability. Part A: Global and Sectoral Aspects. Contribution of Working Group II to the Fifth Assessment Report of the Intergovernmental Panel on Climate Change. Field, C.B., V.R. Barros, D.J. Dokken, K.J. Mach, M.D. Mastrandrea, T.E. Bilir, M. Chatterjee, K.L. Ebi, Y.O. Estrada, R.C. Genova, B. Girma, E.S. Kissel, A.N. Levy, S. MacCracken, P.R. Mastrandrea, and L.L. White (*Eds.*). Cambridge University Press, Cambridge, United Kingdom and New York, USA, pp. 1-32.

Korhonen, P., M. Kulmala, A. Laaksonen, Y. Viisanen, R. McGraw, and J. H. Seinfeld (1999), Ternary nucleation of H_2SO_4, NH_3 and H_2O in the atmosphere, *Journal of Geophysical Research, 104,* 349–26, doi: 10.1029/1999JD900784

Kulmala, M., and A. Laaksonen (1990), Binary nucleation of water sulfuric acid system. Comparison of classical theories with different H_2SO_4 saturation vapor pressures, *Journal of Chemical Physics, 93,* 696-701, doi: 10.1063/1.459519.

Kulmala, M., P. Korhonen, I. Napari, A. Karlsson, H. Berresheim, and C. D. O'Dowd (2002), Aerosol formation during PARFORCE: Ternary nucleation of H_2SO_4, NH_3, and H_2O, *Journal of Geophysical Research*, 107(D19), 8111.

Kulmala, M., H. Vehkamäki, T. Petäjä, M. Dal Maso, A. Lauri, V. M. Kerminen, W. Birmili, and P. H. McMurry (2004), Formation and growth rates of ultrafine atmospheric particles: a review of observations, *Journal of Aerosol Science, 35*, 143-176, doi: 10.1016/j.jaerosci.2003.10.003.

Laaksonen, A., M. Kulmala, C. D. O'Dowd, J. Joutsensaari, P. Vaattovaara, S. Mikkonen, K. E. J. Lehtinen, L. Sogacheva, M. Dal Maso, P. Aalto, T. Petäjä, A. Sogachev, Y. J. Yoon, H. Lihavainen, D. Nilsson, M. C. Facchini, F. Cavalli, S. Fuzzi, T. Hoffmann, F. Arnold, M. Hanke, K. Sellegri, B. Umann, B., W. Junkermann, H. Coe, J. D. Allan, M. R. Alfarra, D. R. Worsnop, M. L. Riekkola, T. Hyötyläinen, and Y. Viisanen (2008), The role of VOC oxidation products in continental new particle formation, *Atmospheric Chemistry and Physics, 8*, 2657–2665, doi:10.5194/acp-8-2657-2008.

Levy, R. C., L. A. Remer, R. G. Kleidman, S. Mattoo, C. Ichoku, R. Kahn, and T. F. Eck (2010), Global evaluation of the collection 5 MODIS dark-target aerosol products over land, *Atmospheric Chemistry and Physics, 10*, 10399–10410, doi:10.5194/acp-10-10399-2010.

Limbeck, A., M. Kulmala, and H. Puxbaum (2003), Secondary organic aerosol formation in the atmosphere via heterogeneous reaction of gaseous isoprene on acidic particles, *Geophysical Research Letters, 30,* 1996, doi:10.1029/2003GL017738.

Liu, Y., Z. Wang, J. Wang, R. A. Ferrare, R. K. Newsom, and E. J. Welton (2011), The effect of aerosol vertical profiles on satellite-estimated surface particle sulfate concentrations, *Remote Sensing of the Environment, 115*(2), 508-513.

Loeb, N. G., S. Kato, K. Loukachine, and N. Manalo-Smith (2005), Angular distribution models for top-of-atmosphere radiative flux estimation from the Clouds and the Earth's Radiant Energy System instrument on the Terra satellite. Part I: Methodology, *Journal of Atmospheric and Oceanographic Technology, 22*, 338–351, doi:10.1175/JTECH1712.1.

Loeb, N. G., S. Kato, K. Loukachine, N. Manalo-Smith, and D. R. Doelling (2007), Angular distribution models for top-of-atmosphere radiative flux estimation from the Clouds and the Earth's Radiant Energy System instrument on the Terra satellite. Part II: Validation, *Journal of Atmospheric and Oceanographic Technology*, 24, 564–584, doi:10.1175/JTECH1983.1.

Loeb, N.G., K. J. Priestley, D. P. Kratz, E. B. Geier, R. N. Green, B. A. Wielicki, P. O. R. Hinton, and S. K. Nolan (2001), Determination of unfiltered radiances from the Clouds

and the Earth's Radiant Energy System (CERES) instrument. *Journal of Applied Meteorology*, *40*, 822–835, doi: 10.1175/1520-0450.

Luo, G. and F. Yu (2011), Simulation of particle formation and number concentration over the Eastern United States with the WRF-Chem + APM model, *Atmospheric Chemistry and Physics*, 11, 11521-11533, doi:10.5194/acp-11-11521-2011.

Marti, J. J., R. J. Weber, P. H. McMurry, F. Eisele, D. Tanner, and A. Jefferson (1997), New particle formation at a remote continental site: Assessing the contributions of SO_2 and organic precursors, *Journal of Geophysical Research, 102*, 6331–6339, doi: 10.1029/96JD02545.

Mei, L., Y. Xue, G. de Leeuw, J. Guang, Y. Wang, Y. Li, H. Xu, L. Yang, T. Hou, X. He, C. Wu, J. Dong, and Z. Chen (2011), Integration of remote sensing data and surface observations to estimate the impact of the Russian wildfires over Europe and Asia during August 2010, *Biogeosciences, 8,* 3771-3791, doi:10.5194/bg-8-3771-2011, 2011.

Merikanto, J., I. Napari, I., H. Vehkama¨ki, T. Anttila, and M. Kulmala (2007), New parameterization of sulfuric acid ammonia-water ternary nucleation rates at tropospheric conditions. *Journal of Geophysical Research, 112*, D15207. doi: 10.1029/2006JD007977.

Meywerk, J., and V. Ramanathan (1999), Observations of the spectral clear sky aerosol forcing over the tropical Indian Ocean, *Journal of Geophysical Research*, 104, 24,359-24,370, doi: 10.1029/1999JD900502

Nel, A. (2005), Air pollution-related illness: effects of particles, *Science*, *308*, 804–806, doi: 10.1126/science.1108752.

Patadia F., P. Gupta, S. A. Christopher (2008), First observational estimates of global clear sky shortwave aerosol direct radiative effect over land, *Geophysical Research Letters*, 35, L04810, doi: 10.1029/2007GL032314.

Pillai, P., A. Khlystov, J. Walker, V. Aneja (2013), Observation and analysis of particle nucleation at a forest site in the southeastern US, *Atmosphere, 4*, 72-93; doi:10.3390/atmos4020072.

Pope, C., M. Ezzati, and D. Dockery, (2009), Fine-particulate air pollution and life expectancy in the United States, *New England Journal of Medicine, 360*, 376-86, doi: 10.1056/NEJMsa0805646.

Pryor S.C., A. M. Spaulding, and R. J. Barthelmie (2010), New particle formation in the midwestern USA: Event characteristics, meteorological context and vertical profiles, *Atmospheric Environment, 44*, 4413-4425, doi: 10.1016/j.atmosenv.2010.07.045.

Qian, S., H. Sakurai, and P. H. McMurry (2007), Characteristics of regional nucleation events in urban East St. Louis, *Atmospheric Environment , 41,* 4119–4127.

Ramanathan, V., P.J. Crutzen, J.T., Kiehl, and D. Rosenfeld, 2001: Aerosols, climate, and the hydrological cycle, *Science, 294,* 2119–2124, doi:10.5194/acp-8-1577-2008.

Satheesh, S. K., and V. Ramanathan (2000), Large differences in the tropical aerosol forcing at the top of the atmosphere and Earth's surface, *Nature, 405,* 60–63, doi :10.1038/35011039.

Satheesh, S. K., V. Ramanathan, B. N. Holben, K. K. Moorthy, N. G. Loeb, H. Maring, J. M. Prospero, and D. Savoie (2002), Chemical, microphysical, and radiative effects of Indian Ocean aerosols, *Journal of Geophysical Research, 107,* D23, 4725, doi: 10.1029/2002JD002463.

Sena, E. T., P. Artaxo, and A. L. Correia, (2013), Spatial variability of the direct radiative forcing of biomass burning aerosols and the effects of land use change in Amazonia, *Atmospheric Chemistry and Physics, 13,* 1261–1275, doi:10.5194/acp-13-1261-2013.

Seinfeld J. H. and S. N. Pandis (2006), Atmospheric Chemistry and Physics: From Air Pollution to Climate Change, 2nd edition, J. Wiley, New York. ISBN: 978-0-471-72018-8.

Spracklen, D. V., K. S. Carslaw, M. Kulmala, V.-M. Kerminen, S.-L.Sihto, I. Riipinen, J. Merikanto, G. W. Mann, M. P. Chipperfield, A. Wiedensohler, W. Birmili, and H. Lihavainen (2008), Contribution of particle formation to global cloud condensation nuclei concentrations, *Geophysical Research Letters*, 35, L06808, doi:10.1029/2007GL033038.

Stratmann, F., H. Siebert, G. Spindler, B. Wehner, B., D. Althausen, J. Heintzenberg, O. Hellmuth, O., R. Rinke, U. Schmieder, C. Seidel, T. Tuch, U. Uhrner, A. Wiedensohler, U. Wandinger, M. Wendisch, D. Schell, and A. Stohl (2003), New-particle formation events in a continental boundary layer: first results from the SATURN experiment, *Atmospheric Chemistry and Physics*, *3*, 1445-1459, doi: 10.5194/acpd-3-1693-2003

Stroud, C.A., A. Nenes, J. L. Jimenez, P. F. DeCarlo, J. A. Huffman, R. Bruintjes, E. Nemitz, A. E. Delia, D. W. Toohey, A. B. Guenther, and S. Nandi (2007), Cloud activating properties of aerosol observed during CELTIC, *Journal of the Atmospheric Sciences*, *64*, 441–459, doi: 10.1175/JAS3843.1

Torres, O., A. Tanskanen, B. Veihelmann, C. Ahn, R. Braak, P. K. Bhartia, P. Veefkind, and P. Levelt (2007), Aerosols and surface UV products from ozone monitoring

instrument observations: An overview, *Journal of Geophysical Research*, 112, D24S47, doi:10.1029/2007JD008809.

Wielicki, B. A., B. R. Barkstrom, E. F. Harrison, R. B. Lee, G. L. Smith, and J. E. Cooper (1996), Clouds and the Earth's Radiant Energy System (CERES): An earth observing system experiment, *Bulletin of the American Meteorological Society*, *77*(**5**), 853-868, doi: 10.1175/1520-0477(1996)077<0853:CATERE>2.0.CO;2

Yu, F. and G. Luo (2009), Simulation of particle size distribution with a global aerosol model: contribution of nucleation to aerosol and CCN number concentrations, *Atmospheric Chemistry and Physics*, 9, 7691– 7710, doi:10.5194/acp-9-7691-2009.

Yu, F., G. Luo, and X. Ma (2012), Regional and global modeling of aerosol optical properties with a size, composition, and mixing state resolved particle microphysics model. *Atmospheric Chemistry and Physics*, 12(13), 5719-5736.

Yu, F., and R. P. Turco (2000), Ultrafine aerosol formation via ion-mediated nucleation, *Geophysical Research Letters*, *27*, 6, 883–886, doi: 10.1029/1999GL011151.

Yu, F., Z. Wang, G. Luo, and R. P. Turco (2008), Ion-mediated nucleation as an important source of tropospheric aerosols, *Atmospheric Chemistry and Physics*, 8, 2537-2554.

Zhuang, H., C. K. Chan, M. Fang, and A. S. Wexler (1999), Size distributions of particulate sulfate, nitrate, and ammonium at a coastal site in Hong Kong. *Atmospheric Environment*, *33*, 843-853, doi: 10.1016/S1352-2310(98)00305-7.

Chapter 6

6. CONCLUSIONS AND FUTURE DIRECTIONS

The perturbations in the radiative balance of the atmosphere can take place as a result of natural or anthropogenic activities. Two important components responsible for these perturbations are greenhouse gases and atmospheric aerosols. This two-part thesis attempts to quantify the role of these two components in the regional climate of the southeastern U.S.

Because of the increasing energy demands, the production of biofuels is increasing in the U.S. (U.S. RFS, 2010). As a result, the intense agricultural activities and associated management practices associated with biofuel production (i.e., land use change, tillage operations, N - fertilization and irrigation) may lead to enhanced N_2O emissions. Agriculture is the highest individual contributor to this third most potent well-mixed greenhouse gas. Because of the variability in the nutrient uptake efficiency, tillage and irrigation requirements among crops, the N_2O emissions associated with biofuel production strongly depend on the type of crop used. These factors therefore emphasize the importance of the selection of region specific crop varieties that require minimal fertilizer and water inputs. In the U.S., the corn is the current major biofuel crop with ~40% of total corn produced being converted to biofuel (Song et al., 2015). Multiple studies have investigated the regional adaptability (in terms of nutrient uptake efficiency,

water usage and biomass yield) of switchgrass, a potential biofuel crop, in North Carolina and other states in the southeastern U.S. (Fike et al., 2006; Mitchell et. al., 2008; Palmer et al, 2014). However, the current study is unique as it quantified the N_2O emission factor from corn, the current major crop, and switchgrass, the potential crop, relevant to the biofuel production in North Carolina and other states in the southeastern U.S.

The importance of this study in the context of earth's radiative balance is portrayed in Chapter 1. The scientific background on N_2O emissions from the soil was discussed in Chapter 2. The important factors affecting the soil N-cycle and the most relevant findings from previous studies were also discussed this chapter. Chapter 3 elucidates the experimental setup, N_2O chamber sampling procedures, sample processing and N_2O flux calculation. The role of N-fertilizer application rate, soil moisture, soil temperature, and soil inorganic N relative to N_2O emissions was quantified and discussed for both crop types. The response of corn and switchgrass to N-fertilization and the aforementioned environmental or soil variables are also compared in this chapter. In addition, for both the crops, we estimated the N_2O emission factor as a function N-fertilization rate. In corn soils, emission factors ranged from 1.65 ± 0.87 % to 4.33 ± 3.56 % between lowest (60 kg N ha^{-1} yr^{-1}) and highest (180 kg N ha^{-1} yr^{-1}) fertilization rates, respectively. Our study, based on observed N_2O emissions and crop yield, showed that switchgrass can be a potential biofuel feedstock at least in North Carolina.

The inferences drawn from our study warrant the urgent need for additional region specific studies to fill the large information gaps in the GHG emissions and biomass production from biofuel crops. These N_2O observations may be used to parameterize biogeochemical models to study the environmental impact of different N_2O emission scenarios associated with biofuel production. Moreover, the huge spatial and temporal variations in the GHG emissions associated with biofuel production additionally demand a well updated emission inventory and life cycle assessment (LCA) of crops relevant to bio-energy production. In this study, as N-fertilization rate increased, the emission factor for both the crops became greater than the IPCC suggested 1% direct emission factor. The preparation of a regionally specific, accurate emission inventory therefore is crucial in the LCA studies attempting to fill the information gaps on the environmental impacts of crops (including but not limited to land use change, crop variety, regional adaptability, response to N-fertilization rate and other management practices) associated with biofuel production.

In the second part of this thesis, the associations between regional nucleation events and the radiative balance at the southeastern forest site, Duke Forest, Chapel Hill, North Carolina was studied. Particle size distributions (aerodynamic diameter, D_p 10.2 nm to 250 nm), total number concentrations of nucleation mode ($D_p < 25$ nm) and fine mode ($25 < D_p < 250$ nm) particles, and particle growth rates were used to identify regional nucleation events during November 2005 to September 2007 (Pillai et al., 2013). The top of the atmosphere shortwave aerosol direct radiative forcing (SWARF) by these regionally

nucleated particles was calculated using satellite based shortwave flux and aerosol depth at 550 nm.

The significance of regional nucleation events at Duke Forest in the context of regional climate was investigated in Chapter 4. Chapter 5 elucidates the frequent nucleation events occurring over this region and further quantifies the shortwave aerosol radiative forcing induced by these events. In this unique approach we combined the particle size distribution information drawn from multi-year ground based observations to the aerosol optical depth and flux from satellites. To our knowledge, there are no studies conducted in the past in the U.S. to identify the role of regional nucleation events in direct shortwave aerosol radiative forcing.

Despite the higher radiative forcing observed in summer, the radiative forcing efficiency was lower (-54 Wm^{-2}, τ_{550}^{-1}) in summer. The results show that, during spring and summer 2006 and 2007, there is significant forcing efficiency associated with regionally nucleated aerosols. Formations of particles during regional nucleation events introduced significant radiative forcing and need to be examined for other regions of the globe where intense regional nucleation events occur frequently.

REFERENCES

Fike, J.H., Parrish, D. J., Wolf, D. D., Balasko, J. A., Green Jr., J. T., Rasnake, M., Reynolds, J. H., 2006. Switchgrass production for the upper southeastern USA: influence of cultivar and cutting frequency on biomass yields. *Biomass and Bioenergy*, 30:207-213.

Mitchell, R., Vogel, K.P. and Sarath, G., 2008. Managing and enhancing switchgrass as a bioenergy feedstock. *Biofuels, Bioproducts and Biorefining*, 2(6), pp.530-539.

Palmer, I.E., Gehl, R.J., Ranney, T.G., Touchell, D. and George, N., 2014. Biomass yield, nitrogen response, and nutrient uptake of perennial bioenergy grasses in North Carolina. *Biomass and Bioenergy*, 63, pp.218-228.

Pillai, P., Khlystov, A., Walker, J. and Aneja, V., 2013. Observation and analysis of particle nucleation at a forest site in southeastern US. *Atmosphere*, *4*(2), pp.72-93.

Song, Y., Jain, A.K., Landuyt, W., Kheshgi, H.S. and Khanna, M., 2015. Estimates of biomass yield for perennial bioenergy grasses in the USA. *BioEnergy Research*, 8(2), pp.688-715.

U.S. RFS. Regulation of Fuels and Fuel Additives: Changes to Renewable Fuel Standard Program; Final Rule. *Federal Register*. March 26, 2010. 75,pp.14670-14904.

Appendix

Particulate Matter Pollution in the Coal-Producing Regions of the Appalachian Mountains: Integrated Ground Based Measurements and Satellite Analysis

A1. Introduction

The Appalachian Mountains encompass regions with rich coal deposits. The controversial coal mining practice in the region, of stripping off the tops of mountains, is causing both air (Aneja et al., 2012) and water (Palmer et al., 2010; Gilbert, 2010) pollution problems. For efficient extraction of coal, temperate deciduous forests are cleared, topsoil is stripped off, and overburden and interburden rocks are broken apart and removed from above and between coal seams (Palmer et al., 2010). The excess rocks and dirt that do not fit back onto the disturbed ridgeline is dumped into adjacent valleys where it buries headwater streams (Office of Surface Mining Reclamation and Enforcement, 2010). As a consequence, the downstream water quality gets deteriorated (Hendryx and Ahern, 2009). The environmental issues associated with mountaintop mining with valley fills include disturbances in the biological communities and their physical environments. These disturbances in the ecosystem balance are associated with biodiversity loss, erosion, soil and water contamination, and particulate matter pollution (Palmer et al., 2010). As a result of the stress on the natural environment caused by these mining activities, the health and welfare of the surrounding human populations are adversely affected (Ahren et al., 2011;

EPA, 2009). However, the impacts of surface coal mining on air quality have only been sparsely addressed (Aneja et al., 2012) and, therefore, require comprehensive and systematic monitoring and analysis.

The activities associated with surface coal mining, including topsoil removal, drilling, blasting, coal handling operations, coal hauling, transportation and dumping of overburden, along with wind erosion of exposed surface, all inject particulate matter (PM) into the atmosphere. Major air pollutants near the surface coal mines were total suspended particulate matter and respirable particulate matter (Gose and Majee, 2000; Gose and Majee, 2007). The emission inventory for the Greater Metropolitan Region of the New South Wales, Australia, reported that the coal mining industry was the largest industrial emitter of fine particles, particles with aerodynamic diameter $\leq$ 10 μm, PM_{10} (~34% of total anthropogenic emissions) and particles with aerodynamic diameter $\leq$ 2.5 μm, $PM_{2.5}$ (~14%) in 2008. Gose, 2007, reported that drilling operations and wind erosion of coal stockpiles were respectively the two major dust sources in the mining area. Vehicular traffic on haul roads were identified as the largest source of fugitive dust, and can even contribute to 80% of total dust emission (Gose, 2007). The complex topography of the region often lead residents to build their houses very close to coal mine haul roads (Aneja et al., 2012). Coal hauling trucks entrain the temporal buildup of pollutants owing to reduced ventilation of these particulate emissions. PM in the atmosphere has a strong statistical correlation with increased hospitalization, emergency room visits and self-dosage by asthma patients (HEI, 2004). According to the World Health Organization Air

Quality Guidelines 2005 (WHO AQG 2005), public authorities should take actions at the regional, national, and international levels to reduce human exposure to these air pollutants. Analysis of live births during 1996 - 2003 in the four states in the Central Appalachian region – Kentucky (KY), Tennessee (TN), Virginia (VA), and West Virginia (WV) – identified that both socioeconomic and environmental disturbances in mountaintop mining areas may be the major factors contributing to the elevated birth defect rates (Ahern et al., 2011).

Aneja et al., 2012 conducted the particulate matter measurements at Campbell (mine site) and at Willis, a Roda community that live in the narrow hollows with their homes placed directly along the roads. These narrow hollows are located immediately below the mountains and between the mountain tops (Kurth et al., 2015). Proximity to the roads having heavy traffic of the coal hauling trucks and the poor ventilation owing to the complex topography of the region both add severity in the air quality problem of the region. Aneja et al. in 2012 identified coal hauling as the major contributor to the PM_{10} in the Roda community. The levels of respirable particulate matter were up to three times the National Ambient Air Quality Standard (NAAQS) of 150μg m^{-3} (Aneja et al., 2012). In agreement with Gose, 2006, Aneja et al., 2012, also suggested trucks carrying materials from mining site as the major contributor to elevated levels of particulate matter in the Appalachian region. Based on their study, even though the particulate matter pollution in the eastern United States has reduced significantly over the last 30 years, the observed PM_{10} mass concentration in Roda, VA, which is representative of the Appalachian coal

mining region, showed significant PM_{10} levels compared to major cities in the Eastern United States. The same study also revealed the presence of antimony, arsenic, beryllium, cadmium, chromium, cobalt, lead, manganese, mercury, nickel, and selenium in the collected samples from both Campbell and Willis (a group of metals identified as toxic or potentially toxic by the U.S. EPA National Ambient Air Toxics program). Moreover, all of these metals present in the Roda samples were known to be present in coal (Finkelman, 1995). Many states have adopted strategies or control measures, which were typically included within the State Implementation Plans (SIPs) adopted pursuant to the Clean Air Act, to limit emissions of criteria air pollutants such as particulate matter. However, the SIP standards for fugitive dust emissions are ambiguous, and thus potentially unenforceable – such as the requirement in the Virginia SIP that coal mine operators take "reasonable precautions" to control fugitive dust but without specifying the "precautions" that must be taken. Therefore, monitoring and analysis of particulate matter on a regular basis will have significant contributions in improving the management of dust emissions associated with coal mining (The NSW Department of Planning and Industry & Investment, Environmental Compliance and Performance Report, 2010).

The fact that the ground-based observations of particulate matter concentrations are limited in both space and time, it is important to determine the potential of satellite-based observations in understanding the particulate matter pollution in this region. Satellite-derived AOD has significant spatial and temporal coverage and therefore is a potential candidate as a surrogate for predicting the surface air quality. The studies conducted in the

past, in different regions of the world, attempted to estimate the surface $PM_{2.5}$ or PM_{10} from ground-measured or satellite-derived aerosol optical depth (AOD, τ) (Engel-Cox et al., 2006; Filip and Stefan, 2011; Pelletier et al., 2007; van Donkelaar et al., 2006; van Donkelaar et al., 2010; van Donkelaar et al., 2011). These studies demonstrated the promising predictive power of satellite derived AODs for fine particulate matter. The objective of the current study is to estimate the extent of surface particulate matter pollution in Roda, Virginia, i.e., a community representative of other communities in the Appalachian coal mining region. Based on VA county-wide surface coal production data for 2008, the Wise County had the largest production of surface coal in 2008. We had conducted the air sampling of PM_{10} (but not $PM_{2.5}$) during 3-14 August, 2008, at two locations in the small community of Roda, Virginia, located very near to mountaintop mining sites.

As part of this analysis, a multiple regression model was developed by combining satellite retrievals of AOD with ground-based meteorology and particulate matter measurements at an additional location in Bristol, TN. The observed $PM_{2.5}$ concentrations at another location in Hazard, KY are used to validate the regression relation. This relation is then extrapolated to our measurement site (Roda, VA) to predict the surface $PM_{2.5}$ concentrations. The current study demonstrates the potential of combining spatially and temporally frequent satellite AOD retrievals with meteorological observations, in regions devoid of air quality monitoring, to understand the surface particulate matter pollution.

A2. Data and Methodology

A.2.1. Site Description

PM_{10} measurements were conducted at two locations in Roda, Virginia (Figure A.1). The sampling sites, Campbell (36°57′35″ N, 82°49′57″ W, 592 meters) and Willis (36°57′8″ N, 82°49′14″ W, 568 meters), are approximately a mile apart (Aneja et al., 2012). Around the time of the measurements, about 44% of Virginia's surface coal production was taking place in Wise County (Coal production data, 2008). The Campbell site is located along a haul road very near to the entrance of various coal mines, and therefore observations from this site represent PM emissions from the haul road with potential contributions from the mine sites. Site Willis is located along the same haul road approximately a mile away from Site Campbell and coal mines, and therefore represents the microenvironment to which the residents in Roda are exposed (Aneja et al., 2012).

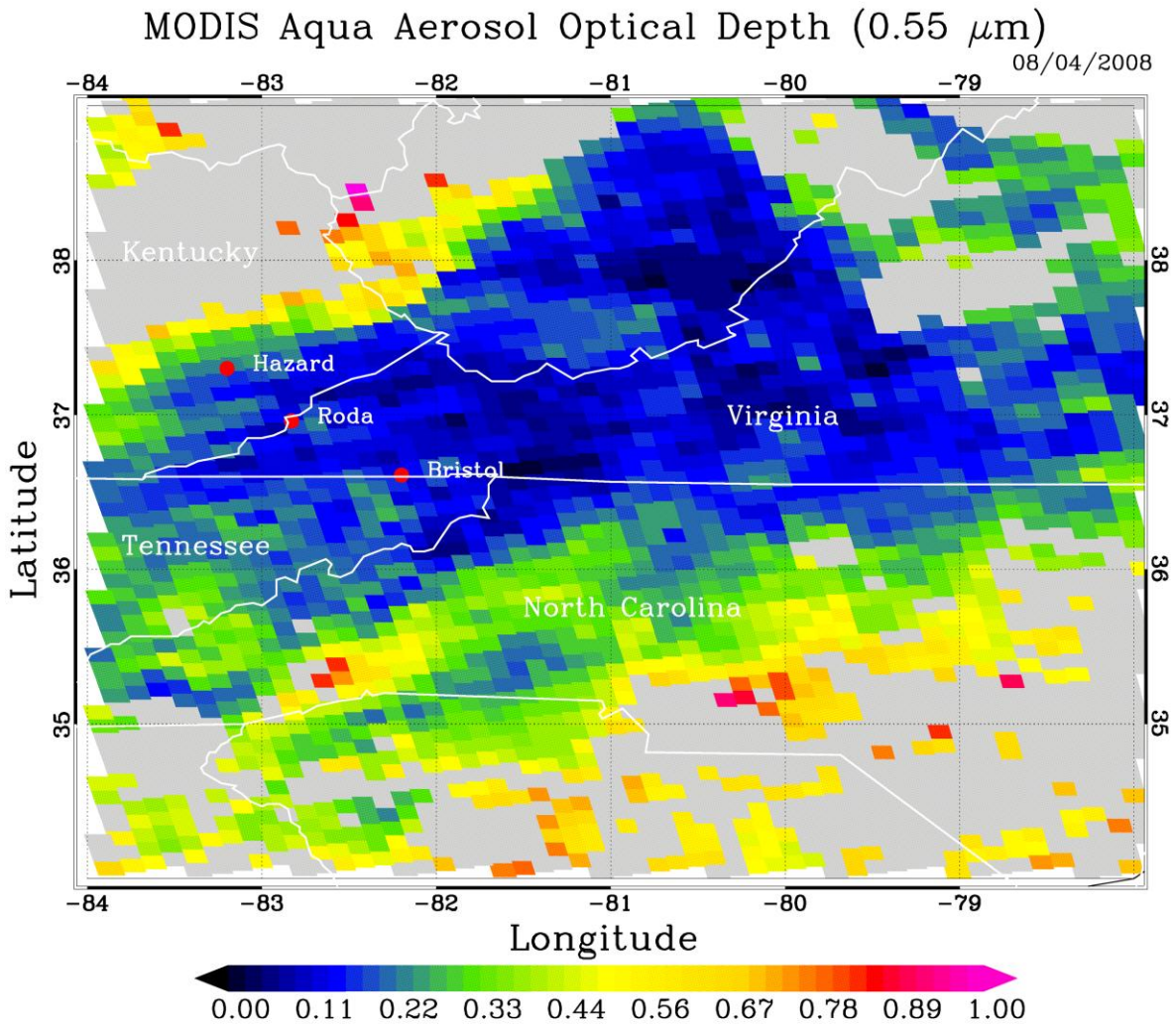

Figure A.1. Particulate Matter measurements during 3-14, August 2008 were conducted at two locations in Roda, Virginia at site Campbell (a mine site) and at site Willis (a site close to the haul road). The air quality and meteorology data from the two closest stations to the Roda, Virginia used in this study include Bristol, Tennessee, and Hazard, Kentucky. The Aqua MODIS aerosol optical depth at 550 nm on 4th August, 2008 is also shown.

A.2.2. Particulate Matter Measurement

Air sampling of PM_{10} was conducted for twelve days during August 3-14, 2008, at Campbell and Willis sites in Roda, Virginia (Figure A.1). By comparing the observations of particulate matter concentrations between the mine site (Campbell) and the location along the haul road (Willis), we can identify the contribution from coal hauling. The PM_{10} samplers used are Andersen/GMW Model GUV-16H high volume air samplers with size selective inlets to collect particles with effective aerodynamic size smaller than ten micrometers. Calibration and operation of the samplers were performed in accordance with the manufacturer's specifications and the US Environmental Protection Agency (US EPA) regulations (US EPA, 1983). Laboratory calibrations of the samplers are conducted prior to and after the field deployment. Moreover, the on-site calibration was performed every day during the measurement period. The sampling was conducted for 24 hours continuously for the twelve days. A detailed description of the site characteristics and the PM samplers used, along with the sampling method, are provided in Aneja et al., 2012.

A.2.3. Air Quality Data

The air quality data were obtained from the two official PM monitoring stations located nearest to Roda, Virginia: one in Bristol, Tennessee (36.608N; 82.164W, 550 m elevation) and the other in Hazard, Kentucky (37.283 N; 83.209W, 280 m elevation) (Figure A.1.). These data were downloaded from the US EPA's Air Quality System (AQS) AirData website (http://www.epa.gov/airquality/airdata/). 24 hour-averaged $PM_{2.5}$ data were available with 2-day intervals at Bristol for all of 2008 and $PM_{2.5,}$ and PM_{10} data with 6-day intervals were available at Hazard from January to May 2008.

A.2.4. Meteorology

The daily average meteorological data – including air temperature (^{0}F), relative humidity (%), wind speed (miles/hour), surface pressure (inches), and rainfall (inches) – were obtained for Bristol, TN (36°37'39" N; 82°10'15" W), Hazard, KY (37°24'43" N; 83°25'26" W), and Roda, VA (36.97°N, 82.56°W). These data were downloaded from the National Weather Service. Days with reported rainfall events are excluded from the analysis.

A.2.5. Satellite Data

Satellite-derived AOD retrievals from Moderate Resolution Imaging Spectro-radiometer (MODIS) sensor onboard the Earth Observing System (EOS) Terra and Aqua satellites are available in high spatial and temporal resolutions. By collocating MODIS collection-5 Aerosol Optical Depth (AOD) with Aerosol Robotic Network (AERONET) AOD, Levy et al., 2010 suggested that, over land, the estimated uncertainty of MODIS AOD fall within the error bounds of $\pm 0.15\tau \pm 05$. The MODIS 3km and 10km aerosol data were obtained from the National Aeronautics and Space Administration (NASA) Goddard Space Flight Center web interface to the Level 1 and Atmosphere Archive and Distribution System (LAADS) (http://ladsweb.nascom.nasa.gov/data/). MODIS Terra and Aqua level 2, collection 5.1 high confidence retrievals of 550 nm AOD at 10km x10km resolution are used in this study. The results are also compared with 3km AOD retrievals from MODIS Aqua satellite.

A.2.6. The Weather Research and Forecasting (WRF) Model

The state-of-the-art Weather Research and Forecasting (WRF) model version 3.5.1 was used to simulate the meteorology of the study region centered at latitude: 37.4^0N, longitude: -83.1^0W. Three model domains with 9 x 9 km^2, 3 x 3 km^2, and 1 x 1 km^2 horizontal resolutions with 51 vertical levels from ~8 m to ~20 km AGL were chosen for this simulation. The size of these three horizontal domains are respectively 810 km x 774 km; 453km x 453km, and 283 km x 268 km. The Yonsei University (YSU) Planetary Boundary Layer (PBL) parameterization scheme (Hong et al., 2006; Hu et al. 2013) is used in this simulation along with the revised MM_5 surface layer scheme (Jiménez et al. 2012), Noah Land Surface Model (LSM) (Tewari et al. 2004), WRF Single-Moment 5-class Microphysics (Hong et al. 2004), RRTMG long wave and shortwave Radiation (Iacono et al. 2008), and Kain–Fritsch Cumulus schemes (Kain 2004). National Centers for Environmental Prediction (NCEP) North American Mesoscale (NAM) analysis data (6 hourly at 12 km horizontal grid resolution) (Rogers et al. 2009) are used for the initial and boundary conditions of WRF meteorological fields. The WRF model is run from 12 UTC on 2nd August to 0 UTC on 15th August, 2008. WRF outputs corresponding to first 12 hours are excluded from this analysis. Output files are produced every 10 minutes and outputs from the 1km (inner) domain are used in this study.

A.2.7. Methodology

MODIS 550 nm AOD with best quality data (quality assurance (QA) data flag = 3) are integrated with ground-based particulate matter and meteorological observations for the selected three stations (Bristol, TN; Roda, VA; and Hazard, KY) in the Appalachian

region. As a first step in the integration, these data are collocated in both space and time. Days with reported rainfall events are excluded from this analysis as these are washout events that reduce the concentrations of particulate matter in the air.

Based on the spatially and temporally coincident AOD and meteorology data, a multiple regression model was developed for the surface $PM_{2.5}$ for Bristol, TN for the year 2008. Even though 3 km AOD were able to resolve fine aerosol features such as smoke plumes over land and ocean significantly better than the 10 km AOD (Remer et al., 2013), their data frequency 3km data is considerably small. Moreover, our sampling was conducted for a limited period. For these reasons, we included 10km x 10km AOD in the development of the regression relation. We used high confidence (Quality Flag = 3) 550 nm AOD and cloud free pixels are only selected in this study. To collocate the satellite-derived AODs with ground-based measurements, we may either employ a minimum distance method or an average method (Cheng et al., 2012). In the minimum-distance method, the satellite pixel closest in distance to the surface station is selected and paired with the surface measurement that is closest in time to the satellite overpass. In the second method, an averaging is done for the high confidence (quality flag =3 and cloud free) retrievals of satellite pixels within a selected distance around the surface station. It is then paired with the surface measurements averaged over an appropriate time range. In this study, we chose the method of averaging to collocate the satellite AOD with the surface measurements.

At Bristol, TN, the collocated data is subjected to bivariate analysis between AOD and surface $PM_{2.5}$ and multivariate analysis by additionally incorporating meteorological parameters to derive an empirical relation for the surface $PM_{2.5}$. Once the particulate matter is released or formed in the atmosphere, its vertical and horizontal transports are governed by the meteorological conditions prevailing in the region. Since we are deriving an empirical relation for the surface particulate matter concentration based on satellite-derived AOD, which is a measure of the aerosol loading in the total atmospheric column, the incorporation of surface meteorology – such as surface temperature, relative humidity, wind speed, and surface pressure – may improve this prediction. Days with reported rainfall events were excluded to avoid the aerosol washout events. Before extending it to study the surface particulate matter concentrations in Roda, VA, the derived empirical relation was evaluated using the $PM_{2.5}$ observations at Hazard, KY. The background conditions were not quantified and removed from the concentration of PM_{10} contributed by the coal hauling.

A.3. Results and Discussion

As we have discussed earlier, a bivariate model is developed to find the association between AOD and $PM_{2.5}$. The linear relationship between AOD and $PM_{2.5}$ at Bristol, TN is:

$$PM_{2.5} = AOD*26.62 + 9.4074 \qquad (A.1)$$

The r^2 corresponding to AOD-$PM_{2.5}$ relation is 0.40 and is within the range of r^2 (0.19 - 0.74) reported for cities in the eastern United States by Engel-Cox et al., (2004). In addition to the impact of humidity on its optical properties, meteorology plays important roles in the vertical distribution, dispersion, and settling of the atmospheric particulate matter. Therefore, incorporating meteorology in deriving the AOD-$PM_{2.5}$ relationship is expected to improve the prediction of surface particulate matter. A multiple regression model is developed between meteorological parameters and MODIS AOD for predicting the surface $PM_{2.5}$ at Bristol, TN:

$$PM_{2.5} = -136.6 + AOD*31.96 + T*0.065 - RH*0.16 - WS*2.21 + P*5.09 \qquad (A.2)$$

where AOD is the aerosol optical depth at 550nm; T is the air temperature in ^{0}F; RH is the relative humidity in %; WS is the wind speed in mph; and P is the surface pressure in inches. Days with reported rainfall events are excluded in the derivation of this regression relation. Figures A.2. a and b show the estimated $PM_{2.5}$ along with the observations at Bristol, TN, based respectively on the two variable simple regression model and the multi-variate regression model. An important factor governing the successful prediction of $PM_{2.5}$ from AOD is the vertical distribution of aerosols in the atmosphere. For an unstable atmosphere, the well-mixed boundary layer may result in an improved linear AOD-$PM_{2.5}$ relationship and vice versa. For this reason, even though AOD can be used as

a surrogate for the surface particulate matter concentrations, meteorology plays a significant role in the extent to which the respective values correspond (Figure A.2.). With the incorporation of meteorology in the estimation of the surface $PM_{2.5}$ concentration, r^2 improved from 0.40 to 0.62. Our results suggest that meteorology plays an important role in determining the air quality of the study region. The model was evaluated and validated based on $PM_{2.5}$ observations from Hazard, KY (Figure A.2.).

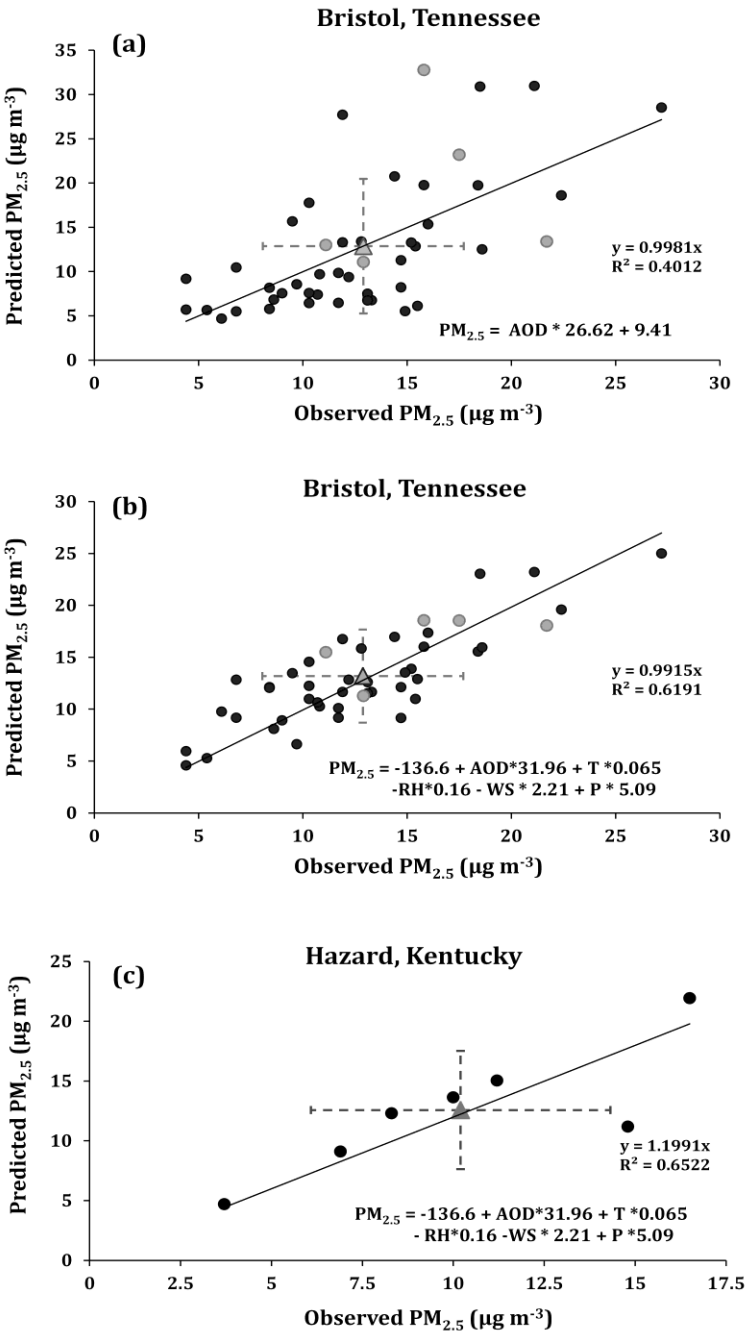

Figure A.2. For 2008, the observed $PM_{2.5}$ is compared with the regression models predicted $PM_{2.5}$ at Bristol, TN (a and b). The $PM_{2.5}$ multiple regression model for Bristol, TN, is evaluated and validated at Hazard, KY (c). (a) Two-variable (AOD) regression model predicted $PM_{2.5}$; (b) Multiple regression model predicted $PM_{2.5}$; (c) The observed $PM_{2.5}$ is compared with multiple regression model predicted $PM_{2.5}$ for Hazard, KY. The $PM_{2.5}$ for August (during the time measurements were made) are highlighted in gray.

The developed model was then extended to Roda, VA, to predict the surface particulate matter concentrations (Figures A.3. and A.4.). We also compared the multiple-regression model (AOD-$PM_{2.5}$-meteorology) (Figure A.2.a) results with the two-variable (AOD-$PM_{2.5}$) model (Figure A.2.b).

Before applying the developed multiple regression model for predicting surface air quality at Roda, VA, the regression relation was evaluated and validated using the $PM_{2.5}$ observations at Hazard, KY. Figure A.2.c shows model-predicted $PM_{2.5}$ compared to observed $PM_{2.5}$ at Hazard, KY. Particulate matter observations at Hazard, KY were available during January – May, 2008 with 6- day intervals. The predicted and observed $PM_{2.5}$ correlated well with an $r^2 = 0.65$.

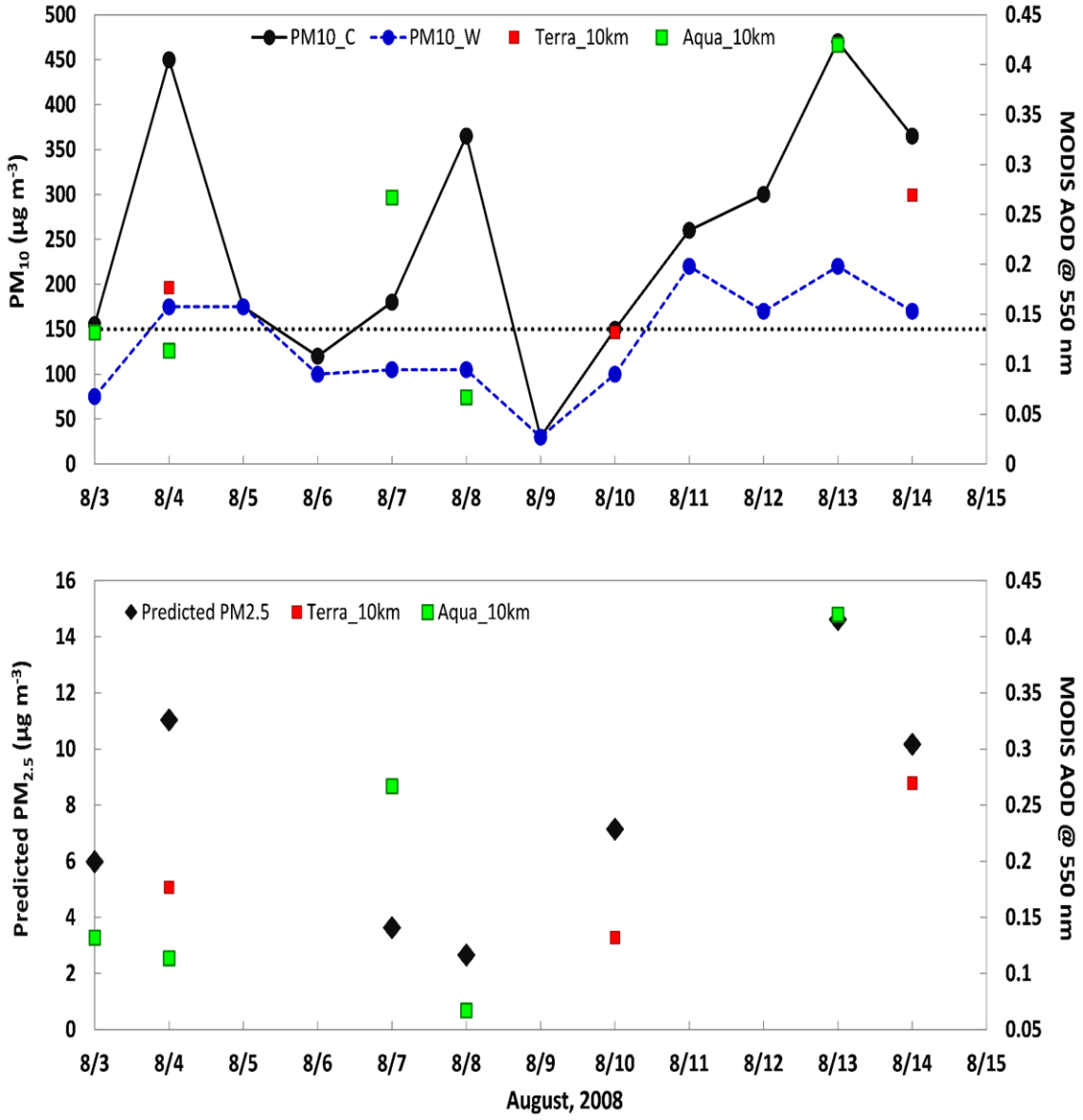

Figure A.3. PM_{10} sampled at site Campbell (PM10_C) and site Willis (PM10_W) are shown during 3 -14 August 2008 (Source: Aneja et al., AE 2012). The spatially and temporally collocated satellite aerosol optical depth (AOD) for MODIS Terra (10x10 km^2 as Terra_10km), and Aqua (10x10 km^2 as Aqua_10m and 3x3km^2 as Aqua_3km) are shown. The multiple regression model predicted $PM_{2.5}$ is also shown.

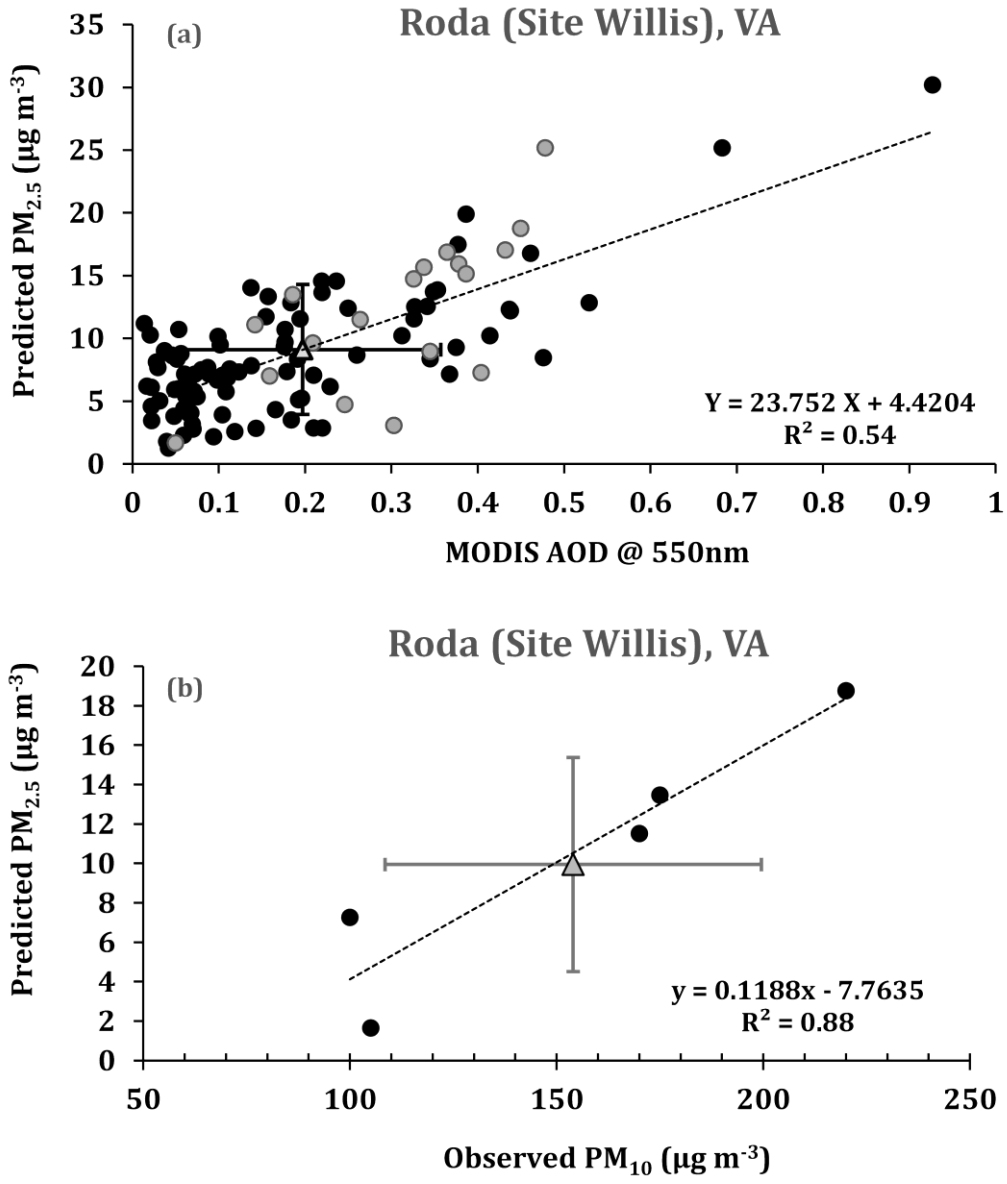

Figure A.4. For Roda, VA, (a) The MODIS aerosol optical depth at 550nm is compared with multiple regression model predicted $PM_{2.5}$ for the year 2008, and (b) The observed PM_{10} is compared with multiple regression model (eq 2) predicted $PM_{2.5}$ during 3 -14 August, 2008. (± 1SD for both observed and predicted $PM_{2.5}$ is also shown)

The PM_{10} concentrations at Roda, VA, are shown in Figure A.3. The 24-hour average PM_{10} concentration during the study period August 3 - 14, 2008 at site Campbell was 250.2 ± 135.0 μg m^{-3} and at site Willis was 144.8 ± 60.0 μg m^{-3}. The PM_{10} 24-hour U.S. National Ambient Air Quality Standard is 150 μg m^{-3}. Site Campbell is located very near to the entrance of various coal mines, and, therefore, PM_{10} concentrations far exceeded those at site Willis. In Figure A.3., spatially and temporally coincident MODIS Aqua and Terra AOD (10km x 10km) are shown compared to the observed PM_{10} for the sampling sites. Satellite-derived AOD is capable of capturing the diurnal variation pattern in the sampled PM_{10} at the Willis site. Site Willis is close to the haul road and is ~ 1 mile away from site Campbell. The particulate matter measurements from Willis site are more representative of the typical exposure in the region as it is further from the mine sites, and therefore we see an improved correlation between satellite-derived AOD and Willis PM_{10} as compared to Campbell PM_{10}.

Using the outputs from WRF model simulation, we further examined the role of meteorology in the air quality of the study region. At Campbell (located at the entrance of mine sites), no or poor correlation observed between WRF simulated planetary boundary layer (PBL) height, wind speed, wind direction, 2m air temperature, or down-welling shortwave radiation. Except for the PBL height and relative humidity, site Willis also showed relatively poor correlation for these simulated meteorological parameters with PM_{10}. At Willis, the daily average PBL height moderately negatively correlated (Figure A.5.) with PM_{10} (r^2 = ~0.50).

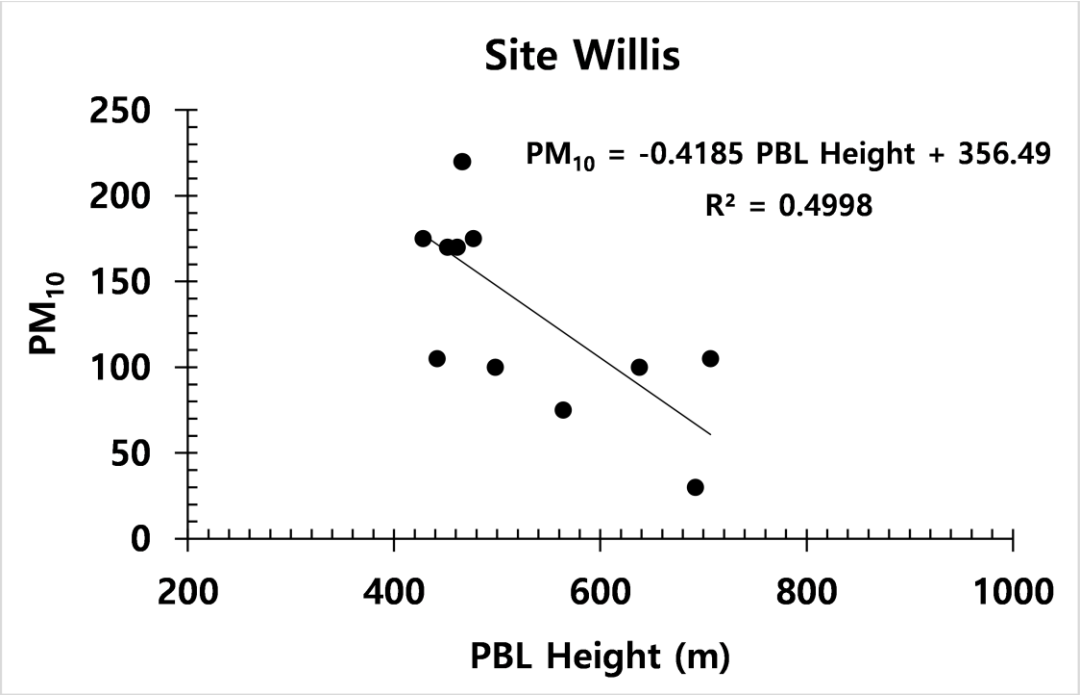

Figure A.5. The correlation between WRF simulated PBL height and PM_{10} is shown for site Willis. The PBL height-PM_{10} showed moderate negative correlation (r^2 =~0.50) at this site. No or poor correlation was observed between PBL height-PM_{10} at site Campbell.

During August 3 - 14, 2008, the WRF simulated average wind direction was north-northwesterly or northerly. The daily average wind direction at site Willis ranged from ~304^0 to ~ 360^0. The corresponding 10m wind speed ranged from 1.85m/s to 3.5 m/s. Aneja et al (2012) noted that at both the sites, the lowest concentration of PM_{10} (~30 μg m^{-3}) was measured on the day that had no truck hauling. We noticed that excluding this particular day in the analysis improved the correlation between PM_{10} and relative humidity at Willis (r^2 = improved from 0.10 to 0.34) and at Campbell (r^2 = 0.08 to 0.25). Other important factors noted during this study are the higher concentration of particulate matter at Campbell and this mine site is ~1 mile northwest of the site along the haul road (Willis). Moreover, the prevailing wind direction in this region during the study period was north/northwesterly. All these factors suggest that the air quality at Willis may be influenced by coal mining and coal hauling.

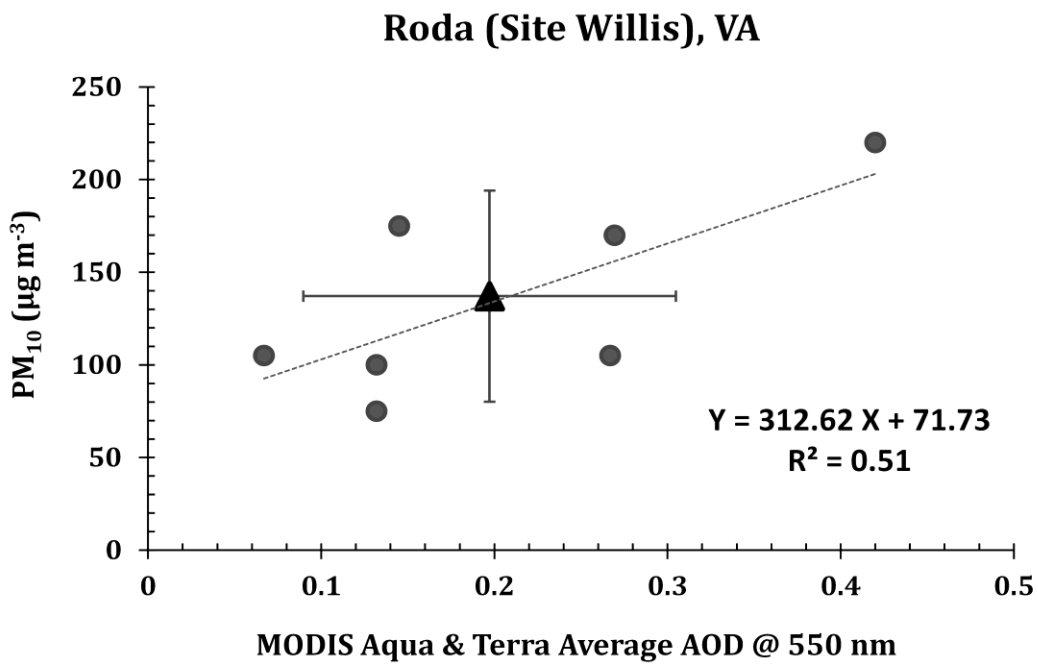

Figure A.6. The correlation between spatially and temporally collocated MODIS aerosol optical depth at 550nm and PM_{10} during 3 -14 August, 2008 are shown for Roda, Virginia.

The multiple regression model-predicted $PM_{2.5}$ correlates well with the observed PM_{10} pattern. During the measurement period, for the days with predicted $PM_{2.5}$, the correlation (negative) between PBL height and predicted $PM_{2.5}$ (r^2 = 0.30) was comparable with that of PBL height and predicted PM_{10} (r^2 = 0.32). For these days, the model predicted $PM_{2.5}$ and PM_{10} exhibited comparable correlation with WRF simulated meteorological parameters. These factors suggest the possibility of the same source for PM_{10} and $PM_{2.5}$ (coal mining operations, including truck hauling). At Roda, VA, the multiple regression model predicted $PM_{2.5}$ was compared with MODIS 550 nm AOD for

the year 2008 (Figure A.4.a). The predicted $PM_{2.5}$ is well correlated with satellite-derived AOD (r^2 = 0.54). Engel-Cox et al., 2006, pointed out that the particulate matter that is transported upwards is a contributing factor in the variability in this AOD-$PM_{2.5}$ relationship. The multiple regression model (eq 2) predicted $PM_{2.5}$ was correlated with measured PM_{10} (Figure A.4.b). The slope of Figure A.4.b suggests a $PM_{2.5}$ fraction of ~9.4% of PM_{10}. We observed a similar relationship between measured $PM_{2.5}$ and measured PM_{10} at Hazard, KY; which has a $PM_{2.5}$ contribution of ~5.6% to PM_{10}. This result is very similar to our predicted $PM_{2.5}$ fraction at Roda, VA. The correlation (r^2 = 0.51) between MODIS 550 nm AOD (mean and ± 1SD is 0.197 ± 0.11) and PM_{10} (mean and ± 1SD is 137.08 ± 56.95 μg m^{-3}) during August 3 - 14, 2008 are shown for Roda, Virginia (Figure A.6.). The World Health Organization (WHO) PM standards are as follows: the 24-hour PM_{10} standard is 50μg m^{-3}; and the 24-hour $PM_{2.5}$ standard is 25μg m^{-3}. Our results show that the predicted $PM_{2.5}$ at Roda, VA, in 2008 is 9.11±5.19 μg m^{-3} with a minimum of 1.27 μg m^{-3} and a maximum of 30.20 μg m^{-3}. On some days in 2008, the predicted $PM_{2.5}$ exceeded the WHO 24-hour standard of 25 μg m^{-3}.

A.4. Conclusions

We have conducted particulate matter (PM_{10}) measurements at Campbell, a site located very near coal mines, and at Willis, a site close to the haul road, both in the active mountaintop mining area of Roda, Virginia located in Wise County. During the 12-day measurement period in August 2008, the 24-hour average PM_{10} concentration at the Campbell Site was 250.2 ± 135.0 μg $m^{-3,}$ and at the Willis Site was 138.4 ± 62.9 μg m^{-3}, while the PM_{10} 24-hour U.S. national ambient air quality standard is 150μg m^{-3}.

The fact that Wise County is Virginia's largest surface coal-producing county at the time may be the reason for elevated levels of particulate matter loading in the region as compared to major cities in the Eastern United States. Therefore, to understand the impact of coal hauling on the ambient air quality by predicting the $PM_{2.5}$ concentration at the site, we have developed a regression model by spatially and temporally integrating high confidence 550 nm AOD retrievals from MODIS satellite sensors, ground based observations of respirable particulate matter concentrations and surface meteorological parameters. The comparison, of multiple regression-model predicted $PM_{2.5}$ (R^2 = 0.62) and two-variable (AOD-$PM_{2.5}$) predicted $PM_{2.5}$ (R^2 =0.4) with the observations, show that including surface meteorology in the regression model improves the agreement between measured and calculated $PM_{2.5}$.

The developed regression model was validated using particulate matter observations from Hazard, Kentucky. At Roda Virginia the ratio between model-predicted $PM_{2.5}$ and measured PM_{10} is a little less than 0.1. The multi-variate model predicted $PM_{2.5}$ exceeded the World Health Organization (WHO) 24 hour $PM_{2.5}$ standard on some days for which quality assured AOD data were available in 2008. The current study sites are representative of communities in the southwest Virginia and parts of Appalachia that are commonly located in narrow hollows where homes are placed directly along the roads that experience heavy coal truck traffic in a region of active mountaintop mining operations. The need for developing control and mitigation strategies to protect the environment and safeguard the public health from particulate matter generated by coal hauling therefore warrant further detailed studies in this and similar regions. The current study demonstrates that integrating satellite-derived aerosol information with observed and model simulated meteorology along with ground-based particulate matter observations may provide improved characterization of air quality in the region of interest.

ACKNOWLEDGEMENTS

We acknowledge support from the Southern Appalachia Mountain Stewards (SAMS) and the Sierra Club. We greatly appreciate the time and interest of the many volunteers, scientists, interest groups, and students who assisted us, in the collection of the data, and shared their knowledge and expertise.

REFERENCES

Ahern, M. M., M. Hendryx, J. Conley, J. Fedorko, A. Ducatman, and K. J. Zullig. 2011. The association between mountaintop mining and birth defects among live births in central Appalachia, 1996–2003. *Environ. Res.* doi:10.1016/j.envres.

Aneja, V. P., A. Isherwood, P. Morgan. 2012. Characterization of particulate matter (PM10) related to surface coal mining operations in Appalachia. *Atmospheric Environ.* 54, pp. 496–501.DOI:10.1016/j.atmosenv.2012.02.063

Cheng, T., H. Chen, X. Gu, T. Yu, J. Guo, and H. Guo. 2012. The inter-comparison of MODIS, MISR and GOCART aerosol products against AERONET data over China. *J. Quant. Spectros. Radiat. Transfer*. 113, 2135–2145, doi:10.1016/j.jqsrt.2012.06.016.

Coal production data 2008, Office of Oil, Gas, and Coal Supply Statistics, U.S. Energy Information Administration (EIA), U.S. Department of Energy. http://www.eia.gov/beta/coal/data/browser/ (accessed November 20, 2014)

Department of Environment and Climate Change. 2007. NSW, Air Emissions Inventory for the Greater Metropolitan Region in NSW. http://www.epa.nsw.gov.au/resources/air/aeibroc07335.pdf (accessed January 4, 2015)

Engel-Cox, J. A., M. H. Raymond, R. Raymond, F. Dimmick, A. C. Rush, J. J. Szykman, J. Al-Saadi, D. A. Chu, and R. Z. Erica. 2006. Integrating lidar and satellite optical depth with ambient monitoring for 3-dimensional particulate characterization. *Atmospheric Environ.* Vol. 40, No. 40, pp. 8056-8067, doi:10.1016/j.atmosenv.2006.02.039

Finkelman, R.B. 1995. Modes of Occurrence of Environmentally-Sensitive Trace 377 Elements in Coal, In: D.J. Swaine and F. Goodarzi (Eds.), Environmental Aspects of 378 Trace Elements in Coal (p. 25). New York: Springer.

Filip, F., and S. Stefan. 2011. Study of the correlation between the near-ground PM_{10} mass concentration and the aerosol optical depth. *Journal of Atmospheric and Solar-Terrestrial Physics*, 73, 1883–1889.

Gilbert, N., 2010. Mountain mining damages streams. *Nature*. vol. 466, pp. 806.

Health Effects Institute (HEI). 1995. Particulate Air Pollution and Daily Mortality: Replication and Validation of Selected Studies, p. 4.

Hendryx, M., and M. M. Ahern. 2009. Mortality in Appalachian Coal Mining Regions: The Value of Statistical Life Lost. *Public Health Report 2009.* 124(4): 541–550.

Hong, Song-You, Jimy Dudhia, and Shu-Hua Chen. 2004. A revised approach to ice microphysical processes for the bulk parameterization of clouds and precipitation. Monthly Weather Review 132, no. 1: 103-120.

Hong, Song-You, Yign Noh, and Jimy Dudhia. 2006. A new vertical diffusion package with an explicit treatment of entrainment processes. Monthly Weather Review 134, no. 9: 2318-2341.

Hong, Song-You. 2010. A new stable boundary-layer mixing scheme and its impact on the simulated East Asian summer monsoon. Quarterly Journal of the Royal Meteorological Society 136, no. 651: 1481-1496.

Hu, Xiao-Ming, Petra M. Klein, and Ming Xue. 2013. Evaluation of the updated YSU planetary boundary layer scheme within WRF for wind resource and air quality assessments. Journal of Geophysical Research: Atmospheres 118, no. 18.

Iacono, Michael J., Jennifer S. Delamere, Eli J. Mlawer, Mark W. Shephard, Shepard A. Clough, and William D. Collins. 2008. Radiative forcing by long-lived greenhouse gases: Calculations with the AER radiative transfer models. Journal of Geophysical Research: Atmospheres 113, no. D13.

Jiménez, Pedro A., Jimy Dudhia, J. Fidel González-Rouco, Jorge Navarro, Juan P. Montávez, and Elena García-Bustamante. 2012. A revised scheme for the WRF surface layer formulation. Monthly Weather Review 140, no. 3: 898-918.

Kain, J. S. 2004. The Kain–Fritsch Convective Parameterization: An Update. J. Appl. Meteor., 43, 170–181.

Kurth, L., A. Kolker, M. Engle, N. Geboy, M. Hendryx, W. Orem, M. McCawley, L. Crosby, C. Tatu, M. Varonka, C. DeVera. 2014. Atmospheric particulate matter in proximity to mountaintop coal mines: sources and potential environmental and human health impacts. *Environ. Geochem. Health.* 37(3). doi: 10.1007/s10653-014-9669-5.

Levy, R.C., L. A. Remer, R. G. Kleidman, S. Mattoo, C. Ichoku, R. Kahn, and T. F. Eck. 2010. Global evaluation of the collection 5 MODIS dark-target aerosol products over land. *Atmos. Chem. Phys. 10*, 10399–10410.

Office of Surface Mining Reclamation and Enforcement, Appalachian Region, Mountain top Mining. 2010, http://www.arcc.osmre.gov/Divisions/TSD/Techservices/MountaintopMining/mtopmining.shtm (accessed November 18, 2015)

Palmer, M. A., E.S. Bernhardt, W. H. Schlesinger, K. N. Eshleman, E.FoufoulaGeorgiou, M. S. Hendryx, A. D. Lemly, G. E. Likens, O. L. Loucks, and M. E. Power. 2010. Science and regulation. Mountaintop mining consequences. *Science*. 327:148-149.

Pelletier, B., R. Santer, and J. Vidot. 2007. Retrieving of particulate matter from optical measurements: a semiparametric approach. *Journal of Geophysical Research*, 112(D06208), 18.

Rogers, Eric, G. DiMego, T. Black, M. Ek, B. Ferrier, G. Gayno, Z. Janjic, Lin, Y., Pyle, M., Wong, V. and Wu, W.S. 2009. The NCEP North American mesoscale modeling system: Recent changes and future plans. In Preprints, 23rd Conference on Weather Analysis and Forecasting/19th Conference on Numerical Weather Prediction.

Tewari, Mukul, F. Chen, W. Wang, J. Dudhia, M. A. LeMone, K. Mitchell, M. Ek, G. Gayno, J. Wegiel, and R. H. Cuenca. 2004. Implementation and verification of the unified NOAH land surface model in the WRF model. In 20th conference on weather analysis and forecasting/16th conference on numerical weather prediction, pp. 11-15.

The Environmental compliance and performance audits: management of dust from coal mines, The Department of Environment and Climate Change and Water, The NSW Department of Planning and Industry & Investment, 2010.

http://www.planning.nsw.gov.au/Portals/0/Development/Compliance/Publications/summary_audit_report_december_2010.pdf (accessed January 4, 2015)

US EPA. 1994. Ground Water and Wellhead Protection. Washington, D.C., United States Environmental Protection Agency.

van Donkelaar, A., R. V. Martin, M. Brauer, R. Kahn, R. Levy, C. Verduzco, and P.J. Villeneuve. 2010. Global Estimates of Ambient Fine Particulate Matter Concentrations from Satellite-based Aerosol Optical Depth: Development and Applications Environ Health Perspectives (6). 118. doi:10.1289/ehp.0901623

van Donkelaar, A., R. V. Martin, R. C. Levy, A. M. DaSilva, M. Krzyzanowski, N. E. Chubarova, E. Semutnikova, and A. J. Cohen. 2011. Satellite-based estimates of ground-level fine particulate matter during extreme events: A case study of the Moscow fires in 2010. *Atmospheric Environ.* 45, 6226-6232, doi:10.1016/j.atmosenv.2011.07.068

van Donkelaar, A., R. V. Martin, and R. J. Park. 2006. Estimating ground-level $PM_{2.5}$ using aerosol optical depth determined from satellite remote sensing. *J. Geophys. Res.* 111, D21201, doi:10.1029/2005JD006996. World Health Organization Air Quality Guidelines. 2005. http://www.euro.who.int/__data/assets/pdf_file/0005/78638/E90038.pdf (accessed January 20, 2015)